NTNU – Trondheim
Norwegian University of
Science and Technology

An Experimental and Numerical Study of Hydraulic Pressure Loss and On-Set of Turbulence

Sindre Eiane Aarsland

Petroleum Geoscience and Engineering (2 year)
Submission date: June 2013
Supervisor: Pål Skalle, IPT

Norwegian University of Science and Technology
Department of Petroleum Engineering and Applied Geophysics

Abstract

A long drillstring consists of numerous of diameter changes, where the most frequent is the change due to tool joints for every pipe length. In the upper wellbore sections, were the annular clearance are wide, are the small diameter changes due to tool joints most likely negligible. When drilling the lower wellbore sections and in slim hole drilling, the annular clearance is decreased, thus the geometric changes could affect the hydraulic pressure loss.

For the purpose of maintaining wellbore pressure control, the ability to accurately estimate hydraulic pressure loss along the wellbore is essential. By investigating the different segments affecting the fluid flow downstream the mud pump, separately and in combination, it is possible to gain a greater knowledge of hydraulic pressure loss. Increased wellbore control ensures a safer operation, but also a more effective operation, with regard to controlled equivalent circulation density and thus rate of penetration.

The main goal in this thesis was to investigate and quantify the contribution to pressure of sequenced tool joints in the string. By building a small scaled lab, experiments were conducted in order to determine the relative difference with and without tool joints, verify existing models and suggest alternative approaches for calculation of the additional pressure drop. Additionally the thesis focus on the impact of on-set of turbulence and its effect on pressure loss, hence the calculation and prediction.

Contraction and enlargement in a borehole causes fluid acceleration, deceleration and kinetic energy loss in the mud. Once an obstacle in the well changes the velocity gradients in the mud, the boundary layer is affected, eddies are formed and local or fully turbulent flow regime can occur. By introducing the gradual contraction and enlargement due to tool joints, the velocity gradient in the mud is altered and an additional pressure drop is introduced.

The different experiments were carried out with the same base-fluid, applying different concentration of polymers for the purpose of increasing the viscosity. In total four different combinations of the inner steel pipe were planned tested, utilizing one Newtonian fluid and three non-Newtonian fluids. Based on the experiments conducted some findings can be highlighted:

- In all tests the presence of tool joints increased the hydraulic pressure loss, also in the laminar region. The highest enhanced pressure loss registered due to tool joints was 90%

- Once tool joints are included in the string the on-set of turbulence is strongly shifted towards lower flow rates, which none of the tested models are able to account for.

- The presence of tool joints in the string introduces a pressure loss equivalent to a rough obstruction in the annular clearance.

- Both modification and the alternative suggested approach, yields more accurate results in the estimation of hydraulic pressure loss with tool joints than the exiting model.

The investigation of the previously suggested models and approaches, showed various results in estimation of the additional pressure drop due to tool joints. Only when applying the lowest viscosity, one of the model suggested by Enfis et al. (2011) showed satisfying results for tool joint correction. Increasing the viscosity of the mud, none of the existing models comprehended with the measured values, due to overestimation of the pressure in the laminar region and estimation of on-set of turbulence.

Three alternative methods have been suggested, of which two have been investigated in depth. The first one presents a modification of the model suggested by Enfis et al (2011). Applying the new suggested modification of the model, the discrepancy between the measured and the calculated pressure drop were decreased in the turbulent regime, but still with overestimated values in the laminar regime.

In the second suggested approach, a regression factor representing increased friction, was presented. By calculating an the frictional enhancement as a function of Reynolds number it was possible to predict a more accurate pressure loss in the higher viscosity range. The regression factor was based on the same principle as Blasius, Moore and Moody in their estimation of pressure loss in pipes with varying surface roughness. The downside of applying a regression approach is the need for continuous experimental investigation in order to create a database based on geometry, annular clearance and fluid rheology.

Sammendrag

En lang borestreng består av endringer i diameter, der den vanligste forandringen er p.g.a. tool joints. I øvre deler av brønnen, hvor ringrommet er stort, vil de små diameter forandringene grunnet tool joints være neglisjerbare. Ved dypere boring og ved slim hole boring er ringrommet mellom vegg og borestreng kraftig redusert, og de små geometriske forandringene kan føre til en signifikant forskjell på det hydrauliske trykktapet.

For å utføre en boreoperasjon på en sikker og effektiv måte er evnen til nøyaktig estimering av hydraulisk trykktap essensiell. Ved å undersøke de forskjellige segmentene i strengen, alene og i sammenheng med andre er det mulig og identifisere og kvantisere effekten de gir.

Hovedmålet i denne avhandlingen var å undersøke og analysere bidraget til flere tool joints i en borestreng. Ved å bygge en lab i liten skala ble eksperimenter utført for å finne de relative forskjellene med og uten tool joints. Eksisterende modeller ble verifisert og nye alternative tilnærminger har blitt foreslått. I tillegg til å fokusere på de relative forskjellene, ble det spesielt fokusert på når laminær strømning avtar og turbulens oppstår..

Sammentrekninger og utvidelser i et borehull forårsaker akselerasjon, retardasjon og kinetisk energitap i boreslammet. Når slammet møter en hindring vil hastighetsgradientene i slammet forandres, det viskøse laget ved veggene forandres og lokal turbulent virvelbevegelse av partikler oppstå. På grunn av den gradvise kontraksjonen eller ekspansjonen ved å innkludere tool joints i strengen vil dette forekomme, som igjen vil føre til et større trykktap.

I de eksperimentelle forsøkene ble 4 forskjellige slam testet, hvor mengden av polymertilsetningen var det eneste som skilte dem Basert på resultatene kan noen funn fremheves:

- I alle slam som ble testet er det en relativ forskjellen mellom tool joints og bart rør, også i det laminære strømningsregimet. Det høyeste registrerte trykktapet grunnet tool joints hadde en relativ økning på mer enn 90%.

- Grunnet tool joints i strengen vil strømningen endres fra laminær til turbulent ved mye lavere strømningsrater and kalkulert.

- Ved å inkludere tool joints i strengen vil man få et ekvivalent hydraulisk trykktap tilsvarende å inkludere en signifikant ru diameter hindring.

Tre alternative metoder for tool joint korreksjon har blitt foreslått, hvor to ble undersøkt i dybden. Den første metoden er en modifikasjon av den av modellen foreslått, Enfis et al (2011), som var mest sammenfallende med de av de målte verdier. Ved å bruke den modifiserte metoden ble forskjellen mellom målt og kalkulert trykktap mindre. Denne metoden ga bare gode resultater viskositeten var lav

Ved økt viskositet i slammet var ingen av de eksisterende modeller eksakte nok, dette grunnet over estimering av trykket i det laminære området og effekten av turbulent strømnings regime grunnet tool joints. For å lettere kunne estimere hvor det turbulente strømnings regimet påtar ble en matematisk korrelasjon ved hjelp av regresjon foreslått. Regresjons faktoren foreslått bygger på de gamle prinsippene for å regne ut effekten av ruhet i materiale, som en funksjon av Reynolds tall og ble brukt for å kalkulere den prosentvise økningen i friksjons faktor som en funksjon av

Reynolds nummer. Basert på sammenligning var regresjons faktoren den eneste faktoren som ga noenlunde overenstemmelse ved høyere viskositet. Den negative siden ved å anvende en regresjonsfaktor er behovet for å lage en database basert på reologi og geometri.

Acknowledgements

This Master Thesis was written at the Department of Petroleum Engineering and Applied Geophysics at the Norwegian University of Science and Technology (NTNU)

First I would like to thank my academic supervisor Pål Skalle for his enthusiasm, encouragement and advice throughout the thesis.

I would also sincerely like to thank Åge Sivertsen.and Håkon Myhren for all those hours spend in the lab with planning, building, evaluating and rebuilding the apertures and features. Without them the experimental part would not be possible

Last I would like to thank my older sister, Silje Aase not only for guidance and help with structuring and language correction, but also for all those hours spent helping with my school work, leading up to this thesis.

……
Sindre Eiane Aarsland

Trondheim 05.06.2013

Table of Contents

List Of Figures

List of Tables

1 Introduction

In order to ensure sufficient downhole pressure and controlled equivalent circulation density (ECD) the ability to calculate and understand frictional pressure drop along the wellbore is essential. Drilling deeper and longer, with decreasing annular clearance, require more accurate estimations with regards to well planning and drilling hydraulics.

The governing equations for one dimensional flow within a pipe is the momentum equation (shown in Equation 1.1) and the conservation of mass (Equation 1.2), both derived from the Navier-Stoke Equation (Sletfjerding 2009).

$$\rho g sin\alpha + \frac{1}{2}\rho\bar{v}\frac{f_m}{D} * \frac{d(\rho\bar{v}^2)}{dx} + \frac{dP}{dx} = 0 \tag{1.1}$$

$$\frac{dh}{dx} + \bar{v}\frac{d\bar{v}}{dx} + gsin\alpha + \frac{1d\dot{q}}{\dot{m}dx} = 0 \tag{1.2}$$

By assuming a horizontal system, without acceleration and isothermal flow, Eq. 1.1 is reduced and it becomes clear that the frictional pressure drop is strongly dependent on the frictional forces between the fluid and the wall, the velocity of the fluid, diameter and density.

In order to obtain an expression of the pressure loss during a drilling operation, contribution from different zones in the string are summed up in the most basic Equation 1.3

$$\Delta P_{annulus} = \Delta P_{Hydraulic\ friction} + \Delta P_{Bottom\ hole\ assembly} \tag{1.3}$$

Summing up the pressure losses according to Equation 1.3, the hydraulic friction terms have to be looked upon as a cluster factor, which have to be studied separately and in connection in order to determine their significance on the ECD. By extracting and highligting some of the most studied parameters the cluster factor becomes as shown in Equation 1.4

$$\begin{aligned}\Delta P_{hydraulic\ friction} &= \Delta P_{Rotation} + \Delta P_{Tool\ \ joints} + \Delta P_{Eccentricity} \\ &+ \Delta P_{Surge\ and\ swab} + \Delta P_{Singulartiy\ losses}\end{aligned} \tag{1.4}$$

Downstream the mud pumps, several irregular restrictions in the flow path is present, were all causes some degree of singularity pressure loss and thus enhanced friction. Pressure loss and flow regime through valves and greater obstacles have been documented in depth in the literature. In recent years the presence of tool joints, with their rapid changes in geometry forming expansions and contractions in the pipe and annulus has been drawn some attention. Although the contribution of one tool joint in the drill string is considered negligible, the total contribution when summing up all the tool joints in a long drill string, could cause a significant pressure drop.

1.1 Objective of the Thesis

The main objective in this thesis was to investigate the effect presence tool joints and the on-set of turbulent flow related to it, utilizing theoretical and experimental studies. By providing experimental data, test and evaluate previously suggested formulas a broader acceptance and awareness may be obtained on the subject. Although previous studies have been fulfilled with success, a broader database and thus confirmation of the existing models is required.

The available studies, both experimental and theoretical, which focus is to determine and create exact models of the hydraulic effect caused by tool joints are present, but limited. In the available studies, the obtained and concluded results are strongly dependent on predetermined assumptions and governing equations chosen. By altering the mud rheology, pipe dimension, fluid flow velocity, pipe eccentricity, drill string rotation and mathematical assumptions the tool joint effect changes and thus the accuracy in the models.

Another important aspect, which was addressed, was the on-set of turbulence and the resulting effect on the pressure loss. Some research's has reported no tool joint effect in the laminar region and thus no shift induced by the tool joint on the offset of turbulence. By only highlighting the hydraulic pressure loss in the turbulent flow regime and not in the laminar an overall picture of the tool joint effect can not be obtained.

1.2 Experimental Approach

In order to experimental test the tool joint effect, a new lab set up was built at the Norwegian University of Science and Technology. Compared with other previous studies some main parameters differs:

- The diameter ratio between the tool joint diameter and the annulus is significantly lower than in other studies, causing a decreased pressure loss. By choosing a wider annular clearance the study can be of relevance in the lower part of the wells in the North Sea.

- Instead of testing the effect of one tool joint, three tool joints have been present in a sequence, making the results more realistic to a real drilling operation.

- An Equivalent rough obstacle has been included in the experimental testing, in order to find an equivalent effect of the presence of tool joints.

2 Previously Published Work

The effect of hydraulic friction has been thoroughly investigated over the years by applying numerical studies, field studies, simulations and experiments. For the purpose of improving the available models with regards to hydraulic friction during drilling, small segments like pipe eccentricity, different fluid rheologies, temperature and string rotation have been approached separately and in conjunction. Recently, some authors have studied the effect and suggested different solutions to evaluate, model and determine the effect of tool joints more accurately. In this chapter the most essential publishing of the previous studies embracing the tool joint effect or with significance to it have been included chronologically divided by experimental studies, theoretical studies and field studies.

2.1 Simulation Studies

In 2007 Simoes et al published a paper, which utilized computer software in order to investigate the effect of tool joints on ECD. A total of 243 simulations were carried out, which altered the pipe geometry, fluid and flow rate. Simulation results showed that the presence of squared tool joints increase the pressure drop between 10-42 % for water and 3-23 % for the polymeric fluids. Changing the tool joint from squared to tapered decreased the pressure drop to 2-26 % in water and to 2-28 % in polymeric fluids. Due to the sudden expansion and contraction in a squared tool joint, the pressure loss enhanced compared with tapered tool joints.

In his paper Simoes suggested statistically correlation divided by the different regions in the tool joint, dependent on the geometry. By dividing the tool joint section in three, shown in Figure 1. Simoes et al. made it possible to evaluate the additional pressure drop with regards to tool joints. The results from Simoes et al. (2007) study have been given in Appendix D.

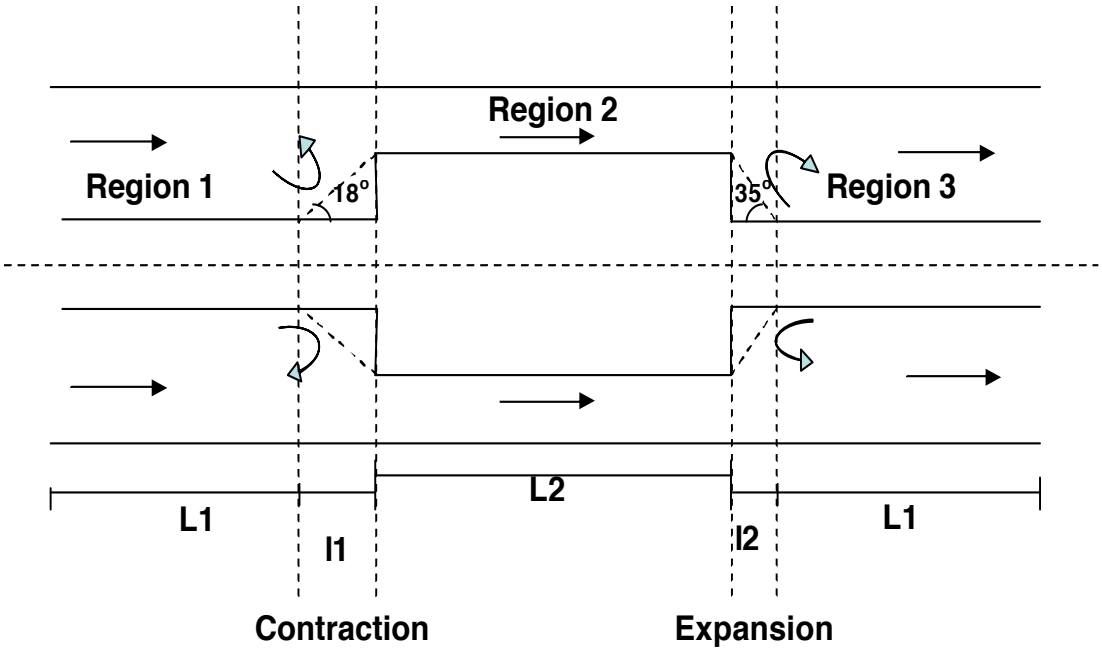

Figure 1: Tool joint regions suggested by Simoes et al (2007)

2.2 Experimental Studies

In 1981 Crane published a small book, which included experimentally tested formulas, suggested by Gibsom, for gradually contraction and expansion in drillpipes. The suggested formulas have been utilized as governing equations for singularity losses, in the studies by Jeong and Shah (2004), Enfis et al (2011), Scheid et al (2009) and Calcada et al (2012). The paper suggested Equation 2.1 – 2.4, depending on the angle of convergence and divergence.

Interval $0° < \theta \leq 45$.

$$K_e = 2.6\sin\frac{\theta}{2}(1 - R^2)^2 \tag{2.1}$$

$$K_c = 0.8\sin\frac{\theta}{2}(1 - R^2) \tag{2.2}$$

Interval $45° < \theta \leq 180$.

$$K_e = (1 - R^2)^2 \tag{2.3}$$

$$K_c = 0{,}5\sqrt{(1 - R^2)\sin\frac{\theta}{2}} \tag{2.4}$$

The study of Jeong and Shah was published in 2004 and investigated the effect of friction pressure loss with regard to tool joints. Jeong and Shah tested and suggested numerical solutions for additional pressure drop with one Newtonian fluid and two polymer fluids Their test facility consisted of two test loops, where one included 6 tool joints and one reference section without tool joints. By applying an annulus of 5 ½" – 2 7/8" and two different flowrates of 5bbl/min and 8,5 bbl/min the friction pressure increased respectively up to 30 % and 75 % with the presence of tool joints in the test flow loop. In their study they concluded that tool joints did not have any effect on friction factor in the laminar region with polymere fluids. The resulting Fanning friction factor plotted against Reynolds number for the one of the polymeric fluids have been displayed in Figure 2.

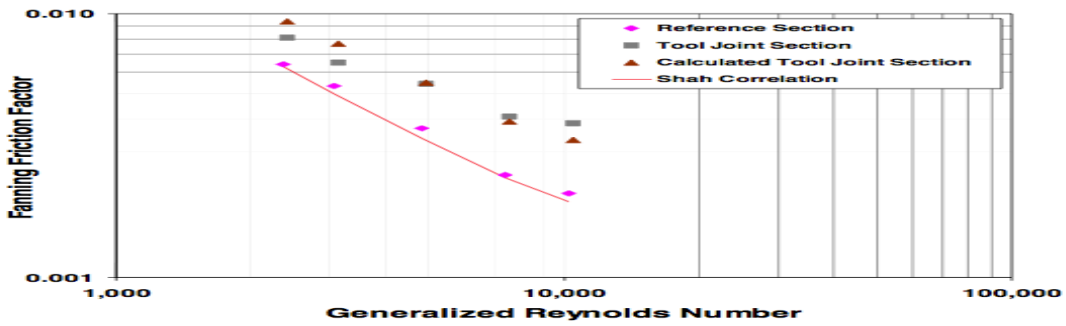

Figure 2: Fanning friction factor plotted against Reynolds number. The difference between the reference section, calculated tool joint section and the measured tool joint section is present by utilizing a polymere fluid (Jeong and Shah 2004).

The pressure loss estimation was calculated and compared with the data from the reference section data with no tool joints incorporated in the string in order to calculate the Shah correlation (ref. Chapter 4) for Non–Newtonian fluids and for comparison reasons. To calculate the effect of tool joint the different pressure contribution was added, shown in Equation 2.5.

$$\Delta P = Dp_{wide\ annulus} + Dp_{narrow\ annulus} + Dp_{expansion} + Dp_{contraction} \qquad (2.5))$$

The new numerical equations presented in the study had an accuracy of 3% and 5 % for additional pressure drop in the annulus for Newtonian and non-Newtonian fluids.

Scheid et al (2009 and 2011) and Calcada et al (2012) experimentally tested the formulas suggested by Jeong and Shah and other friction factor correlations in studies for Petrobras in Brazil. Scheid et al (2011) investigated the effect of well obstructions in the annular space applying four different fluids and rheology models. The study utlized typically applied muds, collected at different rig sites, in order to improve the relevance and applicability to the real world. The mud used had thereby been subjected to real temperature effects, solids and shear effects. In their paper they suggested different correlation factors, dependent on the type of mud used, in order to exactly calculate the friction factor and thus the required pump pressure offshore Brazil. The experimental set up for both Scheid et al (2011) and Calcada et al (2012) have been visualized in Figure 3.

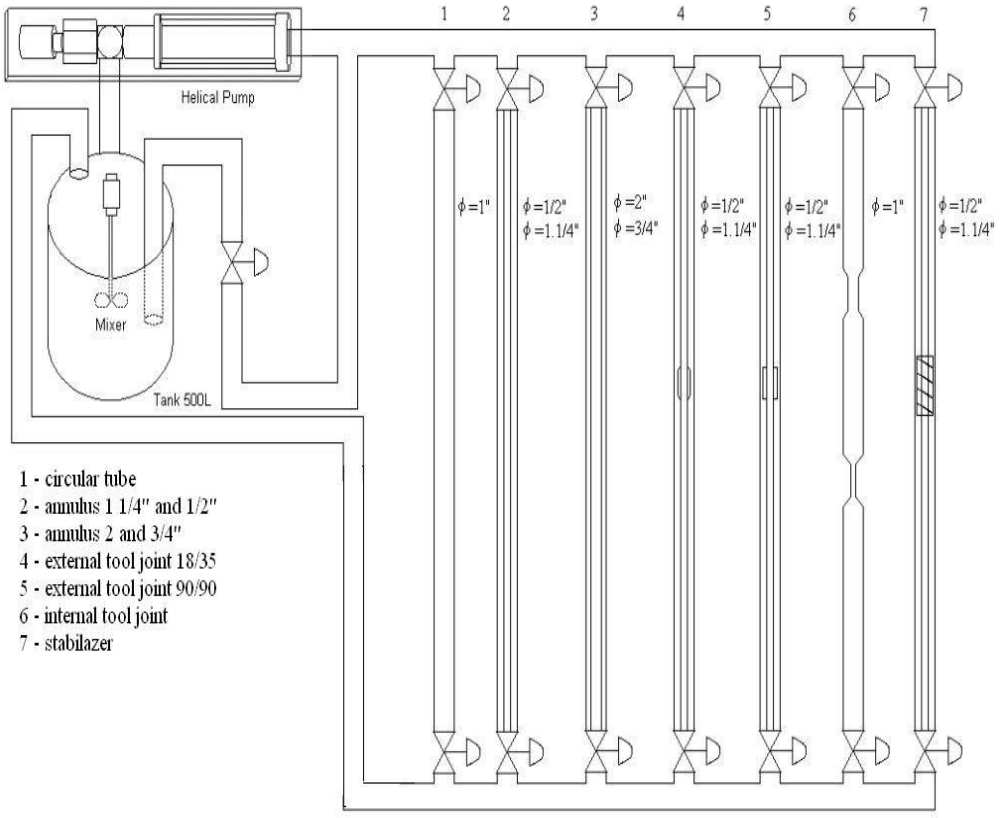

Figure 3: Laboratory set-up in the tool joint experiments by Scheid et al (2011)

Calcada based his study on the published papers by Scheid et al (2009 and 2011). By utilizing CFD (Computer Fluid Dynamics) simulations and the same test loop as Scheid et al (2009 and 2011), Calcada et al suggested further correlations for estimations of frictional factors, which mainly improved the results in the laminar region.

Enfis et al (2011) investigated and suggested solutions for the hydraulic effect of tool joints on annular pressure loss. The study provided by Enfis et al. was based on studies by Jeong and Shah (2004) and Simoes et al (2007). The experiments were conducted with two different annulus, drillpipe and tool joints sizes with relative diameter difference of 0.57 and 0.71. By using water as the drilling fluid the short time pressure loss was more than 200 % by including tool joints in the drill string. Changing the test fluid to polymere fluid, the introduction of tool joints in the string increase the pressure drop to almost 250 % compared to a normal string. Expanding the result and assuming 1 tool joint every 30 ft of drillpipe it was possible to calculate a more realistic pressure drop. The paper concluded, as in the other published paper, that the effect of tool joints could be substantially (up to 30% of annular pressure loss).

2.3 Field Studies

Cartalos and Dupuis (1993) investigated the effect of hydraulic friction with regard to pipe eccentricity and pipe rotation in slimhole drilling. Their study also embraced the effect of decreasing the annular clearance. According to their study the decreased annular clearance could induce the wall shear rate at lower flow rates, hence increase the hydraulic pressure drop. Based on an earlier study, preformed by Cartalos and Piau in 1992, entry and exit effects were neglected in the new formula for tool joint correlations by Cartalos and Dupuis. The old experience had shown that entry and exit effect could be neglected if the fluid where inelastic, while it had to be considered for solutions with high molecular weight or polymer-particle suspensions. The suggested equation by Cartalos and Dupuis for pressure drop with tool joint considered is given in Equation 2.6.

$$\frac{\Delta P}{L} = \frac{1}{L_p \left[\left(\frac{\Delta P}{L}\right)_p \left(L_p - L_{EU}\right) + \left(\frac{\Delta P}{L}\right)_{EU} * L_{EU} \right]} \tag{2.6}$$

McCann et al (1995) investigated the effect of narrow annulus by applying field test from a 2500 ft well and compare the commonly applied hydraulic friction equations. Their study comprised drill string rotation and eccentricity of the pipe and did not mainly focus on the tool joint contribution. In their non-rotating experiments they concluded that the simple models, with no tool joints available was reasonable accurate.

3 Theory of Pressure Loss in Special Pipes

In this chapter an introduction of the theory effecting hydraulic pressure loss and on-set of turbulence, with special regards to studies embracing the effect of tool joints, given. Starting with the rheological models, boundary layer and velocity profile development. In order to calculate the suggested models have friction factors correlation suggested by the compared models been extracted and highlighted. Following is an explanation of roughness, focusing on the effect on flow regime, before extraction expansion effects, a brief explanation of tool joints and the different investigated hydraulic diameters ends the chapter.

3.1 Rheological Models

Numerous of studies have been published on suitability, limitations and correlations with respect to fluid rheology and the responding hydraulic friction equations. As a result of the fluid characterization the pressure equations alter. While the oldest studies embraced the postulated theorem by Newton, newer studies often investigate the effect of utilizing more fluid dependent rheological models.

A Newtonian fluid is defined as a fluid, which has a linear relationship between shear stress and shear rate, defined in Equation 3.1.

$$\tau = \mu\bar{\gamma} \tag{3.1}$$

The Newtonian shear equation have been used as a base for most derivation for hydraulic pressure loss equations. Because of the distinct characterization of drilling fluids, with alternation in properties during a drilling operation, is it a complex process to quantify one correct rheological model. As there is no proportional relationship between the shear rate (ý) and shear strength (τ) in drilling fluids, there are problems in quantification with one exact model throughout the entire drilling cycle. Once the drilling fluids are subjected to the forces and temperature in the well thixotropic and rheopectic characterization can be detected. Thixotropic fluids are fluids which experiences reduced viscosity, if the shear rate is increased to a new constant, e.g. increased constant rotation of the drillstring. A rheopectic fluid is defined as the opposite. None of the most applied rheological models such as the Newtonian model, Power Law model or the Bingham Plastic Model, accounts for these thixotropic/rheopectic characterization in drilling muds Applying the rheological models at hand, calculating hydraulic friction problem can cause large discrepancy from the absolute truth (Bourgoyne et al. 1991).

One of oldest and most applied rheology models in the industry is the Power-Law model, shown in Equation 3.2.

$$\tau = K\acute{y}^{n} \tag{3.2}$$

K is the flow consistency index and *n* is the flow behavior index. Dependent on the flow behavior index the fluid can be characterized as a dilatant ($n < 1$) or a pseudoplastic ($1 > n$) If the fluid is characterized as a pseudoplastic fluid the effective viscosity will decrease as a response to increased shear rate, while for a dilatant fluid the viscosity will decrease with the same increased shear rate. Additionally a more shear thinning fluid (decreased n) will have a flatter flow profile, than a fluid with higher fluid flow index, due to the increased viscosity. A flatter flow profile will thus be more related to the turbulent flow regime, hence the pressure loss enhances (Ogugbue and Shah, 2010).

In the search for an accurate model for friction pressure loss due to tool joints many of the recent studies utilized the power law model. In order to apply the hydraulic pressure loss equations in non-Newtonian fluids, the concept of apparent viscosity has been introduced. By combining the pressure drop equations from Newtonian model and power law model and solving for the apparent viscosity in the power law model the apparent viscosity can be calculated. From most rheological models a relationship for apparent viscosity have been established. Apparent viscosity for Power-Law fluids is defined in Equation 3.3

$$\mu_{apparent} = \left(\frac{12 * \bar{v}}{d_h} * \frac{2n+1}{3n}\right)^n * \frac{Kd_h}{12\bar{v}} \tag{3.3}$$

Focusing on hydraulic pressure loss Langlinais et al.(1983) investigated the accuracy in the Bingham model and Power Law model by monitoring the pressure in two real 6000 ft wells and utilizing six different drilling muds, shown in Figure 4.

TABLE I
PROPERTIES OF CLAY-WATER MUDS

Mud Property	Mud No. 1	Mud No. 2	Mud No. 3	Mud No. 4	Mud No. 5
Density, ppg	8.6	8.8	8.8	8.8	8.85
Plastic Viscosity, cp	5.0	6.5	7.5	13.0	13.5
Yield Point, lb/100 ft^2	1.0	2.5	2.5	5.0	4.0
Flow Behavior Index, n	.874	.784	.807	.784	.824
Consistency Index, eq. cp.	13.1	34.6	33.3	69.2	52.2
Fann VG Readings					
T600	11.0	15.5	17.5	31.0	31.0
T300	6.0	9.0	10.0	18.0	17.5
T200	4.5	6.5	7.0	13.0	12.5
T100	2.5	3.5	4.0	8.0	7.0

Figure 4: The different rheological properties in the field study conducted by Lanlinais et al (1983)

The study highlighted that the predicted losses were greater than measured at low flow rates and vice verca at high flow rates, hence laminar pressure loss was overestimated, while turbulent pressure loss was underestimated. It was also concluded, based on the data available, that the methods for determining equivalent diameter of the fluid flow were of greater importance than the selection of rheological model. The results from the full scale tests have been displayed in Figure 5.

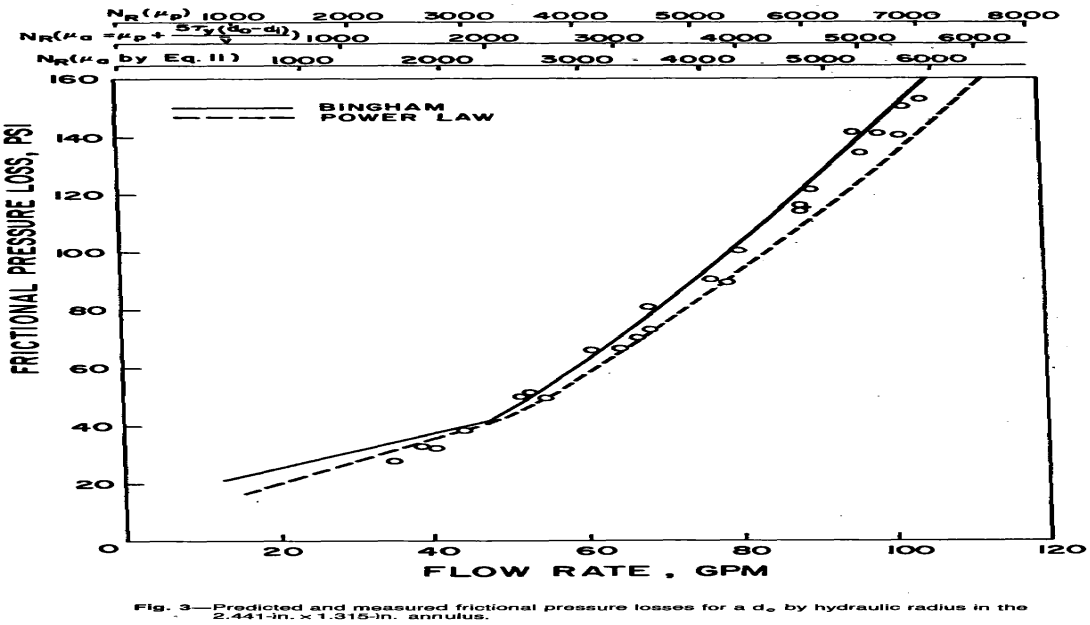

Fig. 3—Predicted and measured frictional pressure losses for a d_e by hydraulic radius in the 2.441-in. × 1.315-in. annulus.

Figure 5: Pressure drop vs flow rate in the investigation provided by Langlinais et al (1983)

Contrary to Langlinais (1983), Ochua (2006) highlighted the importance of choice of rheological model in pressure calculations. Ochua experimentally tested the accuracy of different rheological models and their accuracy with respect to hydraulic friction calculations; Newtonian, Bingham Plastic, Power Law, API RP 13D, Herschel-Bulkley, Unified rheological model, Robertson and Stiff and Casson model. Based on the predetermine assumptions and test factors, Ochua concluded that the API RP 13 D was the best model for the purpose to predict the hydraulic friction measurement. The API 13 D model was published in 1995 and aims to match the shear rate from the viscometer with true shear rates experienced in within the drillstring and annulus. API 13 D is a modification of the power law model and is suggested by the American Petroleum Institute. Instead of applying the standard 600 and 300 rpm reading in the Fann Viscometer, API 13 D applies the readings at 3 and 100 rpm. The Power Law equations then becomes as shown in Equation 3.4 and 3.5.

$$n_a = 0.657\, log \frac{\theta 100}{\theta 3} \tag{3.4}$$

$$K_a = \frac{5.11 * \theta 100}{170.2^{n_a}} \tag{3.5}$$

Another study which investigated the effect on hydraulic friction in different drilling muds, was published by Subramani and Azar in 2000. The study aimed to determine which rheological models that coincided and generated the most accurate results with regards to pressure drop, when altering mud type and wall roughness in pipe and annulus. The study suggested plots of friction factor versus Reynolds number, which could be utilized for the purpose to calculate friction pressure drop in annular flow, dependent on the mud at hand. In their study Subramani and Azar applied the Colebrook–White equation as a reference in rough pipes and Dodge and Metzner for smooth pipes for Power Law fluids. The findings in the study showed varying results, although the Yield Power Law model showed overall the most coinciding results with regards to friction pressure loss. The study also suggested correlation for pressure loss pipes with regards to the

different rheology models. In Figure 6 below, friction factor have been plotted for the different muds investigated in their studies.

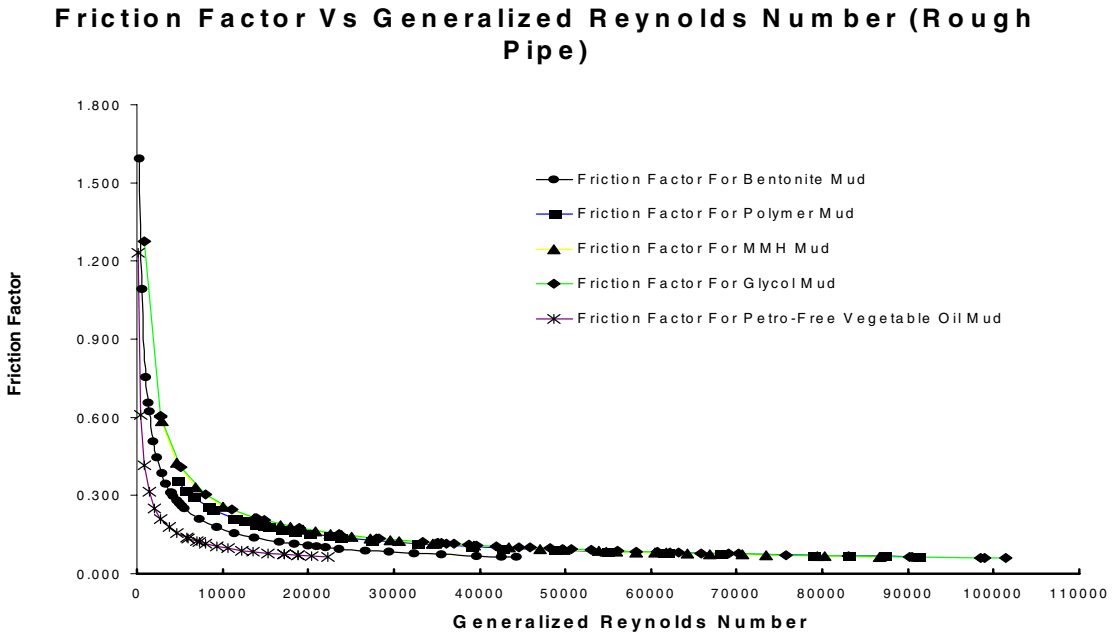

Figure 6: Friction factor vs Generalized reynolds number for rough pipes (Subramani and Azar 2000)

3.2 Fluid Flow Regime

On-set of turbulenc is a well known, but not yet fully understood phenomena in physics. For about 500 years ago Da Vinci illustrated the turbulence phenomena shown in Figure 7.

Figure 7: Da Vinci Scetch of turbulent fluid behaviour (McDonough 2007)

Assuming steady state flow, fluid flow can be classified into laminar or turbulent flow, governed by the Reynolds number, written as in Equation 3.6.

$$\mathrm{Re} = \frac{\rho v d}{\mu} \tag{3.6}$$

According to the basic studies, provided by Reynold, on-set of turbulence in a Newtonian fluid was dependent on four parameters: Pipe diameter, viscosity, flow velocity and density of the fluid (Bourgoyne et al 1991). Studies have proven that the transition from laminar to turbulent flow is also dependent on surface roughness and geometry changes in the flow path. The transition between laminar and turbulent flow does not occur sudden, but as a function of a transition range, before the flow eventually turn turbulent. In literature, laminar flow is defined as the area where the Reynolds number is less than 1800, with a transition zone between 1800-2100 and a fully developed turbulent flow at 2100, shown in Figure 8 (Skalle, 2011). Reynolds number for transition is established with regards to a slick pipe wall, hence roughness will decrease the transition area and the flow will turn turbulent at an earlier stage.

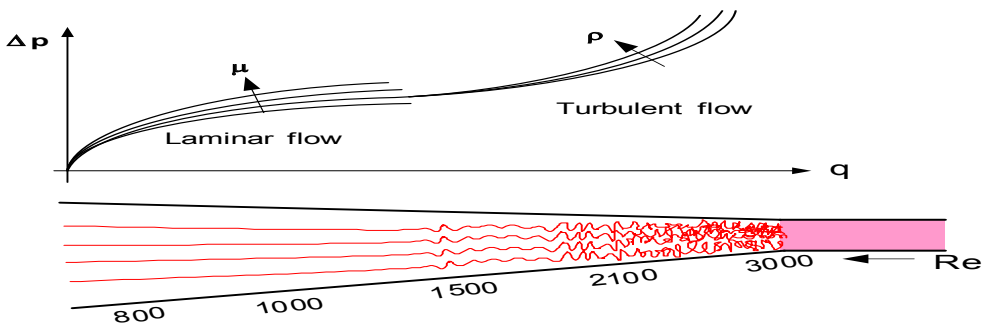

Figure 8: Transition from laminar to turbulent flow (Skalle 2011)

The easiest way in order to determine the flow regime is to plot experimentally recorded pressure drop versus flow rate, locate the area of transition and then calculate the critical Reynolds number. In the literature different formulas have been suggested for critical Reynolds number, dependent on the rheological model at hand. Metzner and Reed suggested the most standard model for Reynolds number for Power law fluids, utilized in the drilling industry, shown in Equation 3.7 (Skalle, 2011)

$$Re = \frac{{D_e}^n \bar{v}^{2-n} * \rho}{k(\frac{2n+1}{3n})^n * 12^{n-1}} \tag{3.7}$$

For the purpose of accurately estimation of the ECD and keep the wellbore pressure at a sufficient level, the flow regime has to be known. Were laminar movement of particles is defined as relative streamline movement over the adjacent layers in the fluid flow, turbulent flow will cause swirls and fluctuations in the velocity of the particles in the flow, varying from 1-20 % from the average velocity gradient in the pipe. As a result of the unsteady velocity gradient, resulting fluctuations in the pressure, temperature and concentration values will be experienced (White, 2008 and Bakker, 2002-2006). A turbulent flow regime will in most cases enhance the additional pressure drop significantly. By increasing the average velocity within a turbulent flow regime a quadric change in the pressure loss will be experienced $\Delta P \ \alpha V^{1.75}$ (White, 2008).

Due to the velocity fluctuations of the different fluid particles, eddies are formed. Eddies interact with each other, the flow and moves relative with the fluid direction. Eddies naturally forms due

to rotation, at the different boundary layers and/or at changes in the geometry. Eddies formed dissipates energy due to viscous shear in the fluid and eventually disappears (Finnemore and Franzini 2002). The phenomena of how much energy that is stored and how much energy which is dissipated in eddies, was described in detail by Kolmogorov in 1941. The process is described as an energy cascade, where large unstable eddies breaks up and transfer the stored energy to smaller eddies. When the eddies are small enough, a stable state is obtained where the molecular viscosity is effective in dissipating the kinetic energy into heat, hence energy is lost and a pressure drop experienced in the fluid. In Figure 9 Kolmogorov energy spectrum is explained where the large scale eddies contains the highest amount of energy. Within the Taylor scale the turbulence is isotropic, before small velocity scaled Kolmogorov eddies are formed where the energy is dissipated to heat. The fundamentals thought behind Kolmogorov energy spectrum is widely accepted in the literature, although lab research has proven that smaller eddies can transform energy to larger eddies (Bakker 2002-2006).

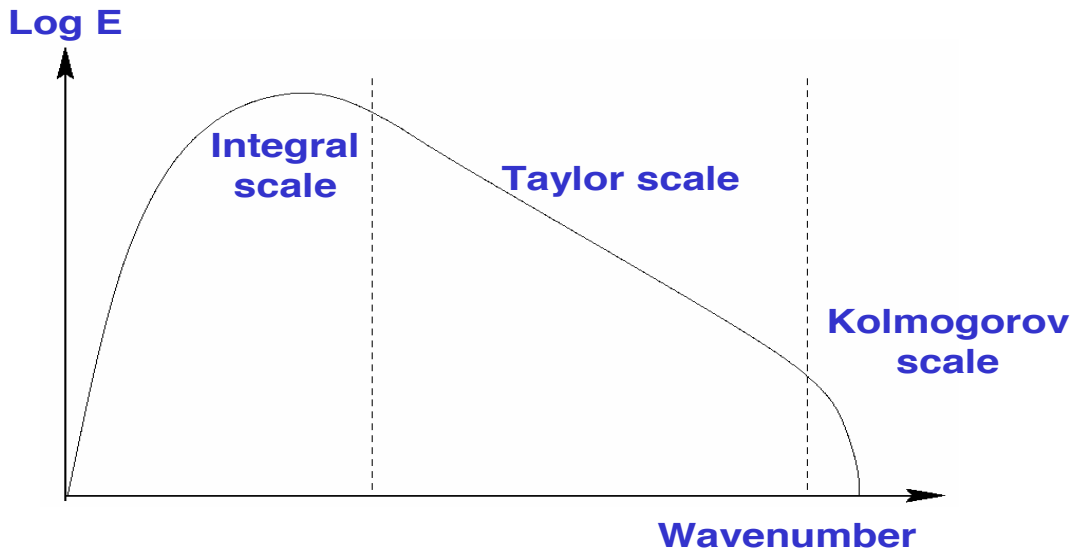

Figure 9: Energy stored in eddies compared to wavelenght of the eddies (Bakker 2002-2006)

3.3 Boundary Layers

Due to the non-slip effect between the fluid and the pipe wall a velocity profile is formed where the particles in contact with the wall is completely stopped. The effect of the non-slip effect propagates in the adjacent layers, causing highest velocity in the middle in order to maintain a stable mass flow rate. The difference in flow due to the viscous effect of the shear forces in the fluid is called boundary layer. According to Cengel and Cambala (2011) boundary layers can be divided into two regions within laminar flow; one where the viscous effect and the velocity change is high, and one where the frictional effect is negligible. Compared to the almost parabolic velocity profile in laminar flow, the velocity profile is more uniform with a sharper drop towards the pipe wall in turbulent flow, shown in Figure 10

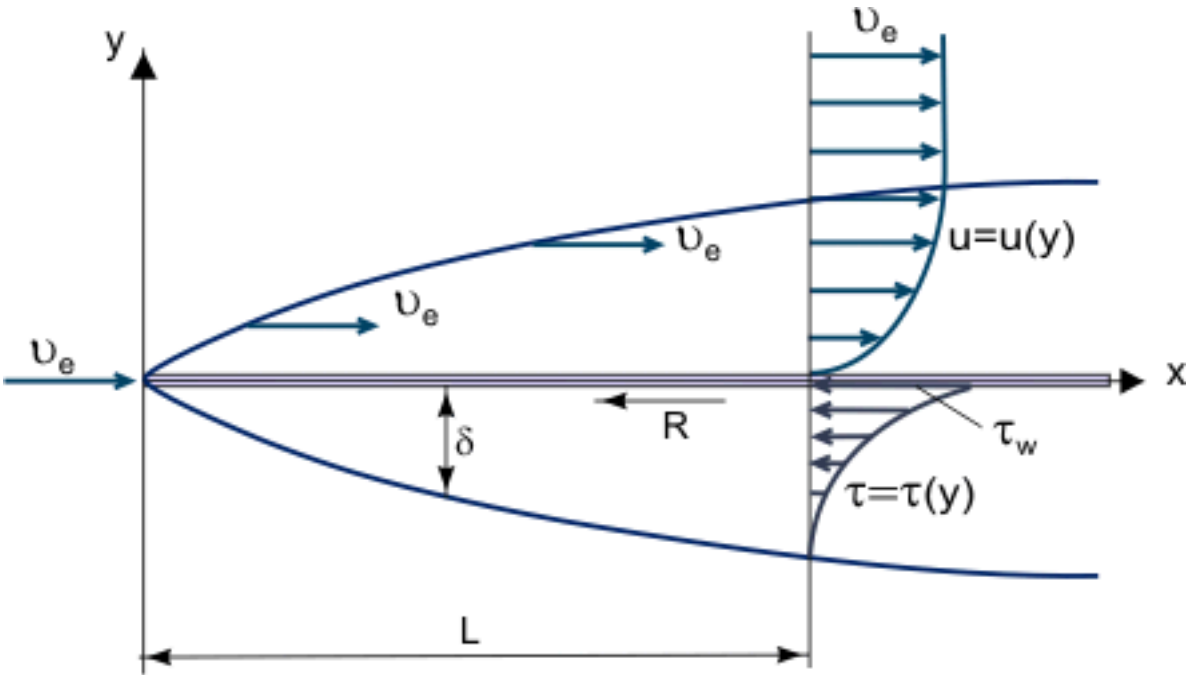

Figure 10: The development of boundary layer (δ) on a flat plate with the resulting velocity profile and shear stress with the wall (Epifanov, Thermopedia)

Dependent on the size of the sub-layers (δ) the velocity alters. The different flow velocites are shown in Figure 11 and is defined as the law of the wall in literature. Boundary layers in the turbulent regimes are divided in 4 regions; The layer closest to the wall is the viscous sublayer where the velocity profile is linear. The thickness of the sublayers are defined as proportional to the kinematic viscosity, but inversely proportional to the average velocity in the fluid flow. Next is the buffer layer where the turbulent flow is significant although the viscous effect is dominating. After the buffer layer, an overlap layer is following where the turbulence is higher, but still not governing the viscous forces. In the middle of the velocity profile is the outer layer where turbulent effect is dominating the viscous forces (McDonough, 2007).

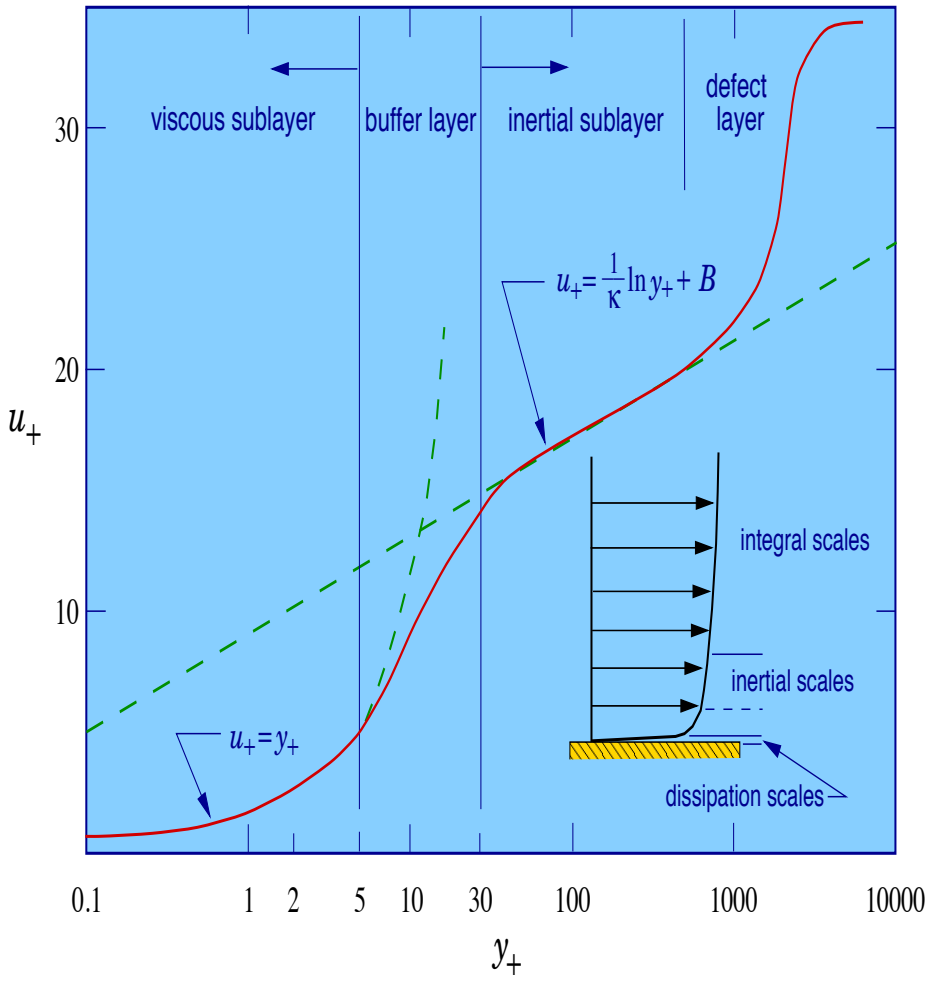

Figure 11: Velocity profile in the different sublayers (McDonough. 2007)

Turbulent flow is not yet fully understood and the best way to quantify the flow is to utilize experimental data in order to quantify numerical values for any constant. The viscous layer is according to Cengel and Cambala (2011) only approximately 1 % of the pipe diameter. However, due to propagation effect to the other adjecent layers, the characteristic of flow is highly determined to the other flow regions. Hence, a change in roughness in the surface pipe, has a higher impact in turbulent flow than in laminar flow with regard to friction factor.

3.4 Velocity Profile Development

The development of turbulent and laminar flow profiles is a key element in order to suggest correlations for friction factor and thus exact pressure drop in pipe flow. By shifting from a laminar to a turbulent flow profile the frictional pressure is enhanced due to the momentum transfer of heat because of in-orderly movement of particles and fluctuations in velocity. When turbulent flow is fully developed maximum friction factor in the system is reached (Cengel and Cambala, 2011).

Assuming steady flow, incompressible fluid and non-rotational movement of the fluid the governing equation suggested by Navier-Stoke Equation can be utilized in order to develop flow profiles for laminar and turbulent flow. Sletfjerding (1999) showed that the velocity can be divided in two components in turbulent flow and the Navier-Stoke Equation reduced to Equation 3.8

$$-\rho\overline{uv} + \mu\frac{dv}{dy} = \frac{1}{2}(y - r)\frac{dP}{dx} \tag{3.8}$$

The first component in Equation 3.8 is the Reynolds stress or turbulent stress. Reynolds stress is considered as shear between fluctuations in the fluid and a product of the slowing moving flow retarding faster moving slow, in accordance to the law of the wall (ref. Chapter 3.3). The second component in Equation 3.8 is the viscous stress, r is the radius of the pipe and y is the distance from the wall.

Based on Equation 3.8 researchers have tried to understand and create patterns for the turbulent flow, but due to the non-recognizable pattern in the Reynolds stress no one have succeeded completely. By utilizing boundary layer theory and empirical results as base, most authors have suggested dimensionless correlations, some summed up in the following chapter (Sletfjerding, 1999).

In laminar flow Reynolds stress is considered as zero and Equation 3.8 can be utilized to derived Hagen-Poiseulle velocity profile for flow in pipe shown in Equation 3.9

$$V(y) = -\frac{dP}{dx}\frac{1}{2\mu}\int_0^y (r - y)dy = -\frac{dP}{dx}\frac{1}{2\mu}(ry - \frac{1}{2}y^2) \tag{3.9}$$

3.5 Friction Factor Correlations

Dependent on predetermine parameters different friction factor correlation have been suggested. Due to the relative simple flow pattern the friction factor in the laminar region is considered linear and is for the annular space given in the equation 3.10

$$f_{laminar} = \frac{24}{Re} \tag{3.10}$$

Dependent on the base theory different authors have suggested correlations for friction factor in turbulent flow including roughness, velocity profile, fluid type, Reynolds number, Haalands number, Boundary layer and etc.

One of the most accepted equations for friction factor, incorporating roughness, related to fully developed turbulent flow is the Colebrook-White equation shown in Equation 4.15. The Colebrook-White equation was developed from the work and equations suggested by Nikuradse, Prandtl and Von Karman. Utilizing boundary layer theory Colebrook and White claimed that the roughness length (defined as the diameter of equivalent sand grains), dominate the effect of the viscous length (defined as small scale movement near the wall) in fully developed rough flow, shown in Equation 3.11 (Sletfjerding, 1999).

$$\frac{1}{f^{0,5}} = -4\log\left(\frac{\varepsilon/D}{3,7} + \frac{2.51}{Re\sqrt{f}}\right) \tag{3.11}$$

Developed from the Colebrook equations the Moody chart was drawn, where Darcys friction factor is drawn as a function of the relative roughness (ε/D) (Cengel and Cimbala 2010). In hydraulic friction loss a problem one have to keep in mind that literature separates between the Fanning friction factor and the Moody friction factor, ref Equation 3.12 (Skalle 2011).

$$f_M = \frac{4\tau_w}{\frac{1}{2}\rho\bar{v}^2} = 4f_F \tag{3.12}$$

Due to the time consuming process calculating the iterative Colebrook equation, many explicit correlations have been suggested. The majority of research papers published utilize the same governing equations, with altering explicit correlations for friction factor, dependent on the testing parameters and lab set-ups. In order to verify and compare previous published papers, some friction factor have been presented briefly following in the next sub-chapters. To compare the suggested correlations the universial pressure law, or the fanning friction factor have been utilized as a reference shown in Equation 3.13 and 3.14.

$$f = \frac{F_k}{AE_k} = \frac{2\pi r_w \Delta L * \tau_w}{A * \frac{1}{2}\rho v^2} = \frac{2\pi r_w \Delta L * \frac{r_w}{2}\frac{dp_f}{dL}}{A * \frac{1}{2}\rho v^2} = \frac{\pi d^2 \frac{dp_f}{de}\Delta L}{2\rho v^2 A} \text{L} \tag{3.13}$$

Solving for the frictional pressure drop in Equation 3.14

$$f = \frac{d_e}{2\rho\bar{v}^2} * \frac{dp_f}{dl} \tag{3.14}$$

3.5.1 Newtonian Fluids

Blasius suggested one of the oldest equations for friction factor correlations. The equation is shown in Equation 3.15. The equation assumes fully developed flow profile and Newtonian fluids, hence only wall roughness effect the friction factor, ref Chapter 3 (Skalle 2011).

$$\mathrm{f} = 0.079 * \mathrm{Re}^{-0.25} \tag{3.15}$$

Although Blasius suggested equation received acceptance it has been experimental proven that the approximation by Moore is more valid, shown in Equation 4.19 (Thermopedia) and (Skalle, 2011).

$$\mathrm{f} = 0.046 * \mathrm{Re}^{-0.20} \tag{3.16}$$

Contrary to Blasius and Moore, Chen suggested a correlation for Newtonian fluids, including roughness, diameter and Reynolds number (Shah 1990). Equation 3.17 is valid both in the turbulent region and in the transition zone.

$$\frac{1}{f^{0,5}} = 4\log\left(\frac{\varepsilon}{3.7065d} - \frac{5.0452}{Re} log\left[\frac{1}{2.8257}\frac{\varepsilon}{d}^{1.1098} + \frac{5.8506}{Re^{0.8981}}\right]\right) \tag{3.17}$$

3.5.2 Non-Newtonian Fluids

Metzner and Reed (1955) suggested their correlation with regard to a power law fluid and a smooth pipe shown in Equation 3.18.

$$f = a * N_{Re}^{-b}$$
$$a = \frac{logn + 3.93}{50} \tag{3.18}$$
$$b = \frac{1.75 - logn}{7}$$

Notable, Equation 3.18 is an explicit equation and in 1959 Dodge and Metzner suggested an iterative equation valid for power law fluids, shown in Equation 3.19

$$\frac{1}{f^{0,5}} = \frac{4}{n^{0,75}}\log Re\, f^{\left(1-\frac{n}{2}\right)} - \frac{0,4}{n^{1,2}} \tag{3.19}$$

Developed from the work by Dodge and Metzner, many correlations have been presented. In order to delineate the subchapter the rest of the correlations investigated in the thesis have been summed up in Equation 3.20, 3.21 and 3.22 and are obtained from the work provided by Scheid et al (2009).

Ostwald De Waele	$f = 0.060n^{0.462} * Re^{-0.233}$	(3.20)
Frank Shuh	$f = 0.110n^{0.616} * Re^{-0.287}$	(3.21)
Ellis and George	$f = 0.00454 * 0.645Re^{-0.70}$	(3.22)

Much of the experimental data focusing on tool joints correction have been published at the University of Oklahoma. If the fluid exceeded drag reducing parameters the authors have incorporated a correlation named the Shah Correlation. Shah experimental tested different fracturing fluids. The goal for the research was to obtain missing experimental data with regard to friction factor for fluids with larger flow index than $n \geq 0.4$. By developing the approach suggested by Dodge and Metzner (1959), Shah suggested Equation 3.23.

$$f = f_{\infty}(n) + A(n)Re^{-b(n)} \tag{3.23}$$

In his study Shah utilized a reference section making it eligible to calculate the induced friction due to roughness according to the equation 3.24.

$$\sigma = \left[\frac{(\Delta p_r - \Delta p_r)}{\Delta p_s}\right] * 100 \tag{3.24}$$

By plotting σ vs Reynolds number for the experimental data and curvefitting Equation 3.25 values could be obtained for the constants A, B and C, utilizing regression analysis .

$$\log(N_{Re}) = A + B(\sigma)^C \tag{3.25}$$

Once good values were achieved, A, B and C in Equation 3.23, were correlated with the fluids apparent viscosity at 170 seconds^{-1}. The last step in Shahs publications was to compare the experimental data with the predicted values from the model and express pipe roughness correction with regards to percent increased friction pressure shown in Figure 12

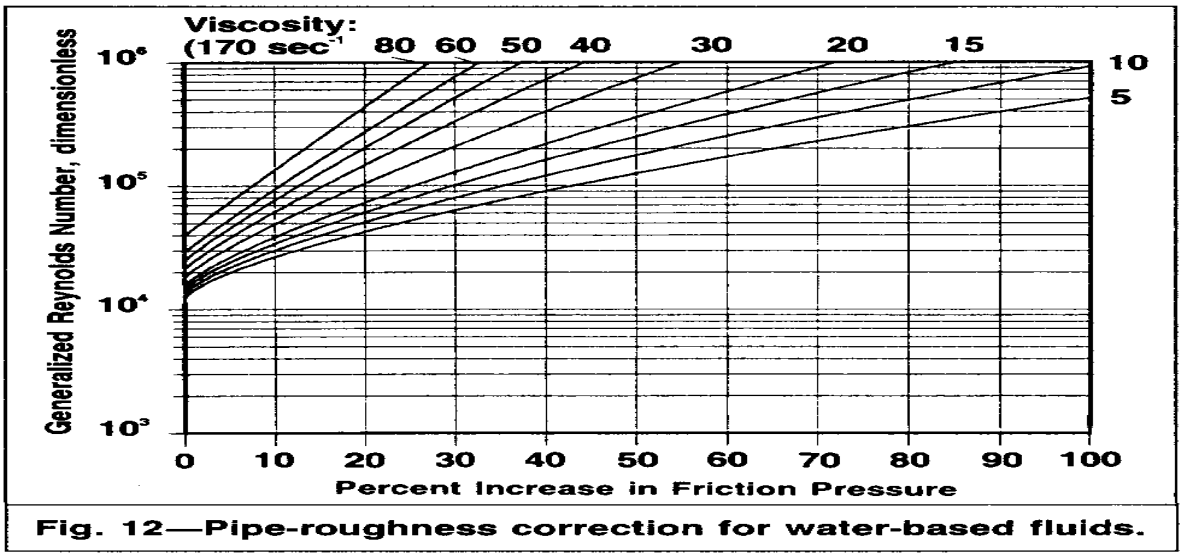

Figure 12: Percentage increase in frictional pressure due to changes in roughness suggested by Shah (1990)

3.6 Roughness

Roughness is a relative parameter and is defined as the thickness of the rough interface in the pipe wall. In order to be quantified as roughness, the roughness in the pipe has to govern the height of the viscous sub layer. Another definition of roughness was given in by Farshad and Rieke (2006) and was based on the experiments by Nikuradse. Roughness or ε, is defined as the mean height of sand grains, which are uniformly distributed, that will increase the hydraulic friction and thus the same pressure gradient behavior as the actual pipe.

Many experiments have been conducted, without success, for the purpose to quantify roughness by geometric factors. The reason for the failed attempts is that experiments have illustrated that the protrusions in the steel wall, which determine the degree of roughness is dependent on size, height, shape, and distribution. In other words, the characteristic geometry differs from material to material, and is too large in order to predetermine governing geometric factors. (Finnemore and Franzini 2002 and Farshad and Rieke 2006).

As there were no instruments in the past to measure the surface roughness directly, pipe roughness was calculated from the Moodys pipe roughness chart. Some of the main roughness is shown in Figure 13.

TABLE 1—MOODY'S (1994) SURFACE-ROUGHNESS ϵ VALUES OF COMMONLY USED PIPE WALL SURFACES

Pipe Absolute-Roughness Values		
Material	Absolute Roughness (in. x 10^{-3})	Absolute Roughness (μm or m x 10^{-6})
Drawn tubing	0.06	1.5
Commercial steel	1.8	46
Wrought iron	1.8	46
Asphalted cast iron	4.7	120
Galvanized iron	5.9	150
Cast iron	10.2	260
Wood stove	6.5–32.7	180–900
Concrete	10.9–109.1	300–3000
Riveted steel	32.7–327.3	900–9000

Figure 13: Moodys surface roughness (Farshad and Riekte 2006)

Nowadays, Measuring roughness with modernize equipment; Stylus instrument or Scanning Electron Instrument, the common way to quantify roughness is the average of 5 samples with regard to the peak to valley height (Sletfjerding, 1999).

3.7 Expansion and Contraction Effects

When fluid flows through a restriction, independent of type, a pressure drop occurs as a function of accelerated or decelerated of the velocity gradient and the change in internal diameter. Downstream the obstacle, the pressure will continue to drop until the point where velocity peaks and flow diameter is at the lowest, called Vena Contracta. According to Husveg (2007) Vena Contracta is typical found downstream an orifice to a axial distance of twice the diameter of the orifice. Downstream the orifice a recirculation zone is created, causing turbulence and corresponding energy dissipation of the fluid, due to the deceleration of the fluid, shown in Figure 14.. In order to regain flow condition as upstream the orifice. Some of the pressure is never regain due to the energy dissipation downstream Vena Contracta (van der Zande et al 1998). Energy dissipation is defined as the dynamic energy, which is transformed into heat, when a fluid flows through an orifice the resulting energy dissipation becomes as in Equation 3.26

$$\dot{E} = \Delta P_{perm} \times Q \tag{3.26}$$

Assuming that all turbulent energy in the area is transformed to heat the energy dissipation rate per unit mass is defined as Equation 3.27

$$\dot{\varepsilon} = \frac{\dot{E}}{m_{diss}} = \frac{\Delta P_{perm} \times Q}{\rho_c \times A_0 \times L_{diss}} = \frac{\Delta P_{perm} \times V_0}{\rho_c \times L_{diss}} \tag{3.27}$$

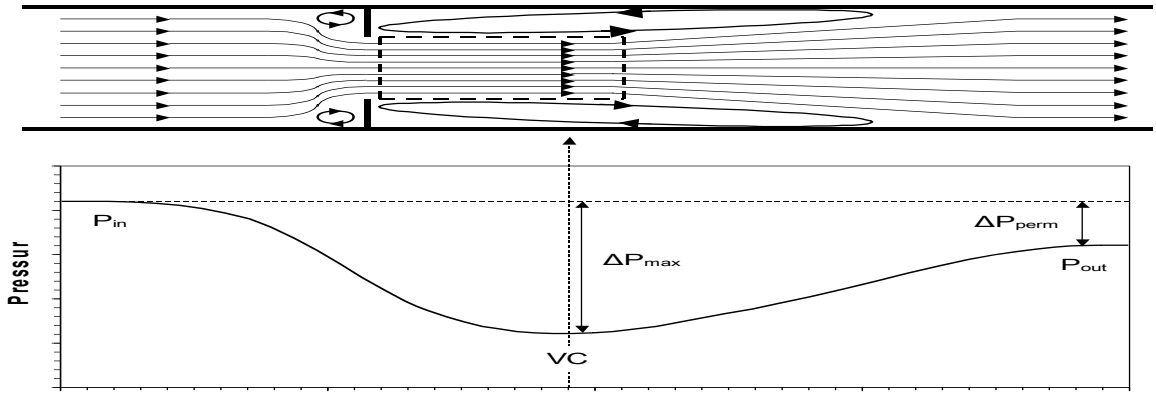

Figure 14: The effect of pressure loss down stream a obstacle in a wellbore. Vena Contracta illustrated where maximum pressure loss is experienced. (Husveg 2007)

As a result of decrease in flow geometry the velocity increase. Calcada et al (2012) measured the velocity increase, due to a tool joint contraction shown in Figure 15. Figure 15 is a result from the CFD analysis carried out before the experiments where conducted by Calcada et al. As the velocity profile illustrates turbulent regions, with velocity oscillations, is experienced in 0.5 m before flow is fully developed again. Due to the eddies formed and to ensure reliable results, the pressure sensors in Calcadas et al. experiments to be placed at least 0.5 meter after the tool joint.

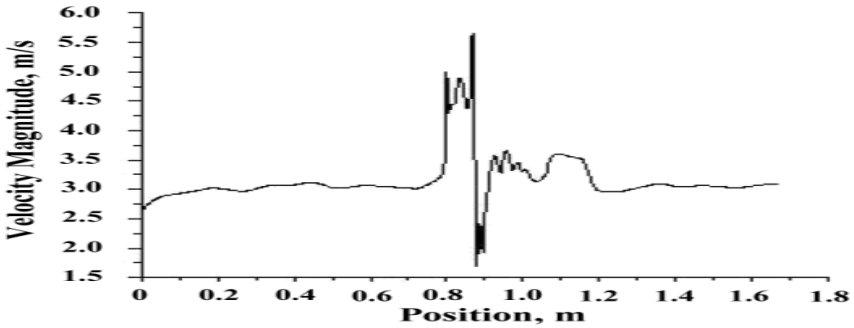

Figure 15: A typical flow profile when the fluid flows through a tool joint. The results was published in relation to the experiments conducted by Calcada et al (2012).

Both Husveg (2007) and van der Zande (1998) investigated the effect of droplet break up with regards to fluid flow through valves, but the general theory and thoughts can be transformed and utilized with regards to pressure loss due to tool joints.

Tool joints, such as valves, are a restriction to fluid flow, due to the decrease in geometry. Tool joints are designed in order to decrease the change in diameter and the restriction to fluid flow to a minimum. In theory, the lower angel of convergence and divergence, the resulting pressure drop decreases. The basic equations for the general loss coefficient due to restriction in fluid flow is derived from the Bernoulli and momentum equations and can be defined as Equation 3.28 (Jeong and Shah 2004)

$$F_e = \frac{(V_2 - V_1)^2}{2g_c} = \frac{{V_2}^2}{2g_c}\left(1 - \frac{A_2}{A_1}\right)^2 = K_e \frac{{V_2}^2}{2g_c} \qquad (3,.28)$$

In 1981 Crane published a paper, which experimental tested formulas for gradually contraction and expansion in drillpipes. The suggested formulas by Gibson was experimental tested by Crane and have been utilized as governing equations for singularity losses in the studies by Jeong and Shah (2004) and Enfis et al (2011). The paper suggested Equation 3.29 – 3.32 depending on the angle of convergence and divergence.

Interval $0° < \theta \leq 45$.

$$\mathrm{K_e} = 2.6\sin\frac{\theta}{2}(1 - \mathrm{R}^2)^2 \qquad (3.29)$$

$$\mathrm{K_c} = 0.8\sin\frac{\theta}{2}(1 - \mathrm{R}^2) \qquad (3.30)$$

Interval $45° < \theta \leq 180$.

$$\mathrm{K_c} = 0{,}5\sqrt{(1 - \mathrm{R}^2)\sin\frac{\theta}{2}} \qquad (3.31)$$

$$\mathrm{K_e} = (1 - \mathrm{R}^2)^2 \qquad (3.32)$$

The loss coefficient can be highly reduced by applying a cone geometry in the contraction and expanding zone. According to Finnermore and Franzini (2002) it is possible to obtainae friction coefficient as low as 0.10, given a conic geometry and a smooth surface. Finnermore and Franzini also embraced, through experimental studies, that the effect of a sudden enlargement exceeds the corresponding contraction diameter, due to forming of local eddies because of the diverging flow paths.

Another way to predict the contraction and expansion effect is to introduce a kinetic friction factor due to expansion and contraction. In 2008 Fester et al. experimental tested the effect of contractions in fluid flow of Newtonian and non-newtonian fluids with regards to three diameter ratios; 0.22, 0.5 and 0.85. Their study aimed to obtain reliable experimental data and find corresponding agreement with suggested semi-empirical models in the literature. By including a suggested kinetic correction factor, for psoudoplastic fluids, due to changes in the velocity downstream and upstream the restriction, Fester et al. expanded the availeble data for fluids when flowing through restrictions. Allthough it was proven that the loss coefficent only could be utilized for power law and newtonian fluids, if the Reynolds number acounts for the viscouse properties in the fluids.

3.8 Tool Joints

Tool joints are designed for the purpose to connect drill pipes. In order to provide a safe and strong connection the main body is designed to have an internal/external upset or both. Due to tool joints purpose of tightening and loosing at the connections numerous of times, tool joints are often design to withstand higher strength than the original tube. The necessity to increase the strength at the thread connection decreases the annular geometry, and hence could increase the hydraulic friction along the string (Ochua, 2006). Size and strength of tooljoints are the highly determine factor which determine the tolerance of torsion, i.e. higher tolerance to torsion, larger diameter OD and increased hydraulic friction.

In Figure 16 the different tool joint components have been explained according to the IADC manual. The Pin and Box is consider as the main body of the tool joint and is considered as the area of reduced annular clearance in the pipe. In the upper tool joint a tapered shoulder is shown in the end of the box, while in the second tool joint a squared tool joint is illustrated on the box. As Figure 16 indicate the hardfaced area is optional in the tool joint.

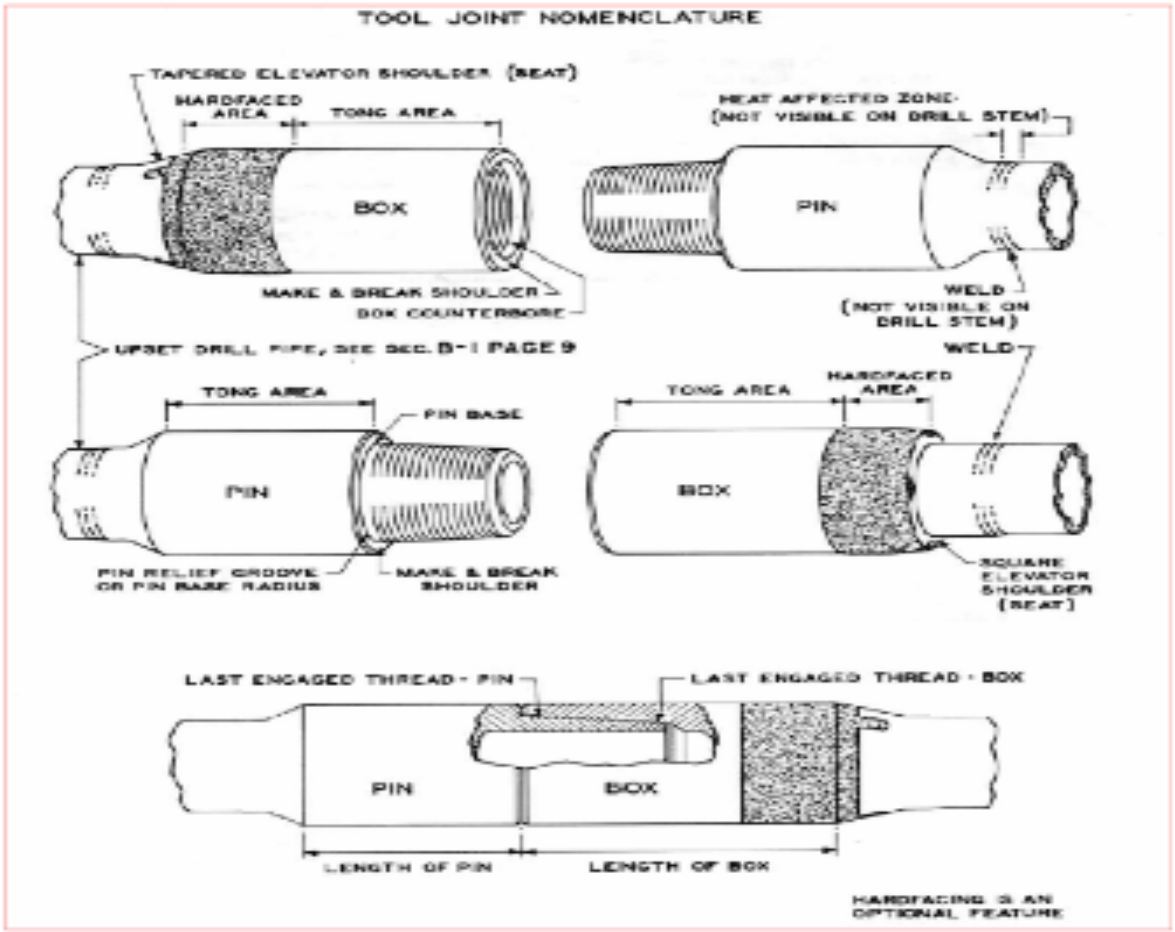

Figure 16: Tool joint nomenclature (Ochua, 2006)

3.9 Equivalent diameter

Most of the studies related to pressure drop have been carried out in circular pipes. In order to apply the equations derived, it is common to calculate an alternative conduit of the diameter of interest. Below some methods have been suggested (Bourgoyne 1991). In this thesis have only the three suggested equivalent diameter been evaluated due to the need of calculating fictional correlated velocity when applying other suggested diameters. In Appendix A, the theoretical results of applying the different suggested equivalent diameters.

1. The first equation is base on the hydraulic radius. The equivalent diameter in annulus is simply the difference between the inner diameter and the outer diameter of interest:

$$r_H = \frac{\pi(r_2^2 - r_1^2)}{2\pi(r_1 - r_2)} = \frac{d_2 - d_1}{4} \tag{3.33}$$

$$d_{e1} = 4r_H = d_2 - d_1 \tag{3.34}$$

2. The second and most popular proposed diameter equation is named the slot approximation and defines the effective equivalent diameter as:

$$d_{e2} = 0.816(d_2 - d_1) \tag{3.35}$$

Assuming $d_1/d_2 > 0{,}3$ equation have been proven to give accurate results.

3. The third suggested equivalent diameter suggested equivalent diameter is given in Equation 3.36 and was suggested by Lamb.

$$d_{e3} = \sqrt{{d_2}^2 + {d_1}^2 - \frac{{d_2}^2 - {d_1}^2}{\ln(\frac{d_2}{d_1})}} \tag{3.36}$$

4 Selected Models for Hydraulic Pressure Loss in Special Pipes

Dependent on predetermined assumptions, models have been suggested for off-set of turbulence and thus the resulting pressure drop, some more accurate than others. In order to calculate and use the fundamental equations some basic assumptions have to be made for the purpose to create a mathematical relation between fluid flow, pressure drop and rheology. Bourgoyne et al (1991) lists 5 basic assumptions:

- The drillstring placement is concentric in the hole.
- Drillstring rotation is neglected.
- The open hole is circular and with a known diameter.
- Incompressible fluid.
- The flow is isothermal.

In the following chapter have different pressure loss equations, applied in the calculated results been given for comparison and visualization purposes. The formulas chosen, for further investigation, have been published in the papers by Enfis et al. (2011) and Calcada et al. (2009). Both papers applies many of the same governing equations, with some modifications and alternations.

4.1 Laminar Flow Newtonian Fluid

The suggested equations below have been sampled from Bourgoyne et al (1991) for annular flow. In the derivation a relation between frictional pressure gradient, shear stress and radius have been attained using Newtons second law of motion. In order to correct for annular geometry and velocity the geometry diameter changes have to be accounted for. By multiplying the mean velocity ($\bar{v}$) with the annular cross sectional area, a correlation for annular geometry can be established

$$q = \pi(r_2^2 - r_1^2)\bar{v} \tag{4.1}$$

$$\frac{dp_f}{dL} = \frac{8\mu\bar{v}}{r_2^2 + r_1^2 - \frac{r_2^2 - r_1^2}{lnr_2/r_1}} \tag{4.2}$$

Bourgoyne et al 1991 have also suggested to derive the pressure loss in the annulus applying a slot flow principle and is according to the author accurate if d1 / d2 > 0,3.The derivation of the pressure loss in the annular section can be carried out, assuming a slot flow approximation, with the end result 4.3

$$\frac{\mathrm{dp_f}}{\mathrm{dL}} = \frac{12\mu\bar{v}}{(\mathrm{r_2} - \mathrm{r_1})^2} \tag{4.3}$$

4.2 Laminar flow Non-Newtonian Fluid

The approach to derive a laminar equation for pressure loss for a laminar fluid in annulus is the same for power law fluids as for Newtonian fluids and the derivation of the equations have not been included. Bourgoyne et al (1991) and Skalle (2011) have defined the equation for annular flow applying the power law model slightly different, both generate the same result shown in Equation 4.5 and 4.6.

$$\frac{dp}{dL} = \frac{2K\bar{v}^n(4+\frac{2}{n})^n}{(r_2 - r_1)^{n+1}} \tag{4.4}$$

$$\frac{dp}{dL} = 4K(\frac{12\bar{v}}{d_2 - d_1} * \frac{2n+1}{3n})^n * \frac{1}{d_2 - d_1} \tag{4.5}$$

Utilizing the apparent viscosity concept Reynolds number for power model can be defined as (Skalle 2011):

$$Re = \frac{{D_e}^n \bar{v}^{2-n} * \rho}{k(\frac{2n+1}{3n})^n * 12^{n-1}} \tag{4.6}$$

4.3 Turbulent Flow Newtonian Fluid and Non-Newtonian Fluids

As mentioned in Chapter 3, turbulent flow equations are based on empirical correlations, in order to correct for e.g. roughness. Bourgoyne et al (1991) have suggested the same formula for Newtonian fluids and Non-Newtonian fluids. Deriving the frictional pressure loss from the Fanning friction factor a relationship can be obtained. By comparing the area of conduit, kinetic energy and force exerted at the wall due to fluid movement the derivation for friction factor is summed in Equation 4.7

$$f = \frac{F_k}{AE_k} = \frac{2\pi r_w \Delta L * \tau_w}{A * \frac{1}{2}\rho v^2} = \frac{2\pi r_w \Delta L * \frac{r_w}{2}\frac{dp_f}{dL}}{A * \frac{1}{2}\rho v^2} = \frac{\pi d^2 \frac{dp_f}{de}\Delta L}{2\rho v^2 A} \text{L} \tag{4.7}$$

Solving for the frictional pressure drop:

$$f = \frac{d_e}{2\rho \bar{v}^2} * \frac{dp_f}{dl} \tag{4.8}$$

$$\Delta Pf = \frac{2f\rho \bar{v}^2}{de} * \Delta L \tag{4.9}$$

Substitution e.g. Moores 4.10 equation into Equation 4.9 an Equation for pressure loss can be obtained, shown in Equation 4.11

$$f = \frac{0.046}{Re^{0.20}} \tag{4.10}$$

$$\Delta \text{P} = \frac{0.092 * \rho^{0.8} * \bar{\text{v}}^{1.8} * \mu^{0.2} * L}{\text{De}^{1.2}} \tag{4.11}$$

4.4 Enfis et al. (2011) Tool Joint Correlation

Enfis et al (2011), hereby referred to as Enfis, defined numerical equations in order to calculate the pressure loss due to tool joints. The derivations are based on some basic assumptions:

- Steady state flow
- Incompressible flow
- Tool joint is horizontally placed
- Toll joint contraction and expansion are considerably

Applying the basic assumptions Enfis defined the pressure difference upstream and downstream the tool joints as in Equation 4.12.

$$\Delta P = \frac{\rho}{2} V_N{}^2 \left\{ K_c + K_e \left(\frac{A_N}{A_W}\right)^2 \right\} + \Delta P_{f1} \tag{4.12}$$

V_N is defined as the mean fluid viscosity in the narrow zone. Due to the missing measurement in the narrow zone the overall fluid velocity have been applied in the calculation.

The contraction and expansion coefficient are strongly dependent if the tool joints are squared or tapered. Based on Cranes equations, K_c and K_e was defined as in Equation 4.13 and 4.24

$$K_e = (1 - \mathrm{R}^2) \tag{4.13}$$

$$K_c = 0{,}5 \sqrt{(1 - \mathrm{R}^2) \sin \frac{\theta}{2}} \tag{4.14}$$

The pressure loss, which is not included in the contraction or expansion effects is dependent on the wall shear stress and is the interaction between the drilling mud component and the drillstring and annulus pipe wall. The additional pressure loss is divided between the narrow zone and the wide zone when passing the tool joints shown in Equation 4.15.

$$\Delta P_{f1} = \Delta P_N + \Delta P_W = \frac{4\tau_{w,N} L_N}{D_{hyd,N}} + \frac{4\tau_{w,W} L_W}{D_{hyd,W}} \tag{4.15}$$

The experiments conducted only utilized Power Law fluids, hence wall shear stress in the laminar region was defined as in Equation 4.16

$$\tau_w = K \left[\frac{12V}{D_{hyd}} \left(\frac{2n+1}{3n} \right) \right]^n \tag{4.16}$$

While the shear stress in the turbulent flow region defined as:

$$\tau_w = \frac{1}{2} f \rho V^2 \tag{4.17}$$

Friction factor was found by utilizing water in the reference section in the lab set up. Enfis found that friction factor was approximately the same as smooth pipe in his test section. For Non-Newtonian fluids Enfis applied the Shah correlation for drag reducing fluids presented in Equation 4.18.

$$f = f_\infty(n) + A(n) Re^{-b(n)} \tag{4.18}$$

If the fluid is without drag reduction properties the Dodge and Metzner equation was utilized in the form of Equation 4.19.

$$\frac{1}{f^{0,5}} = \frac{4}{n^{0,75}} \log Re\, f^{\left(1-\frac{n}{2}\right)} - \frac{0,4}{n^{1,2}} \tag{4.19}$$

4.5 Calcade et al. (2012) Tool Joint Correlation

Calcada et al (2012), hereby referred to as Calcada, based their study on Scheid et al (2011 and 2009). They investigated the effect of hydraulic friction on internal and external flow, with regards to specific muds in order to gain a data base for the most applied muds in the Brazilian drilling industry. The study concluded that the most exact friction factor utilizing water based muds were Equation 4.20-4.22 suggested by Ostwald de Waele, Frank Shuh and Ellis and George.

$$\mathrm{f} = 0.060\mathrm{n}^{0.462} * \mathrm{Re}^{-0.233} \tag{4.20}$$

$$\mathrm{f} = 0.110\mathrm{n}^{0.616} * \mathrm{Re}^{-0.287} \tag{4.21}$$

$$\mathrm{f} = 0.00454 * 0.645\mathrm{Re}^{-0.70} \tag{4.22}$$

The approach by Calcada is almost similar to Enfis approach besides some parts. The equation for the tool joint coefficient in the enlargement zone, where Calcada estimate the enlargement coefficient as Equation. 4.23

$$K_e = R(1 - \mathrm{R}^2) \tag{4.23}$$

Instead of applying Equation 4.12 Calcada simply multiply the enlargement and contraction coefficient by Equation 4.24 and adds up the contributions utilizing the universal pressure law.

$$P_{c,e} = F_{c,e} * \rho$$

$$F_{c,e} = K_{c,e} * \frac{V_1}{2} \tag{4.24}$$

The difference between Enfis and and Calcadas suggested models has been visualized in Chapter 4.4. For further research have only Ostwald de Waele, herby Ostwald, and Ellis and George Correlation (Equation 4.20 and 4.22) have been applied.

4.6 Theoretical Results Tool Joint Correlation

On the basis of the framework conditions, different mathematical models and correlations are more suitable than other. In the following subchapter the effect of the investigated mathematical models have been highlighted. Due to the fact that the suggested models by Calcada and Enfis applies different friction factor correlations and hydraulic diameter, they have been extracted and visualized in Appendix A separately.

Plotting the effect of tool joint correction, suggested by Enfis and Calcada, the differences in the end result was visualized in Figure 17. For visualization purposes some assumptions have been made:

- If the fluid was applying drag reduction properties Enfis applied the Shah correlation. Due to the time consuming process of calculating and curve fitting the results this has been neglected and Dodge and Metzner suggested friction factor has been applied.
- Both Ellis and George and Ostwald de Waele friction factor correlation have been investigated for Calcada.
- Turbulent pressure has been plotted where the turbulent pressure loss exceeds the laminar.
- n and K are assumed to be the same as the medium viscosity mud in the experiments.
- Tool joint effect is equivalent in the turbulent and the laminar section.

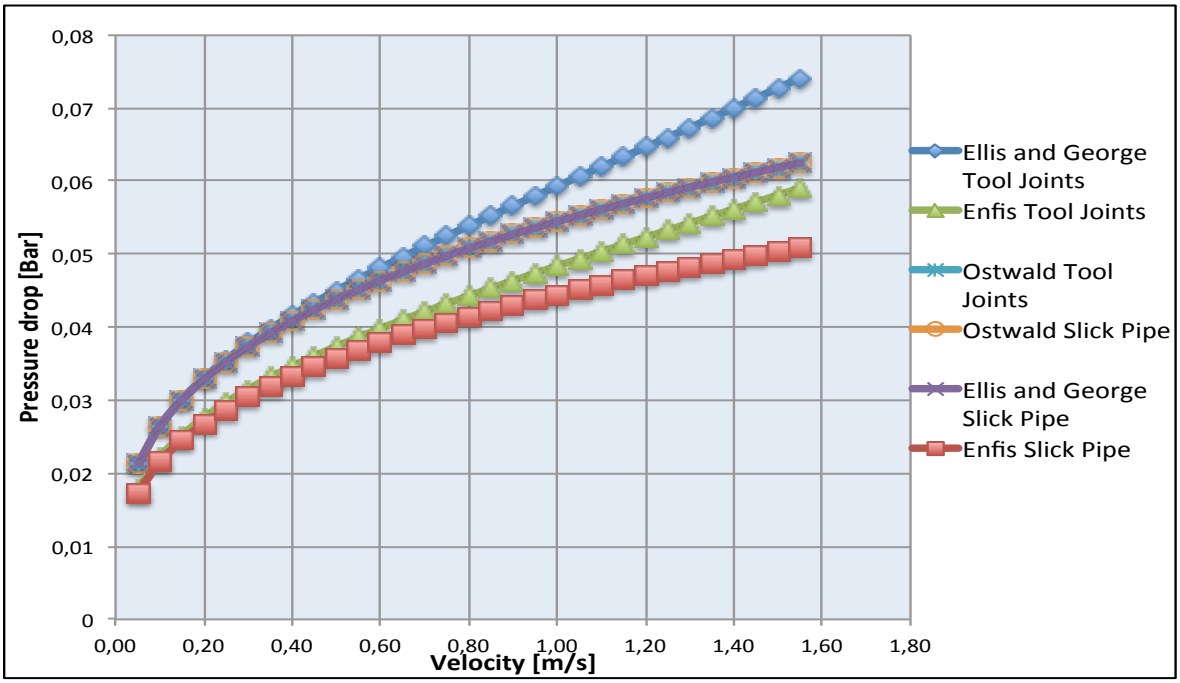

Figure 17: Calculated results of Enfis. and Calcadas suggested approaches for tool joint correction for a medium viscosity mud. Tool joint effect included in both the laminar and the turbulent section

Studying Figure 17 some main obeservation can be highlighted. Due to the tool joint effect pressure loss is enhanced with 17.79% by Ellis and George correlation and Ostwald, while the pressure loss for Enfis suggested approach was 15.3%.

Figure 18 the same assumptions have been made as in Figure 17, except tool joint effect is only assumed to effect in the turbulent flow regime. By only including tool joint in the turbulent section, both Calcada and Enfis suggested approaches implies turbulent flow regimes at the highest flow rates.

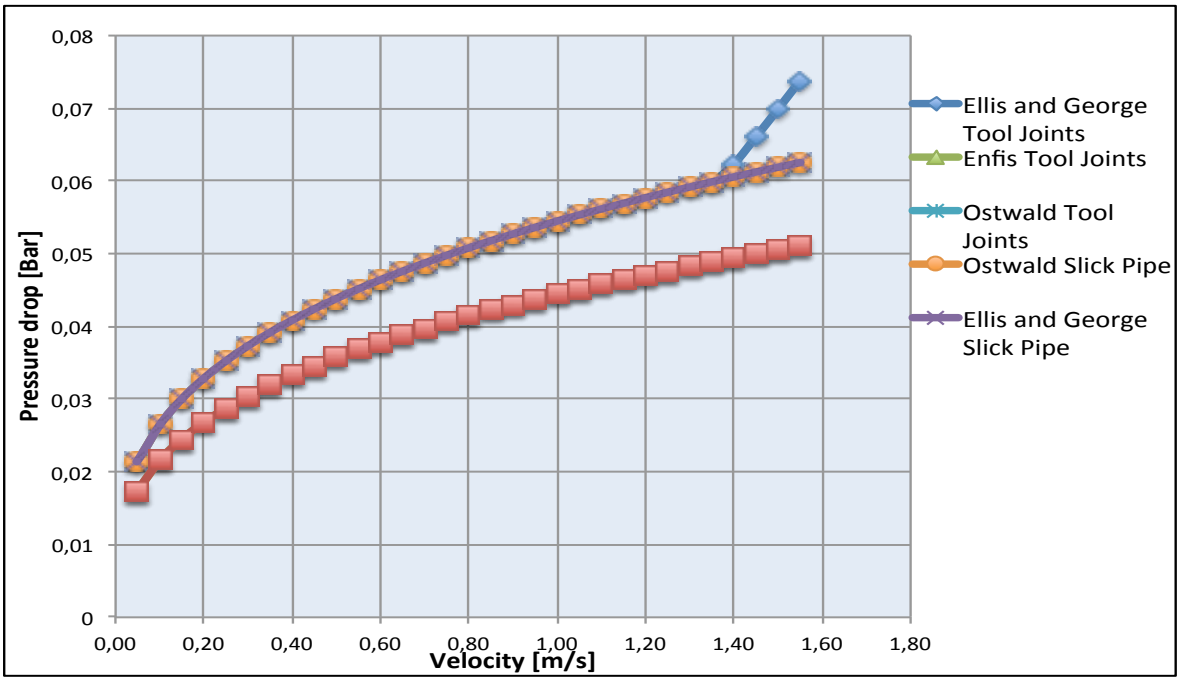

Figure 18: Calculated results of Enfis. and Calcadas suggested approaches for tool joint correction for a medium viscosity mud. Tool joint effect only included in the turbulent region.

Based on older papers, which suggest no tool joint correction in the laminar region ,Figure 18 have been applied for comparison reasons for the medium mud. The same calculation approach have been appied for the low viscosity mud for comparison reasons.

In order to gain a deeper understanding of the calculated results ,a summary of the differences in the models is given:

- Calcada applies the same share for the narrow as for the wide zone. Enfis applies Equation 4.25, which differentiate between the narrow and wide diameter. The difference of applying a narrow diameter in the tool joint section is decreased overall pressure loss in the calculations. On the other hand, the effect would probably the small contribution of applying a smaller diameter in in the short tool joint section not make any difference at all in a real drilling situation.

$$\Delta P_{f1} = \Delta P_N + \Delta P_W = \frac{4\tau_{w,N} L_N}{D_{hyd,N}} + \frac{4\tau_{w,W} L_W}{D_{hyd,W}} \qquad (4.25)$$

- In Calcada and Enfis study, the estimation of hydraulic diameter differs. Calcada applies the slot approximation when estimating the hydraulic diameter, while Enfis applies the normal hydraulic diameter, which decreases the estimated pressure loss compared to Calcada.

- The choice of Friction Factor correlation is different. Calcada investigates the effect by applying different correlations, while Enfis applies Dodge and Metzner or the Shah correlation.

5 Experimental Investigation

This chapter includes the experimental setup, the process control, signal evaluation and an error analysis an error analysis. At the end of the chapter the experimental results are given. For presentation purposes the results have not been discussed in this chapter. Pictures of the real lab set up have been included in Appendix C

5.1 Test Matrix

In total four different combinations of the inner steel pipe were, planned utilizing one Newtonian fluid (water for calibration) and three Non-Newtonian fluids. During each test it was planned to vary the pump speed from 1 to 25 HZ in steps of one, but due to the viscosity this was altered fto 1-45Hz for all the viscosities except the high viscosity fluid in order to cover a greater range of Reynolds numbers. To visualize the equivalent effect of roughness and/or obstacles in a well an additional metal mesh was incorporated at the same distance as the first tool joint downstream the pipe inlet. The planned test matrix is shown in Table 1. All tests was carried out at least twice.

Table 1: Planned test matrix

Inner pipe configuration	Newtonian fluid	Low viscosity	Medium Viscosity	High Viscosity
No tool joints	0-25Hz	0-45Hz	0-45Hz	0-25Hz
Tool joints	0-25Hz	0-45Hz	0-45Hz	0-25Hz
Additional Roughness 1	-	0-45Hz	0-45Hz	-
Additional Roughness 2	-	0-45Hz	0-45Hz	-
Total number of planned tests, including repetitions				24

5.2 Test Loop and Process Control

In order to experimental test the incorporation of tool joints in the string a experimental set up was built at NTNU consisting of; a centrifugal pump, outer steel pipe, inner steel pipe, a 200 liter mud tank, a flow meter and one differential pressure transducer. Tool dimension have been given in Table 2 and the test set up schematics in Figure 19.

Table 2: Test loop components

Component	Type/Dimension	
Pump	Wangen KL30S helical rotor screw pump	
Flow meter	RS Combined Liquid Flow. Stock No-257-026	
Differential pressure transmitter	FCX Series Differential Pressure Transmitter	
Component	Length	Diameter (mm)
Outer steel pipe	6 m	54 mm (Inner)
Inner steel pipe	5,90 m	25 mm (Outer)
Distance pressure measurements points	4,36 m	

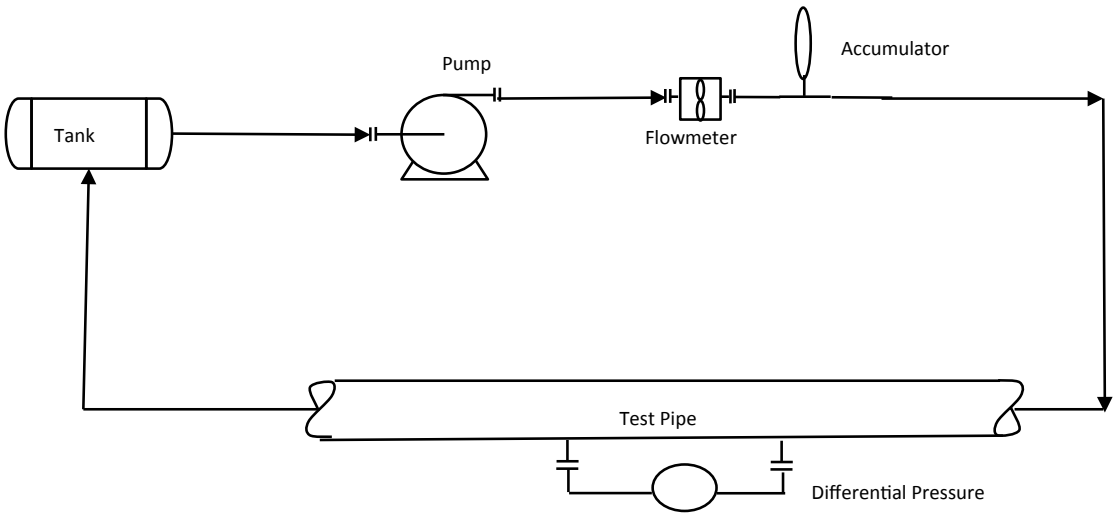

Figure 19: Test Loop Schematics

In order to test the different inner configuration the outer steel pipe had to be stripped and reassembled. By reassembling the outer configuration the risk of changing the outer environment, and thus introduce errors in the results present.

5.3 Test Loop Components

Downstream the tank the first component is a Wangen KL30S helical rotor screw pump, which was utilized due to low pulsation. From the pump a flow meter of the type RS Combined Liquid Flow. Stock No-257-026 is connected. The relative simple flow meter has an accuracy specification of (plus/minus) 2 %. Before the flow meter was utilized, a simple calibration procedure was carried out to ensure the accuracy were the results are included in Chapter 5.3.4. The predesigned conversion factor from electric signal to fluid flow rate was 1 V = 10 l/min, creating a linear relationship given in Equation 5.1

$$y = ax - b \tag{5.1}$$

- y is the fluid flow in l/min
- a is slope factor, converting volt to l/min, in the electrical measured input and has to be confirmed by calibrations
- x is the flow meter input in Volts
- b is the resistance in the wiriring or the offset in the measurements and has a value of 2 V

In the start up phase of the experiments, two Druck PTX 1400 pressure sensors were utilizedAnalysis of the test data concluded that the pressure sensors did not provide accurate and reliable results. To ensure the accuracy of the experiments the pressure sensors were changed to a FCX Series Differential Pressure Transmitter.

The pressure sensors, was as the flow meter, electrical and the output signals had to be converted from volts to bar by the linear relationship in Equation 5.2

$$y = ax - b \tag{5.2}$$

- y is pressure measurement in bar and have a range from 0 to 0,35 bar
- a is defined as the slope factor, converting volt to bar.

$$\mathrm{a} = \frac{0{,}35\mathrm{Bar}}{10V - 2V} \tag{5.3}$$

- x is the pressure input in Volts
- b is resistance in the wiring and equivalent to 2V.The value have been confirmed by measuring the resistance in the wiring applying a multimeter

In order to ensure fully developed flow and accurate pressure readings, sufficient length between the first pressure measuring point from the entrance important. In the study provided by Calcada flow patterns were simulated utilizing CFD and it was determine that 0.5 meter was sufficient length to neglect disturbance in their set up. To be absolutely sure, the first pressure sensors were placed 1,44 meter from the entrance of the pipe.

To transfer the info into readable data, the sensors were connected through a data input called NI USB-6009, which feed the graphical software, called Labview by National Instruments. Labview is a relative simple way in order to feed the input data and write the desired output data. Figure 20 shows the user interface, while Figure 21 show the block diagram of the Labview code.

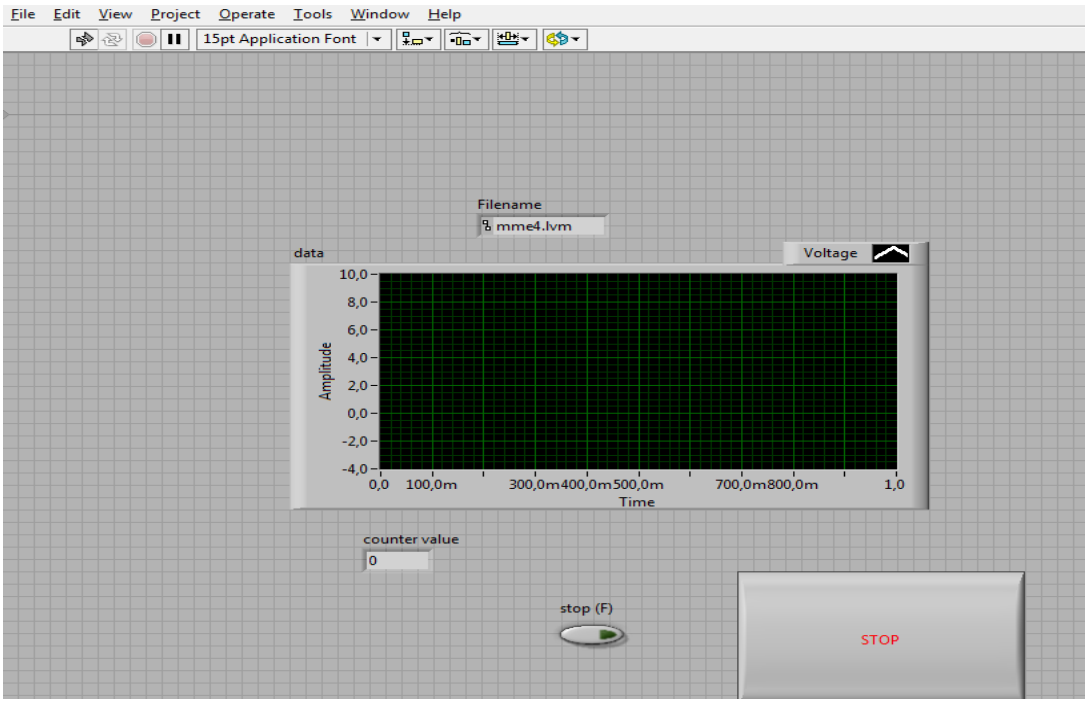

Figure 20: Labview user interface (Mme 2013)

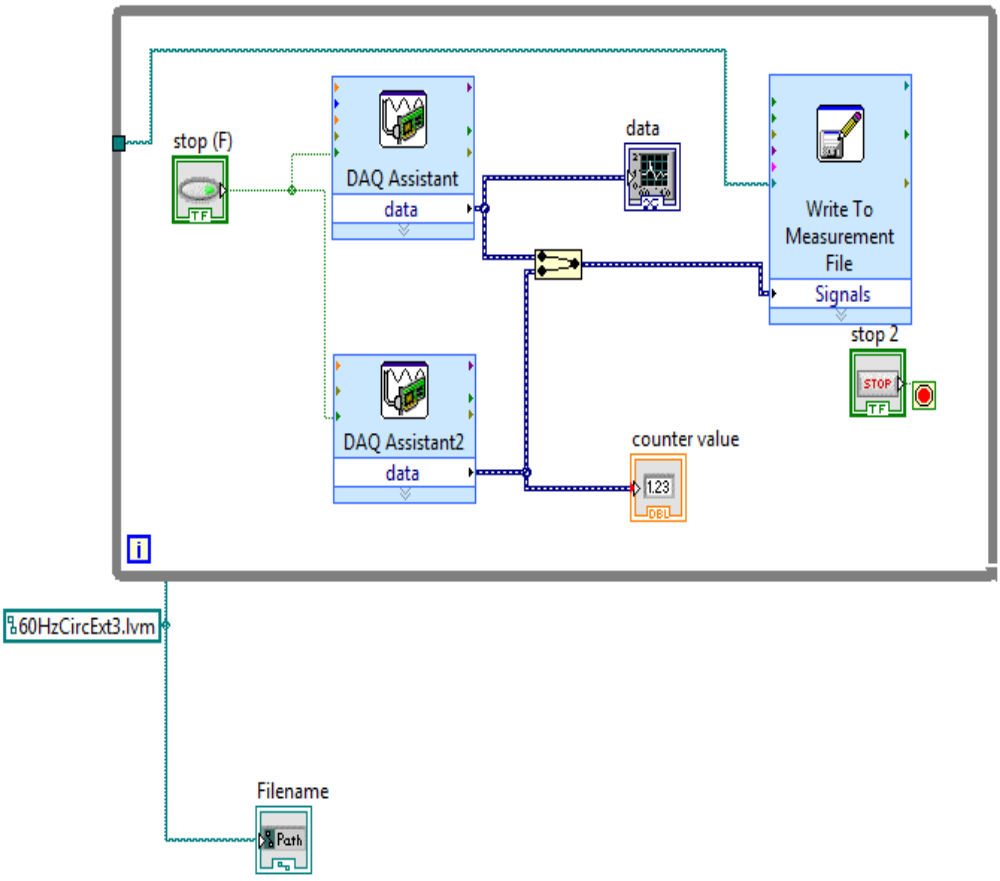

Figure 21: Labview input code in labview (Mme 2013)

5.3.1 Tool Joints and additional Roughness Details

The tool joints utilized in the experiment set-up were made of POM (Polyoksymetylen). POM is often utilized in pumps, isolation in electrical applications and gears. Surface roughness can in theory be neglected when utilizing plastic. By performing experiments with an additional rough obstacle, the tool joints effect can be pin pointed. The measurements of the tool joint components are summarized in Table 3, while Figure 22 shows a relative scaled figure.

Table 3: Test loop components

Component	Measurments
Outer pipe inner diameter	5.40 cm
Inner pipe outer diameter	2.5 cm
L_1	1.54 cm
L_1 angle	36°
Box+Pin hight	3.50 cm
Box+Pin length	5.00 cm
L_2	0.69 cm
L_2 angle	18°
Total length	7.23 cm

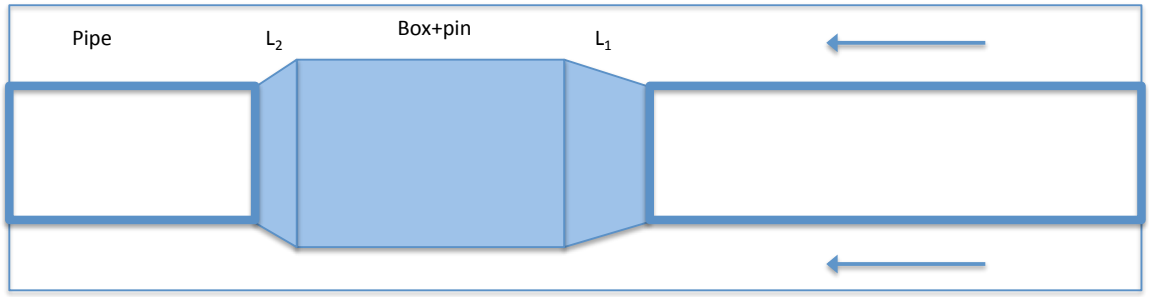

Figure 22: Relative scaled figure of the inner pipe, tool joint and casing

Three tool joints were included in the string with 1.1 meter distance between the center of each tool joint. The first pressure transducer was placed in a distance of 1.46 meters in order to ensure full developed flow, while the second pressure transducer was distanced 1.1 meter from the center of the last tool joint and 0.5 meter from the outlet in order to neglect outlet effects, shown Figure 23.

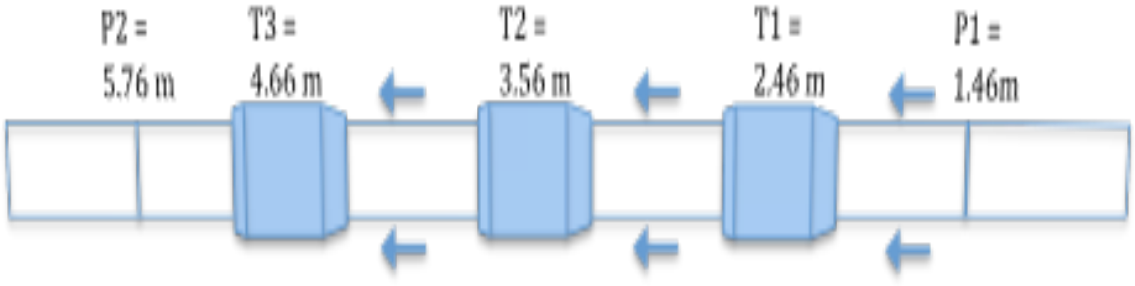

Figure 23: Tool joint steel pipe

The additional rough obstruction in the string were place at the same distance as the first tool joint T1, downstream the mud pump. By placing the additional roughness in the string so far from the second pressure point allowed for sufficient entrance length for the flow to settle some degree. The additional roughness in the string was cut out of a metal mesh and attached in 3 and 5 rounds shown in Figure 24.

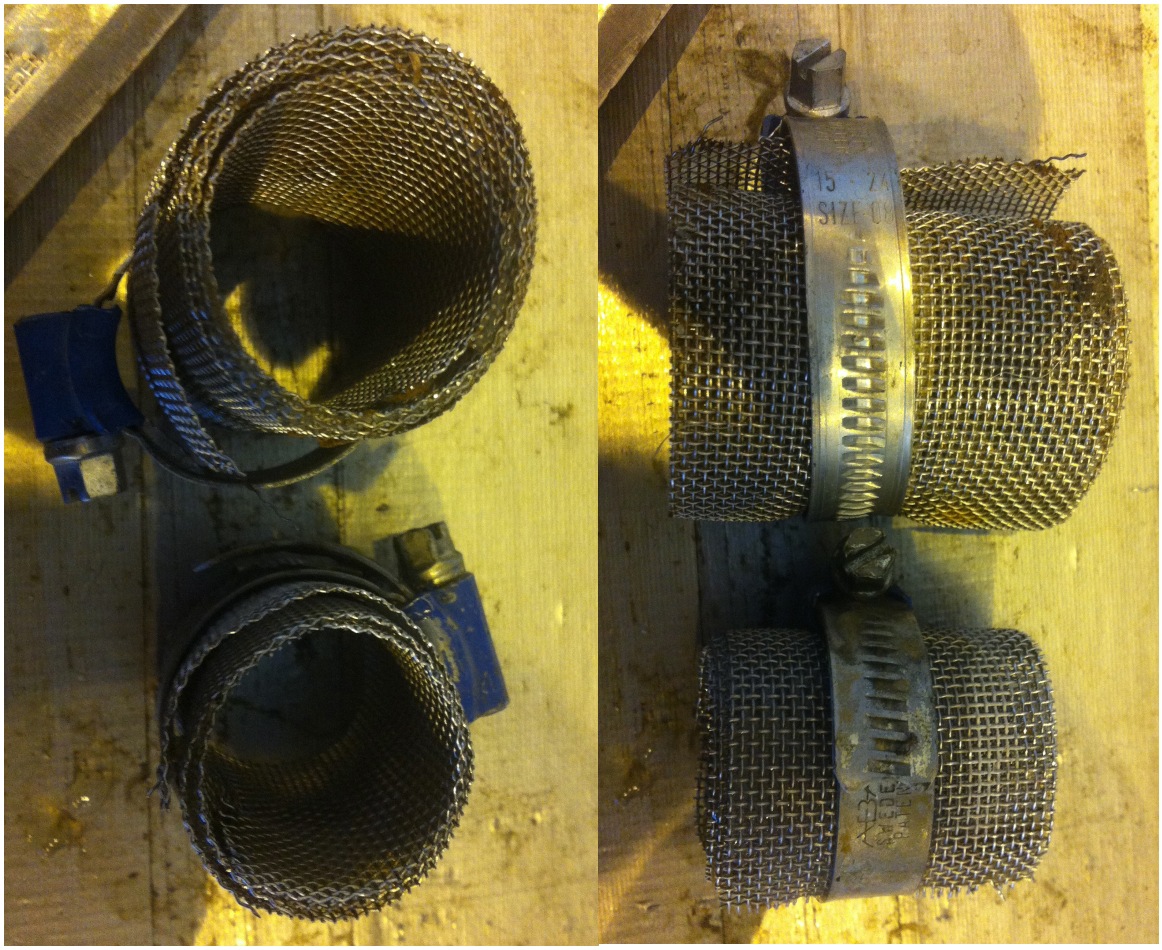

Figure 24: Additional rough obstacle in the string.

5.3.2 Experimental Procedure

The procedure utilized in the laboratory set up was, as most experimental researches, a product of trial and error. From the start of the experiments all components have been changed, one by one, due to uncertainty or errors. In the end set-up a procedure was created. When utilizing the highest viscosity mud the flow rate was not as high as for the two other muds due to the risk of destruction of the flow meter.

Preparations prior to commencement of the experiments:

- The configuration of the inner steel pipe was chosen
- The mud pump was started and circulated in order to free the system of air bubbles. The line from the pipe to the pressure transducer was disconnected at the apertures side. The line was flushed until all air bubbles were circulated out. When utilizing mud as base fluid this procedure was carried out prior to the mixing to ensure that no mud was in connection with the pressure transducer.

Mixing of mud:

- When mud was utilized in the experiments at least 4 hours of mixing was necessary prior to the experiments.
- The pump was started prior to mixing in order to ensure circulation. The pump was kept at a sufficient high circulation rate to prevent flocculated mud to get stuck in the flow meter, pressure transducer and parts of the pipe. Also by providing a higher circulation rate the mixing time of the mud is decreased.
- The mud pump was not stopped at any time after the Xanthan mud was mixed into the water to ensure that settling did not occur.
- The mud was considered finished when no visible flocculation could be registered in the flow meter.

Sampling:

- The pump rate was varied from 0-45Hz in steps of 1Hz when utilizing mud as a base fluid, and 0-25Hz in steps of 1Hz when utilizing water.
- At each flow rate sampling was conducted for at least 30 seconds with 100 samplings per second, creating in total at least 3000 samplings at each flow rate.
- When changing the flow rate, the system was circulated at least 1 minute for stabilization purposes, before registration at the new flow rate was conducted.
- The viscosity was measured prior to and at each 5th flow rate at each experiments. Due to the stability of the Xanthan Gum there was more or less no discrepancy in the measurement.
- Sampling started at the highest flow rate moving downwards before going up again at the second sampling run.
- When in doubt of the accuracy of the measurements the inner configuration was altered, new testing conducted before a the inner configuration was changed back and security tested.

5.3.3 Data Processing and Signal Evaluation

A major problem to overcome in the data processing, to provide accurate results, was to create a filter for the purpose to cancel noise and disturbance in the system. To compare with existing models and thus provide exact results one absolute value for each flow rate should be obtained.

The pump applied in the experimental set-up is a helical screw pump with low pulsation, but there is no such thing in the world as a pulse free pump. The simplest way in order to cancel out noise in the system is to decrease the sampling rate. Decreasing the sampling rate is a primitive way to cancel out undesirable noise, but the sampling rate should be adjusted to utilize the knowledge of known frequency in the signal, hence neglect the undesirable frequency noise. In other words, by decreasing the sampling rate a better signal to noise ratio can be obtained.

In order to create a filter, which did not exclude relevant data nor included the strong unsignificant amplitudes and peaks, the type of noise disturbance has to be determined. In the following figures the output signals from the flow meter and pressure sensor have been utilized simply to illustrate how the created filter works. It has to be emphasized that the noise disturbance is more uniform in the flow meter than in the pressure pulse and just simply averaging the output readings from the flow meter would not create large discrepancy from the filter results. The entire matlab script is given in Appendix B.

The disturbance in the testing equipment is varying depending on:

- Output signal from the pressure transducer or the flow meter
- The flow rate
- Vibration in the system
- Fluid composition

When increasing the pump rate, pulses generated from the pump strongly decreases. This makes the output signal clearer and less filtering of the data is necessary. By setting the pump to 14Hz the flow generates an output signal varying around 6.4 Volts (30-40l/min), shown in Figure 25.

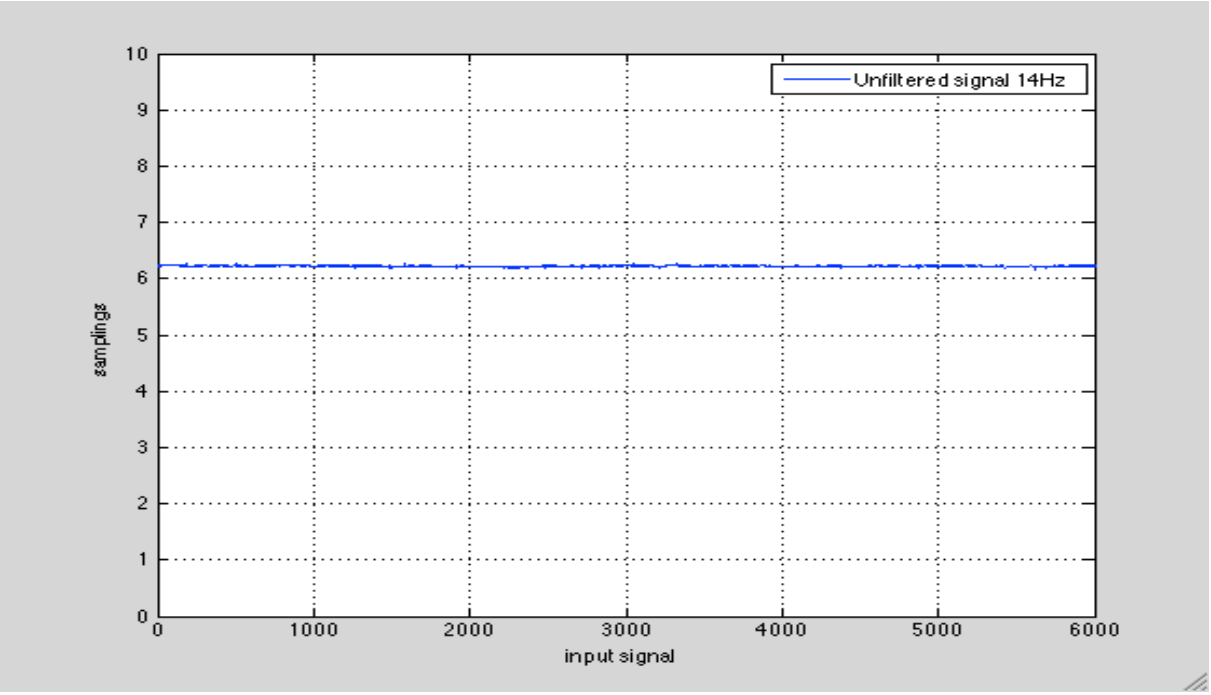

Figure 25: Signal output from the flow meter at 14 Hz speed in the pump. No filter applied

The relative stable signal output from the flowmeter and a system in steady state would indicate a relative stable pressure output. As the plot in Figure 26 shows, this is not the reality. The pressure transducer applied is extremely sensitive and the smallest shift in flow rate or outer environment can create disturbance.

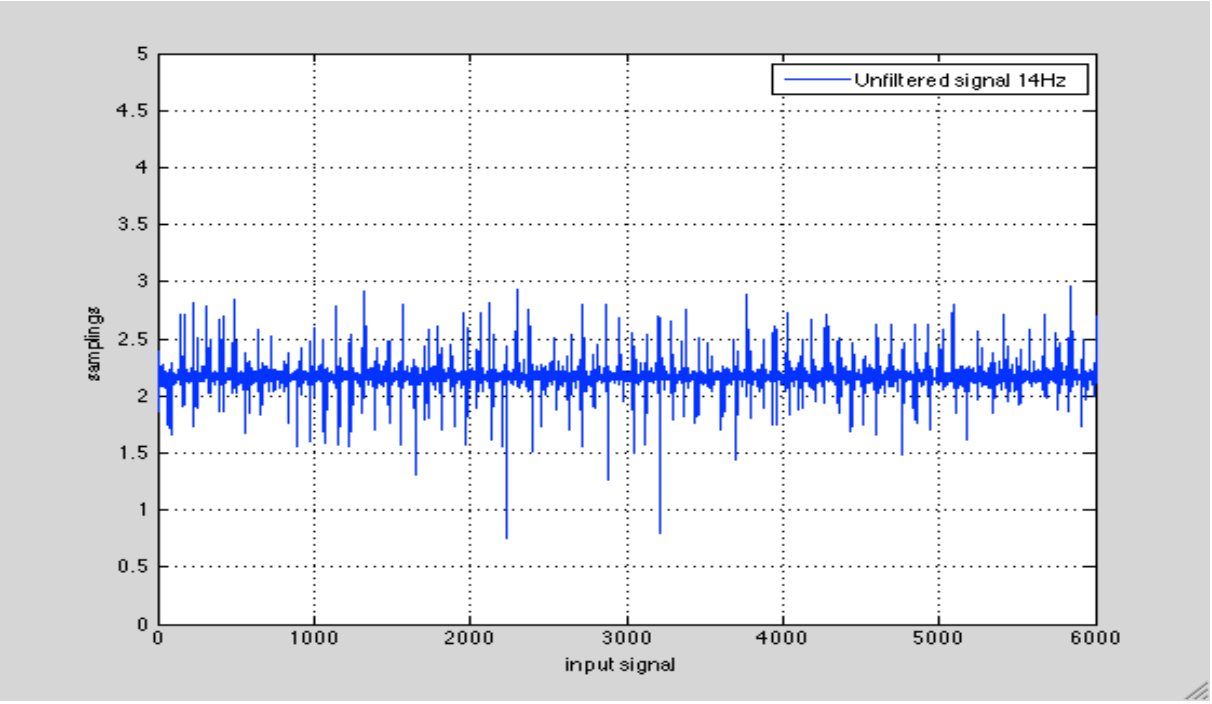

Figure 26: Signal output pressure sensors at 14 Hz seen in the pump. No filter applied.

In Figure 26 the noise generated is relative uniform with some large peaks in both directions. Mathematically, one can express this by decomposing the signal to Equation 5.4

$$y(n) = x(n) + e(n) \tag{5.4}$$

y(n) is the signal output, x(n) the desired signal and e(n) is the noise corrupting the signal.

The experiments were carried out at constant conditions except from the changes in the flow rate. Thus, a relativly simple way to estimate the true value would be to just average the output values and compute a mean value. However, doing it this way will introduce fluctuations in the output signal due to the random peaks, caused by noise in the system. Since it can not be expected a constant pressure output from the pump, this is clearly not the best way of doing it.

In order to analyze the signal a bit more, a frequency analysis was done in Matlab. The frequency content in a signal, can tell a lot about the signal and its properties. By applying a Fast Fourier Transformation (FFT) it is possible to visualize the signal in terms of frequency instead of time.

In Figure 27 a power spectral density spectrum for the signal is shown an example of the uniform disturbance in the same signal as in Figure 26 has been illustrated.

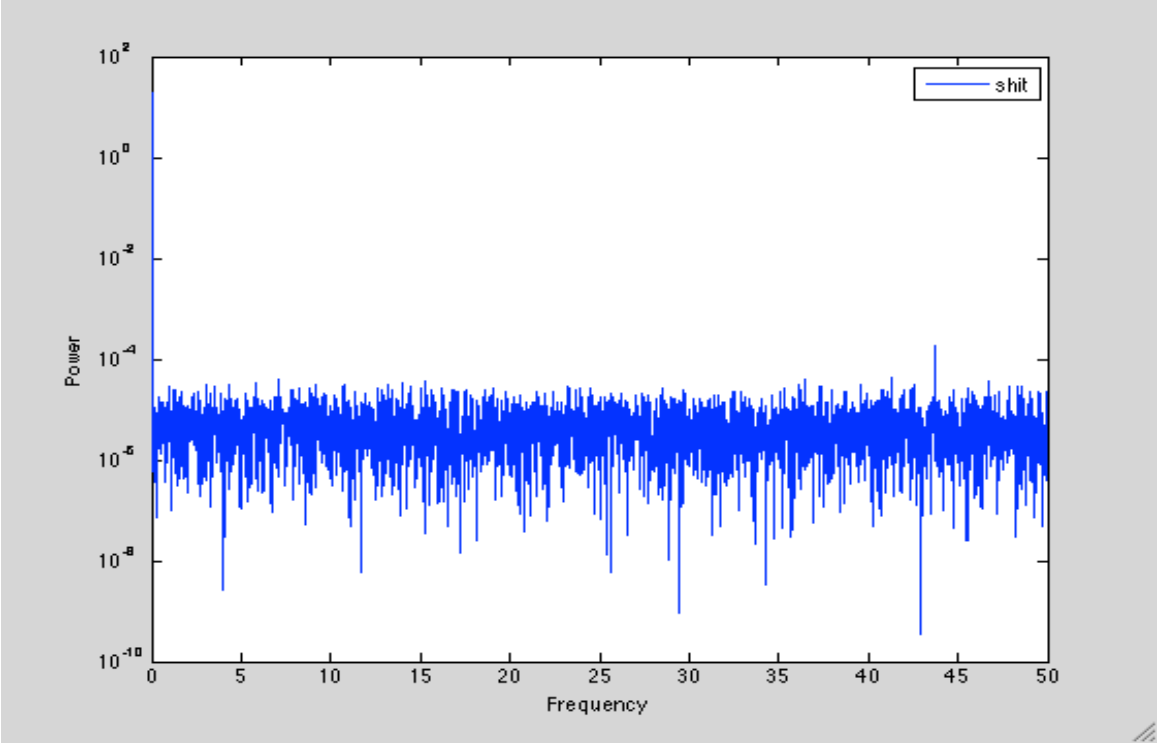

Figure 27: Frequency Spectrum in the 14Hz pressure samplings shows the white noise corrupting the signal in the frequency domain.

White noise is a random signal, which contains equal power for all different frequencies. This is in fact the explanation for the flat frequency spectrum in Figure 27. In this case a finite bandwidth for the signal is present, and the flat frequency spectrum in this bandwidth, implies that white noise with 0 mean and fixed variance is present throughout the output signal.

From the frequency spectrum, it was seen that the signal contains high frequent white noise. It is now possible to utilize this prior knowledge when a filter is to be designed. For instance, a lowpass filter is designed to let low frequencies through, while at the same time, attenuate frequencies that are higher than the pre specified cut-off frequency. This is clearly a good choice in this case. By attenuating all the high frequencies above the pre determined cutoff frequency, it is possible to get rid of most of the disturbance. Hence, a much clearer estimate of the signal is obtained. In Figure 28, a lowpass filter is applied on the raw data from the pressure sensors. For illustration purposes a relative high cut-off frequency is applied. Nevertheless, even though a lower cutoff frequency could have been chosen, a very good result is obtained.

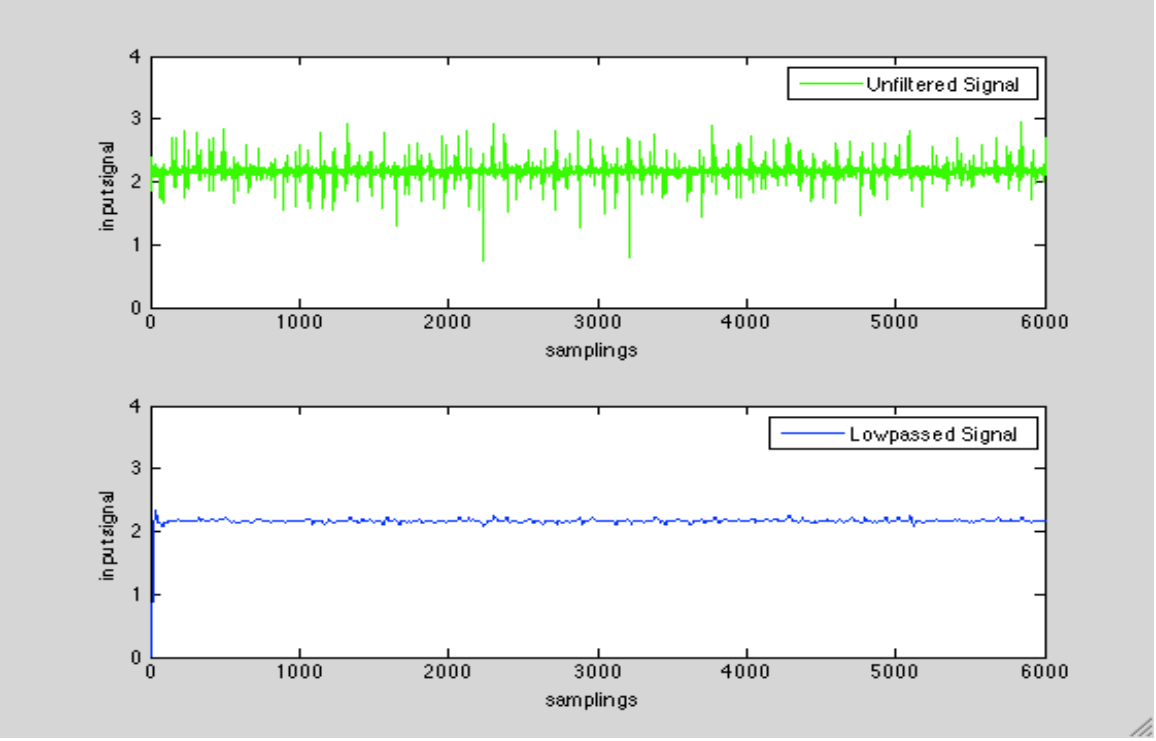

Figure 28: Lowpassed signal with relative high cut-of frequency compared with the unfiltered signal.

A normal way in order to get rid of disturbance in laboratory experiments is to determine an allowed discrepancy between the measurements, before creating a moving average function in steps of e.g. 10 or 100. One major disadvantage by smoothing the signal compared to applying a lowpass filter is the creation of new data, which has not been recorded. When smoothing of the output data is done, one manipulates the data to new values. Smoothing a lowpassed signal will help to get rid of the small fluctuations that are left in the signal. In Figure 29 the third subplot shows a smoothed version of the lowpassed signal in the second subplot. In this case, a moving average with an interval of 250 is used. What this means is that each sample is set as the average value of the 125 neighbor samples on each side.

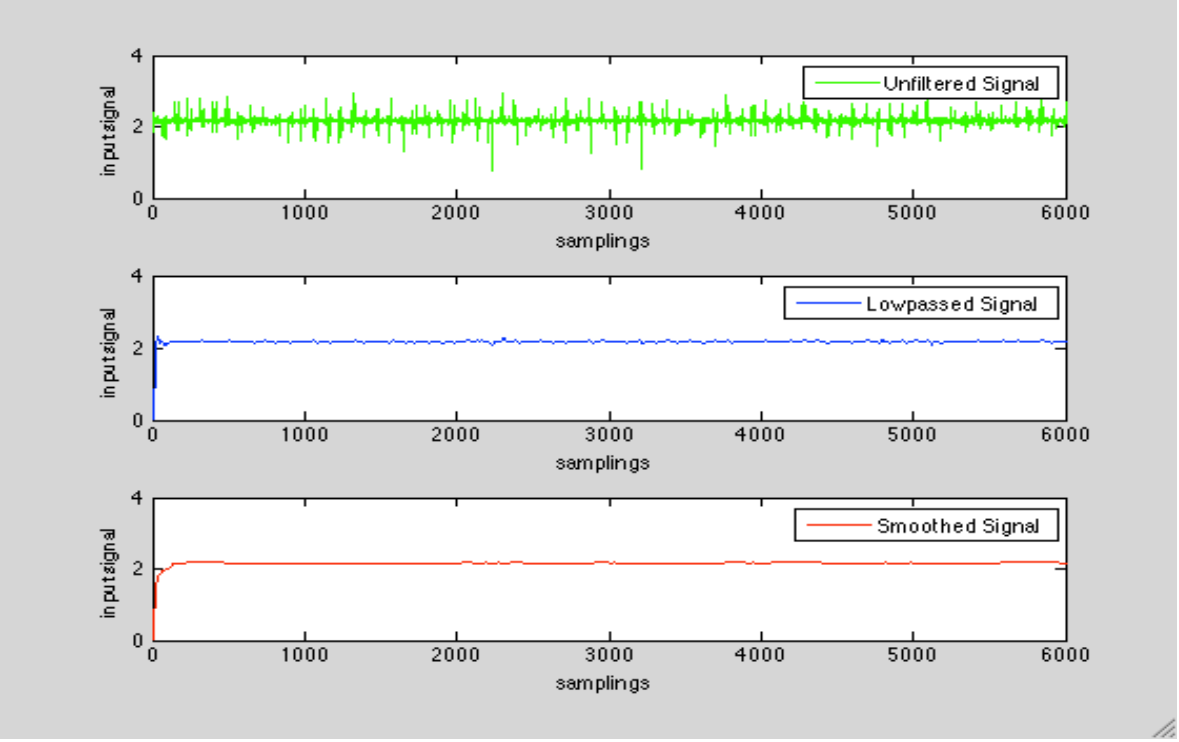

Figure 29: A comparison of the unfiltered signal, lowpassed signal and the smoothened lowpassed signal.

5.3.4 Limitations and Calibration

As the lab set up was built by trial and error one important limitation were connected to measurements of the flow. During the testing the upper limit of in the signaled electrical output (10 Volt) was met in the flow meter. Due to time limitations it was not possible to order a new flow meter. The flow was measured linearly from the Hz set up from the pump and due to the accuracy in the pump and inaccuracy in the flow meter it was decided to extrapolate from the pump set up, flow rates from 27Hz to 45 Hz shown in Figure 30. Extrapolating values is not within good standards for experimental routine, but as the accuracy of the pump was proven by calibration result the validity was accepted. At lower flow rates the rate is more unstable in the flow creating some discrepancy in the further readings. By neglecting the zero value, due to instability in the readings, a formula for linear relationship was obtained:

$$y = 0{,}3186x + 1{,}911 \tag{5.5}$$

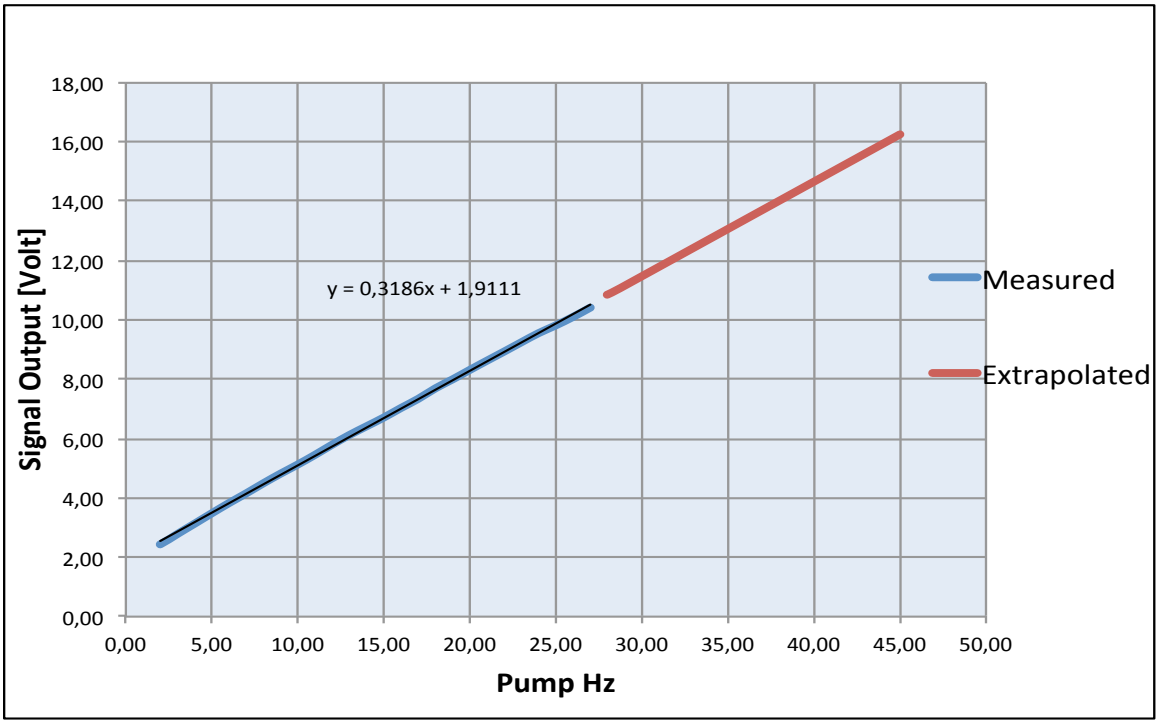

Figure 30: Extrapolated values for flow rate. In the Figure volt output in the flow meter is plotted against pump Hz

For further insurance of the accuracy of the pump and thus the conversion factor from Volt to liter per minutes, fluid was flushed through the system, into a separate tank for a certain time limit before it was weighted. The results in liter per minute is shown in Table 4.

Table 4: Values from the calibration test. All values in liter per minute

Hz	Weighted 1	Weighted 2	Average	Flow Meter1	Flow Meter 2	Average
5	16,5	17,85	17,175	14,60	14,41	14,50
10	35,7	36,3	36	28,33	29,50	28,91
15	54,6	54,6	54,6	42,87	44,93	43,90
20	71,7	71,7	71,7	57,80	59,79	58,80
25	90,6	87	88,8	72,82	73,91	73,36
30	106,8	106,2	106,5			
35	124,5	123,6	124,05			
40	141,9	141	141,45			
45	155,7	155,7	155,7			

Figure 31 show the weighted averaged values versus the weighted. By applying linear regression it is possible to calculate the correlation factor according to equation 5.6.

$$\text{correlation factor} = 1 + \frac{3{,}4805 - 2{,}9857}{2{,}9857} = 1{,}167 \tag{5.6}$$

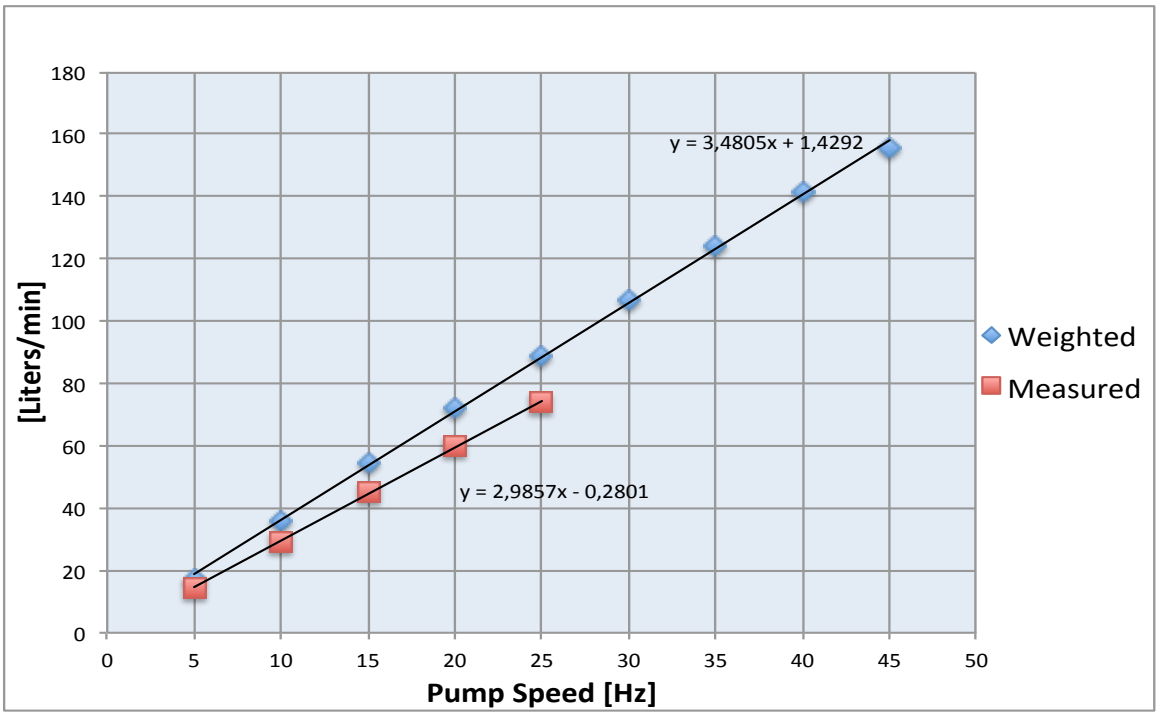

Figure 31: Averaged measured flow in the flow meter plotted against averaged weighted amount of water for calibration purposes.

5.4 Sources of Errors in the Input Variables

In all physical experiments, altering variables introduces systematical errors in the apparatus and random errors in connection to the measurements. In order to quantify and analyze the effect of the different errors a thoroughly review was required. Due to the time consuming and page consuming process presenting the uncertainty in all the experimental samplings, have only the uncertainty in the end Reynolds number and Fanning friction pressure for the slick pipe section in the low viscosity mud been presented. A complete example of the calculation has been given in Appendix C.

Another important aspect of the uncertainty analysis is the lack of flow measurements after the pump reaches 27Hz to 45Hz and thus no random errors. In order to quantify an estimate of the uncertainty the random error in the 27Hz reading has been utilized for the rest of the samplings.

$$\delta f = \sqrt{(\delta f_{random})^2 + (\delta f_{systematical})^2} \tag{5.7}$$

5.4.1 Random Errors

When analyzing the tool joint effect some three main sources of random errors had to be highlighted.

1. A significant source of error in the data obtained from the pressure transducer and flow meter was the pressure pulses from the pump. One simple and primitive method to neglect the random errors in a steady state system is to utilize the time. Since no parameter changes within the given flow rate random errors were severely diminish by the amount of data gathered from each measurement. All measurements were measured at least 30 seconds and with 2 min circulation within the given flow, for stabilization prior to data samplings.

2. Compared to previous studies, the lab set up built with one outer steel pipe. In order to change the inner parameters, i.e. change the tool joint configuration the lab had to be reassembled. By reassembling the lab set up some small errors can be introduced. One advantage of utilizing the same steel pipes throughout the experiments is the insurance that all all the tests are subjected to the same shear due to roughness and erosion in the pipes.

3. As described in Chapter 3.1 drilling fluids has time dependent properties. During circulation, rheopetectic of thixotropic behavior could shift the samplings and thus the end results. Furthermore, due to the time demanding experiments remixing of the mud was needed. By remixing the mud it is impossible to gain the exact parameters two times in a row.

An estimation of the random errors was obtained by a standard deviation based on the average value with the governing Equations from 5.8 – 5.10 expressed by the pressure

$$\overline{\Delta P} = \frac{1}{n}\sum \Delta P \tag{5.8}$$

$$\sigma_{\Delta P}{}^2 = \frac{1}{n-1}\sum (\Delta P_i - \overline{\Delta P})^2 \tag{5.9}$$

$$\delta \Delta P_{random} = \frac{\sigma_{\Delta P}}{\sqrt{n}} \tag{5.10}$$

5.4.2 Systematical Errors

Systematical errors are errors connected to the apparatus in the experiments. All apparatus have a given calibration error (δq). In the given experimental setup errors in the flow meter and pressure transducer have been investigated. But there will also be errors in the electrical wiring and acquisition sub. Compared to random errors there is no way in order to detect or control systematical errors, but by awareness it is possible to calculate the propagation effect and thus estimate the significance of the error.

- Systematical errors in the RS Combined Liquid Flow Transducer Stock is 2%
- Systematical error FCX Series Pressure Transmitter is 0.1%

Utilizing fanning friction factor as a base it is possible to estimate the errors caused by the apparatus and thus visualize the overall effect.

$$f = \frac{\mathrm{d}_e}{2\rho\bar{\mathrm{v}}^2} * \frac{\Delta \mathrm{P}}{L} = \frac{\Delta \mathrm{P} \mathrm{de}}{2\rho \mathrm{L}} * \left(\frac{\pi({d_2}^2 - {d_1}^2)}{4Q}\right)^2 \tag{5.11}$$

Neglecting the small difference in density, length and diameter gives us the uncertainty parameters in Equation 5.12, with the resulting derivation in 5.13-5.16.

$$f = f(\mathrm{P}, \bar{\mathrm{v}}) \text{ or } f = f(\mathrm{P}, \mathrm{Q}) \tag{5.12}$$

$$\mathrm{d}f = (\frac{\mathrm{df}}{d\Delta \mathrm{P}} \partial \Delta \mathrm{P} + \frac{\mathrm{df}}{d\bar{\mathrm{v}}} \partial \bar{\mathrm{v}}) \tag{5.13}$$

$$\delta f = \frac{\mathrm{de} * \left(\pi({d_2}^2 - {d_1}^2)\right)^2}{2\rho \mathrm{L} * 4^2} (\frac{1}{\mathrm{Q}^2} \delta \Delta \mathrm{P} - \frac{2\Delta \mathrm{P}}{\bar{\mathrm{v}}^3} \delta \bar{\mathrm{v}}) \tag{5.14}$$

$$\frac{\delta f}{f} = (\frac{\delta \Delta \mathrm{P}}{\Delta \mathrm{P}} - \frac{2\delta \bar{\mathrm{v}}}{\bar{\mathrm{v}}}) \tag{5.15}$$

$$\frac{\delta f}{f} = \sqrt{(\frac{\delta \Delta \mathrm{P}}{\Delta \mathrm{P}})^2 + (\frac{2\delta \bar{\mathrm{v}}}{\bar{\mathrm{v}}})^2} \tag{5.16}$$

Applying the same procedure on the Reynolds number the systematical errors becomes as 5.17

$$\frac{\delta Re}{Re} = \sqrt{(\frac{\delta \bar{v}}{\bar{v}})^2} \tag{5.17}$$

Calculating the relative errors for flow rate and pressure drop and plotting it against Hz of the pump the magnitude of error at the different flow rates can be displayed, shown in Figure 32. As the figure show, the relative uncertainty in the lower region in the flow meter is extremely high, with differences of more than 10%, while the differences in the pressure is relative low.

The smooth slope of the error in velocity shown in Figure 32, it is possible to conclude that due to the high systematical error in the flow meter the random error can be neglected. In the pressure curve some discrepancy can be detected due to the random error. Between 5-10Hz some large random errors can be detected before the pressure curves smooth out. At around 10Hz the relative error of the pressure sensor exceeds the relative error of the flow meter.

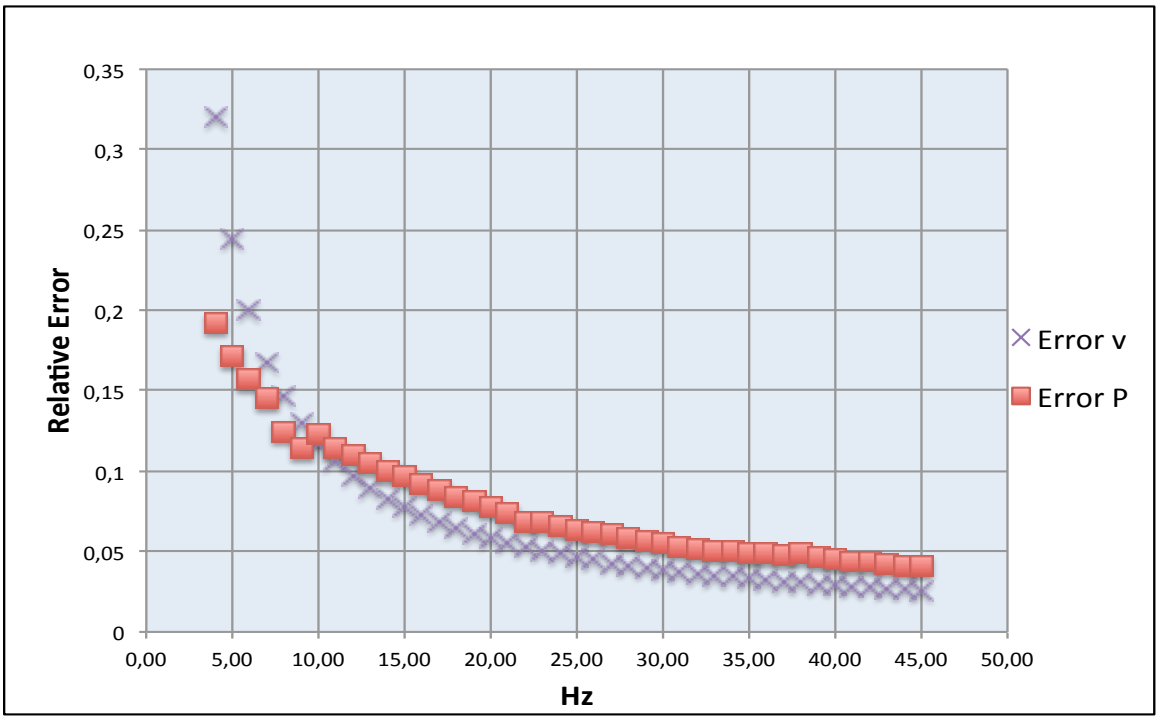

Figure 32: Magnitude of relative error in the velocity and pressure plotted in steps of the pump.

Looking closer at the effect of the error in velocity and pressure on the end result in Reynolds number and Fanning Friction Factor, Figure 33 and Figure 34 can be visualized. Applying the assumptions made, the Reynolds numbers for the highest readings becomes 5530 ± 136. The fanning friction factor is inversely plotted in Figure 34 meaning that the plot starts at the highest pump rate, due to the responding lowest friction factor. The corresponding Fanning friction factor for Reynolds number 5530 was 0.00318 ± 0.00018.

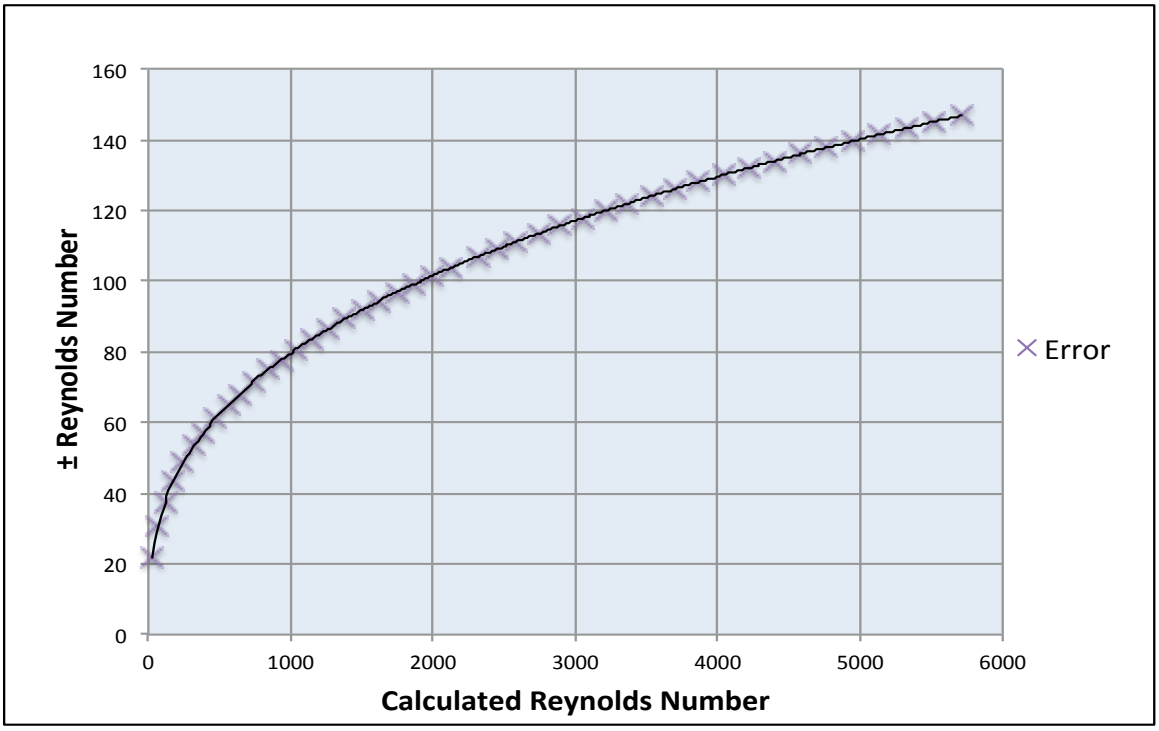

Figure 33: Reynolds number plotted against the ± error in the readings for low viscosity mud.

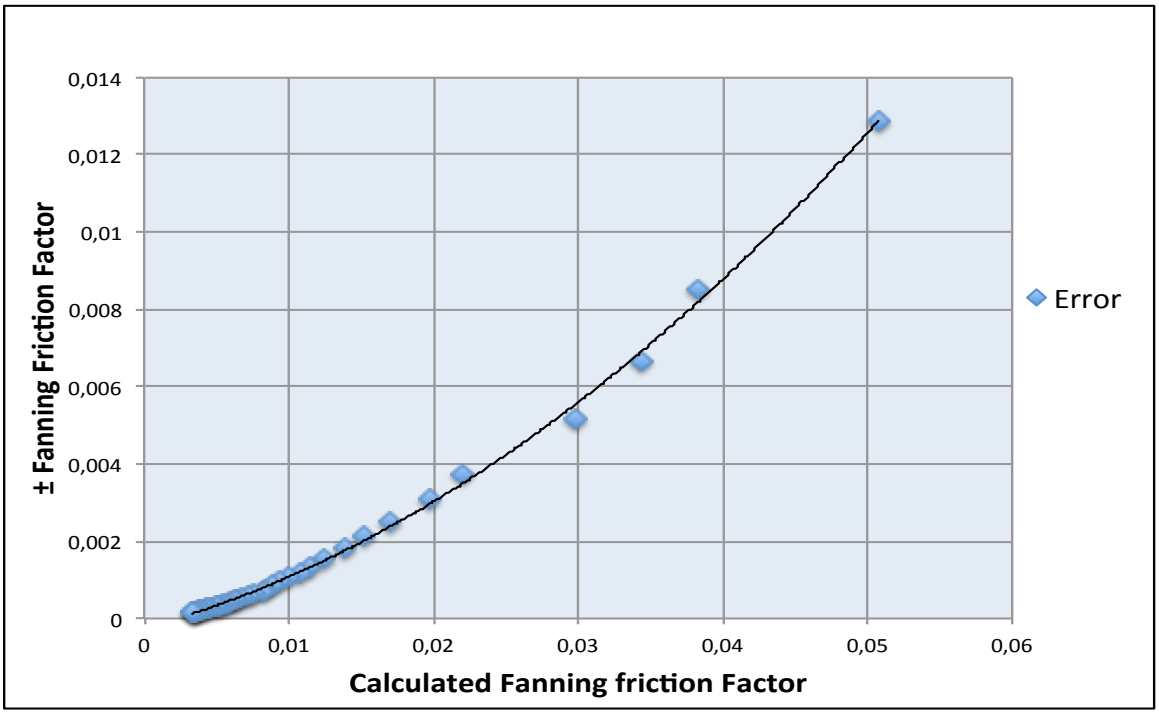

Figure 34: Fanning Friction Factor plotted against the ± error in the readings for low viscosity mud.

5.4.3 Fluid Rheology

To ensure the correct rheological values, rheology was measured with Fann Viscometer. Due to the experimental set up it was difficult to quantifying the exact amount of fluid in the system at all time, and thus quantify the relative amount of viscosifier, although efforts were made to keep it at around 200 liters. For the purpose of creating a Power Law fluids Xanthan Gum Viscosifier provided by Schlumberger was applied.

Three different concentrations were tested, characterized as high concentration, medium concentration and low concentration of Xanthan Gum Viscosifier. Due to the good properties the relative concentration of viscosifier was not more than 1 liter or around 0.5 % for the high concentration 0.3% for the medium and 0.15% for the low concentration mud, with the resulting shear stress and rate in Table 5.

Table 5: Shear stress and shear rate for the applied Power Law muds

Shear rate	τ High [pa]	τ Medium [pa]	τ Low [pa]
1021.8	12,748	8,6686	5,6091
511.9	9,6885	6,6289	4,0793
340.6	8,6686	5,6091	3,5694
170.3	7,1389	4,5892	2,5496
10.21	3,0595	2,0396	1,0198
5.10	2,5496	1,5297	1,0198

In Figure 35 the resulting shear stress is plotted against shear rate for the three different applied power law fluids. Instead of applying standard Fann Viscometer calculations, regression was applied in order to calculate K and n, shown in Table 6.

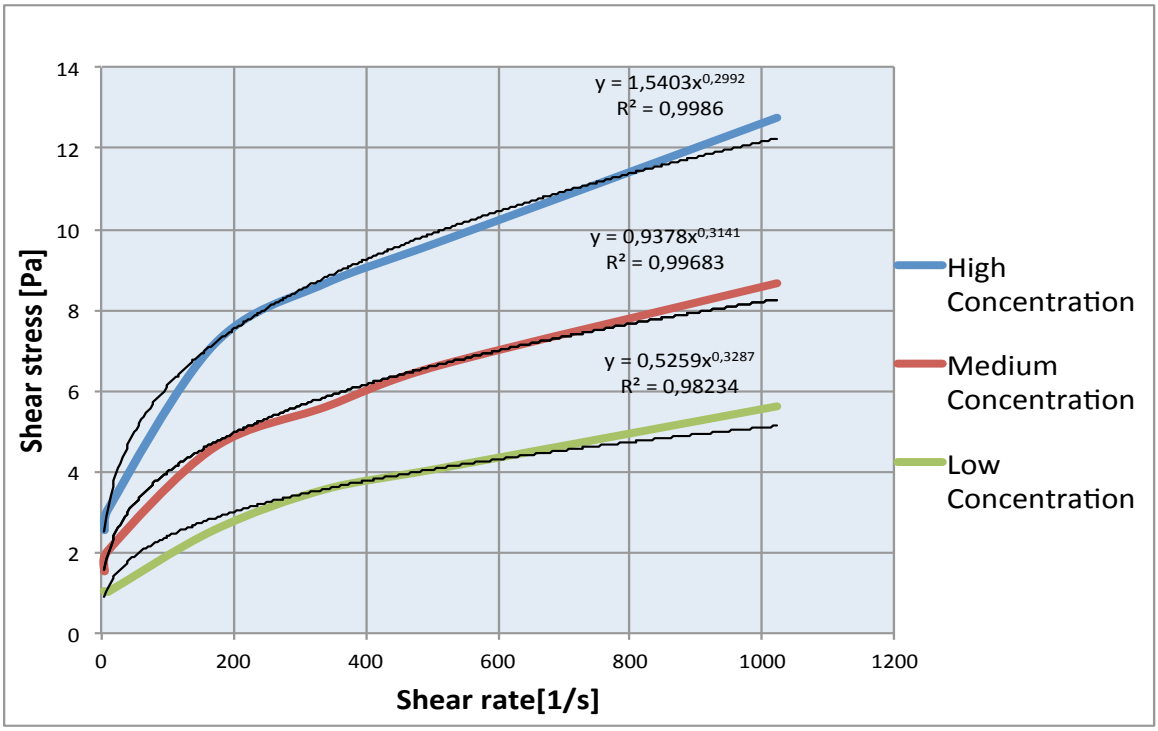

Figure 35: Shear stress plotted against shear rate for the applied power law fluid

Table 6: Resulting n and K from Figure 35.

	High concentration	Medium Concentration	Low Concentration
n k	0,2992 1,5403	0,3141 0,9378	0,3287 0,5229

5.5 Experimental Results

In this chapter the main results from the have been presented. The results have been displayed mainly as a function of pressure loss versus flow rate for comparison between the different muds and with Fanning friction factor versus Reynolds number. First the Newtonian fluid is presented, followed by the low viscosity, medium viscosity and high viscosity mud.

5.5.1 Newtonian fluid

Due to the fact that Newtonian fluids turn turbulent relatively instant, it was decided to only test velocity in the pipe up to 0.8 m/s or 25Hz in the pump. Comparing the average values of tool joint incoporated in the string, shown in Figure 36, with the average values from the experiments with no tool joint in the string, a significant additional pressure loss was introduced. The presence of tool joints in the string increases the pressure drop by 46 % at the highest flow rate.

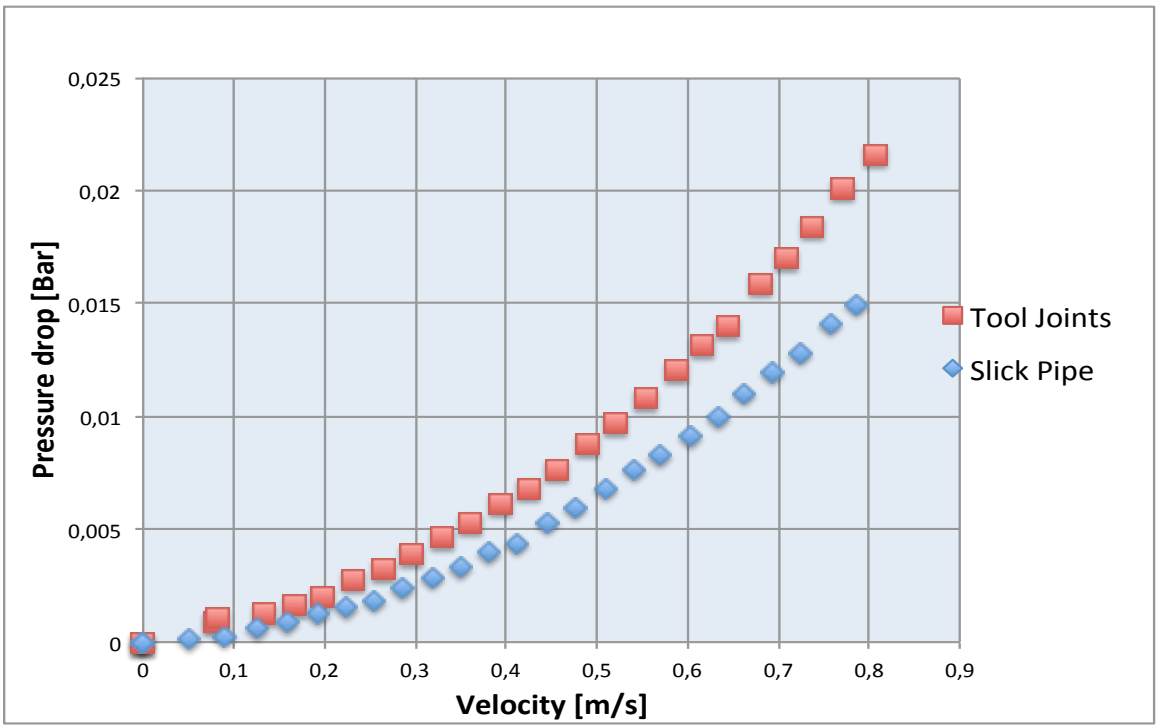

Figure 36: Measured pressure loss plotted against velocity with and without tool joints in the string

Plotting the Fanning friction factor (ref. Equation 3.14) against Reynolds number for the resulting pressure drop in Figure 37 it is possible to visualize the effect in non-dimensional form. Prior to reaching Reynolds number higher than 5000 the friction factor is varying due to the difficulty in measuring the low-pressure differences.

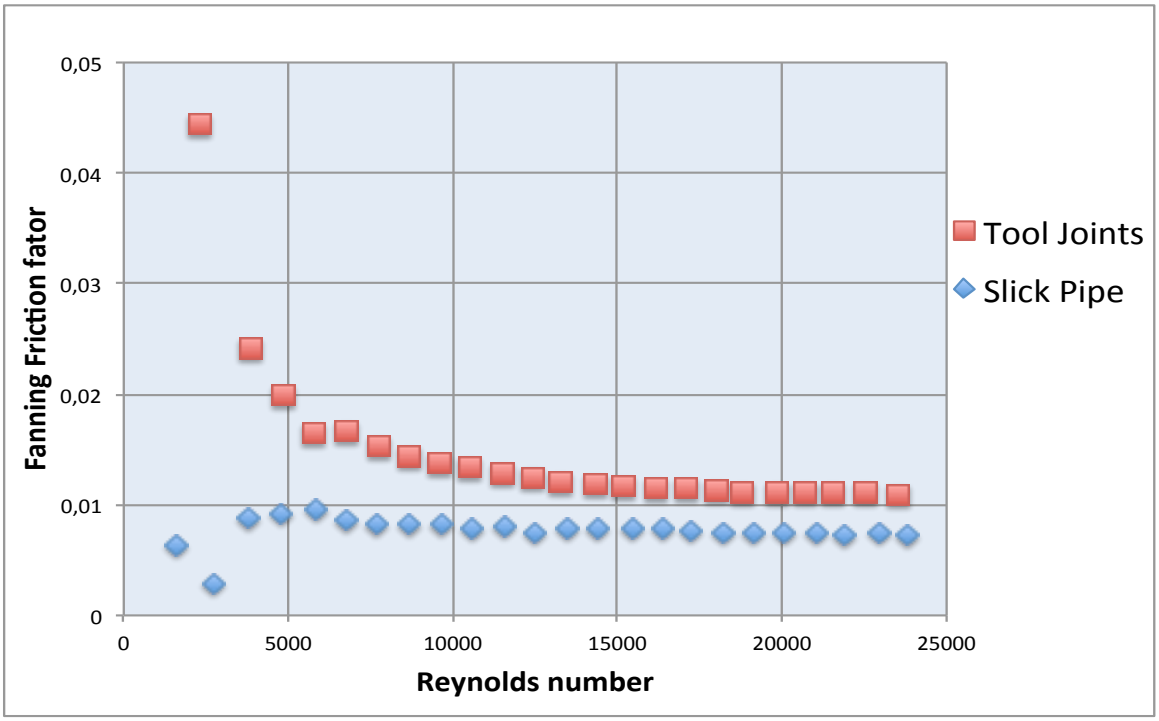

Figure 37: Measured Fanning friction factor plotted against Reynolds number for Newtonian fluid.

Plotting the resulting friction factor against Reynolds number in Figure 37 in a logarithmic plot in Figure 38, it is even easier to visualize the trends based on the gradient of the slope.

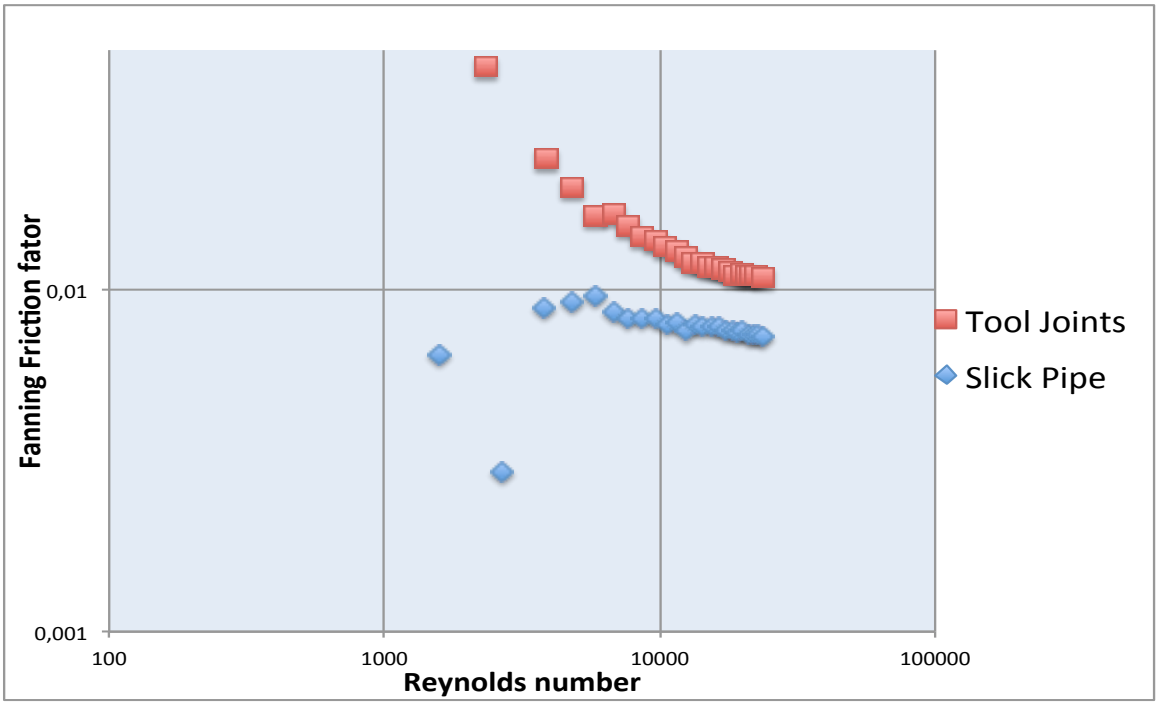

Figure 38: Logarithmic plot of measured Fanning friction factor plotted against Reynolds number for Newtonian fluid.

In the tool joint section a more laminar flow profile can be detected, until reaching Reynolds number of 5000, while in the slick pipe section the small pressure differences was not possible to measure accurately.

One important feature of the Newtonian fluids test is the ability to back calculate the roughness and thus incorporate a more accurate roughness in the calculated results. As mentioned in the theoretical results the friction factor was estimated from the moody chart to 48*10-6 m. By assuming the roughness contribution is twice due to the annular spacing and solving for absolute roughness, ε/d 0.00016717. By calculating the friction factor from the universal pressure law shown in Figure 37, the Colebrook-White equation was utilized to back calculate the absolute roughness in the pipe. The absolute roughness is extremely sensitive and back calculating the roughness with small variations in the frictional pressure drop creates small differences. The roughness was averaged where fully turbulent flow was reach and the absolute roughness calculated to 0.00046. This was almost three times higher than the estimated roughness in the annular section and almost six times higher than the value obtained from the Moody chart, meaning that there is significant contribution from the erosion in the test pipes.

5.5.2 Low Viscosity Mud

The tool joint effect in the string with the low viscosity mud enhances the pressure loss almost 90 % at fluid velocity of 1,55 m/s shown in Fiure 39. The enhanced pressure loss due to the tool joints in the string are indisputable, with pressure losses of 0,047 bar and 0.024 bar for the tool joint section and the slick pipe section respectively. Comparing the pressure loss with the calculated Reynolds number the pattern of on-set of turbulence is relatively distinct in the tool joint section, but not in the slick pipe section. At around Reynolds number 1800 in the tool joint section a discrepancy in the laminar pattern can be detected, resulting a clear turbulent pressure loss slope. In the slick pipe section no clear transformation to a turbulent flow pattern can be observed.

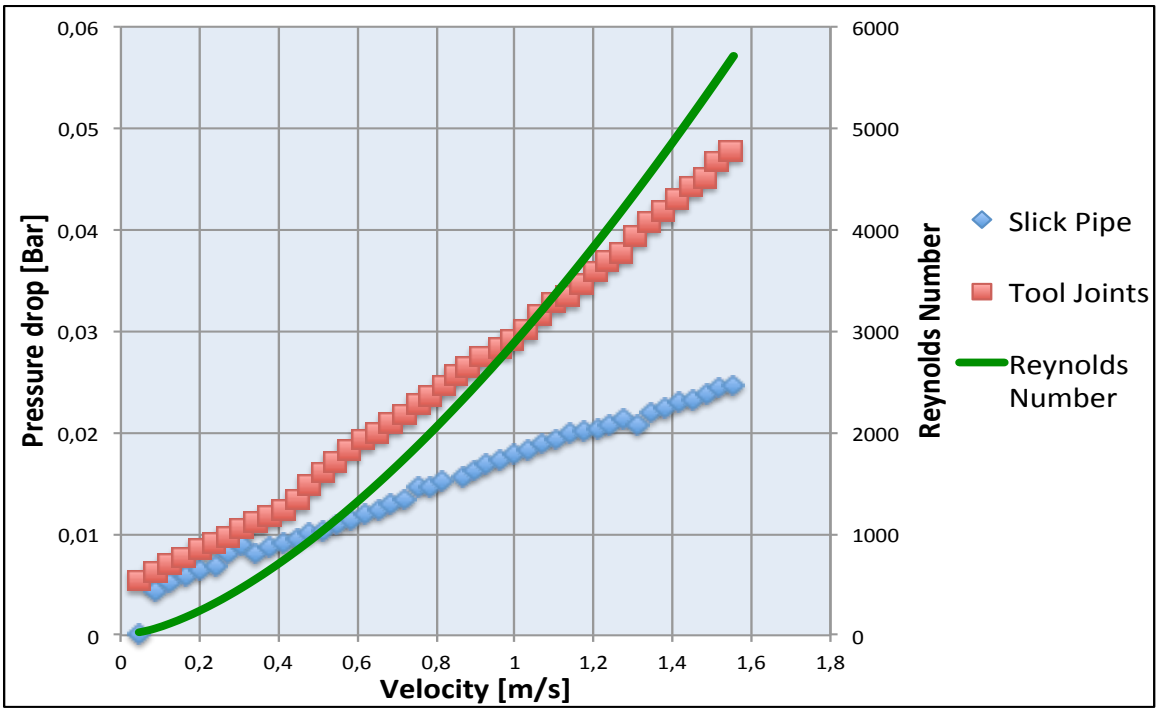

Figure 39: Measured hydraulic pressure loss as a function of flowrate with low viscosity mud.

In order to further obtain a picture of the effect on hydraulic pressure loss when introducing tool joints in the string the friction factor was plotted against Reynolds number shown in Figure 40. As illustrated in Figure 40 the tool joint contribution is significant. The relative distinct characterization of laminar friction factor can be detected at low Reynolds number, before the slope flattens out as the flow turns more turbulent. Also by utilizing mud as the base fluid it was possible to measure more exact pressure drop than with Newtonian fluids. The same trend is shown in the logarithmic plot of Reynolds number and friction factor in Figure 41. From Figure 41 it becomes pretty clear that due to the presence of tool joint the flow turn turbulent at Reynolds number around 800-1400.

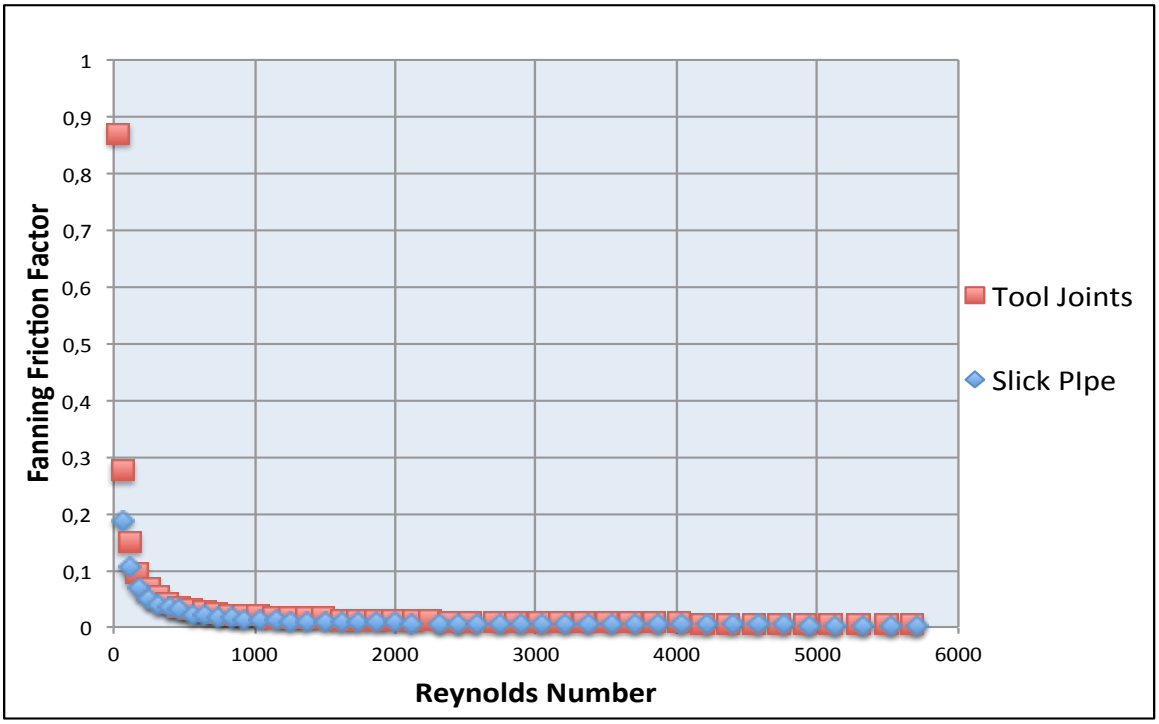

Figure 40: Measured Fanning friction factor plotted against Reynolds number for low viscosity mud

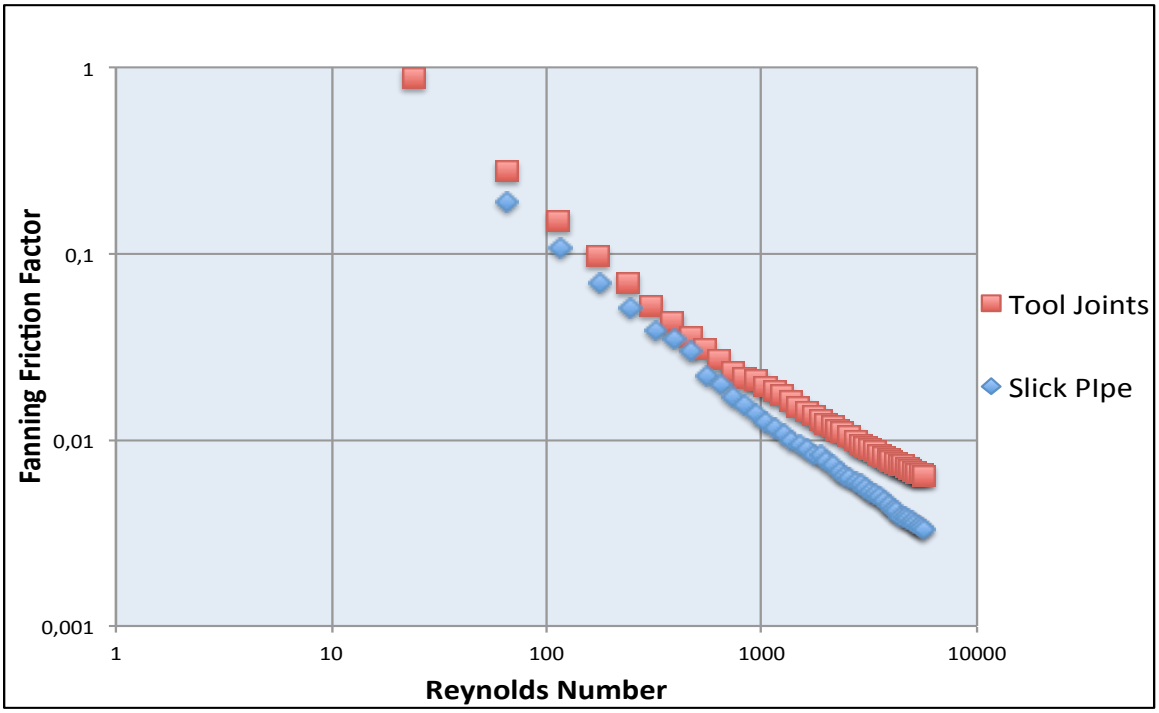

Figure 41: Logarithmic plot of Measured Fanning friction factor against Reynolds number for low viscosity mud

Comparing the hydraulic pressure loss with the rough obstacle in the string a visualization of the presence of tool joints can be obtained is shown in Figure 42 Introducing a rough abrupt restriction in the well, the difference to the tool joint section is almost negligible with an end discrepancy of 0.002 bar or 6,3% in the end. The smaller obstruction induces a decreased pressure drop compared to the tool joint section with discrepancy of 0.005 bar or 13.3%.

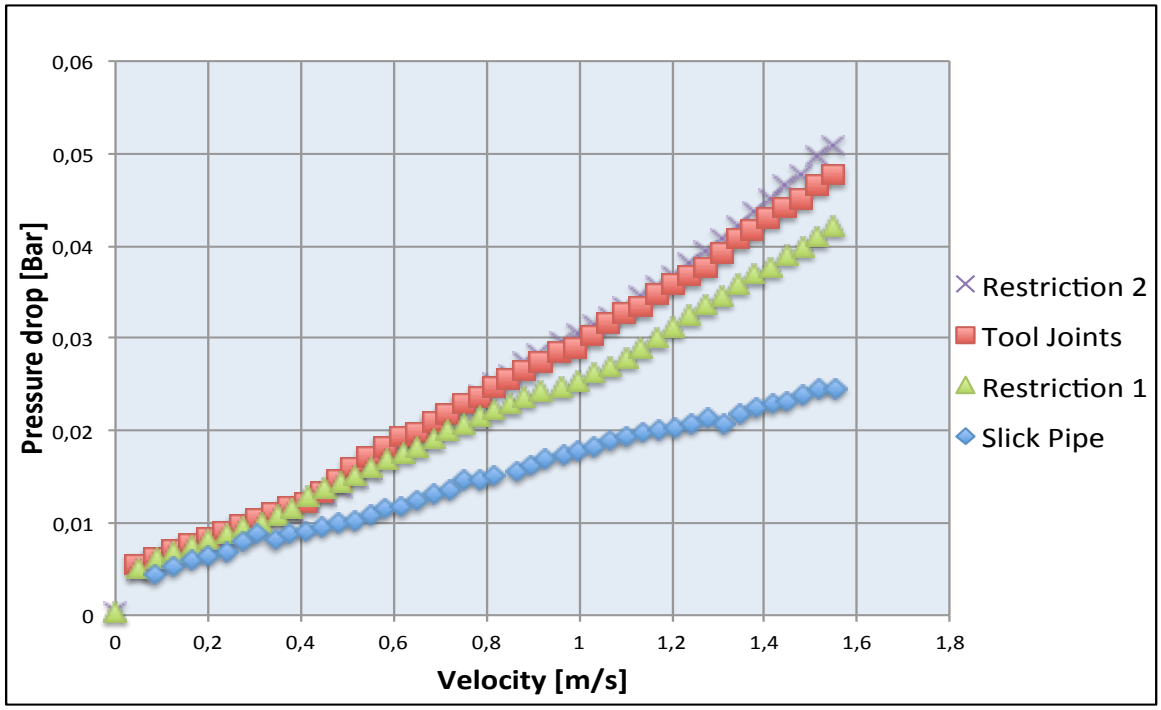

Figure 42: Measured hydraulic pressure loss plotted against velocity for Tool Joint, slick pipe and additional obstacle in the annulus for low viscosity mud

5.5.3 Medium Viscosity Mud

Increasing the viscosity, the patterns from the low viscosity mud becomes better visualized, shown in Figure 43. Already when Reaching Reynolds number at 1200 it looks like the presence of tool joints introduce a turbulent flow regime, and thus enhanced pressure drop. In the slick pipe section the laminar flow pattern seems reasonably stable until Reynolds number of 2200 where the slope changes, to maybe a more turbulent flow regime. The difference in flow regimes alters the pressure drop, creating a difference of 72,75% at the final flow rate.

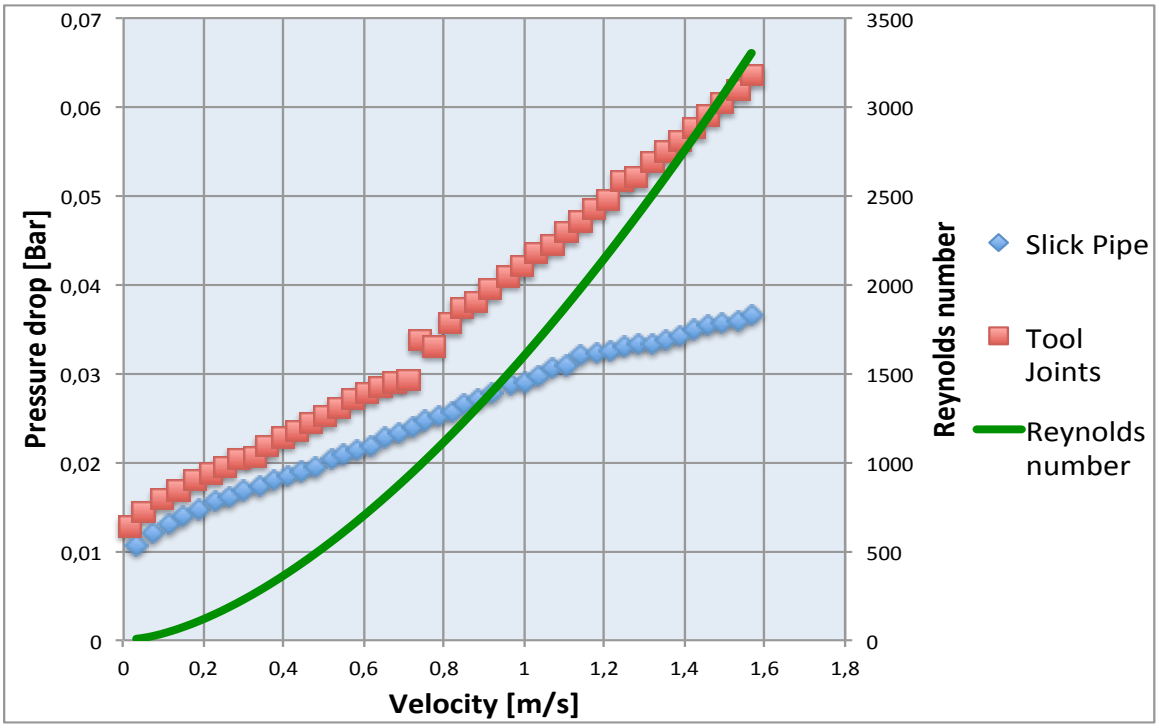

Figure 43: Measured hydraulic pressure loss as a function of flow rate for a medium viscosity mud.

In Figure 44, Fanning Friction Factor is plotted against Reynolds number for the tool joint section and the slick pipe and the same plot is logarithmic plotted in Figure 45. The relative high frictional discrepancy, due to incorporating tool joints in the string, enhances the friction factor significantly at all flow rates applied. At low Reynolds number two measuring errors can be detected in Figure 45. At around Reynolds number of 1000-1500 a shift in the gradient of slope can be detected in Figure 45, which could indictate a turbulent flow regime.

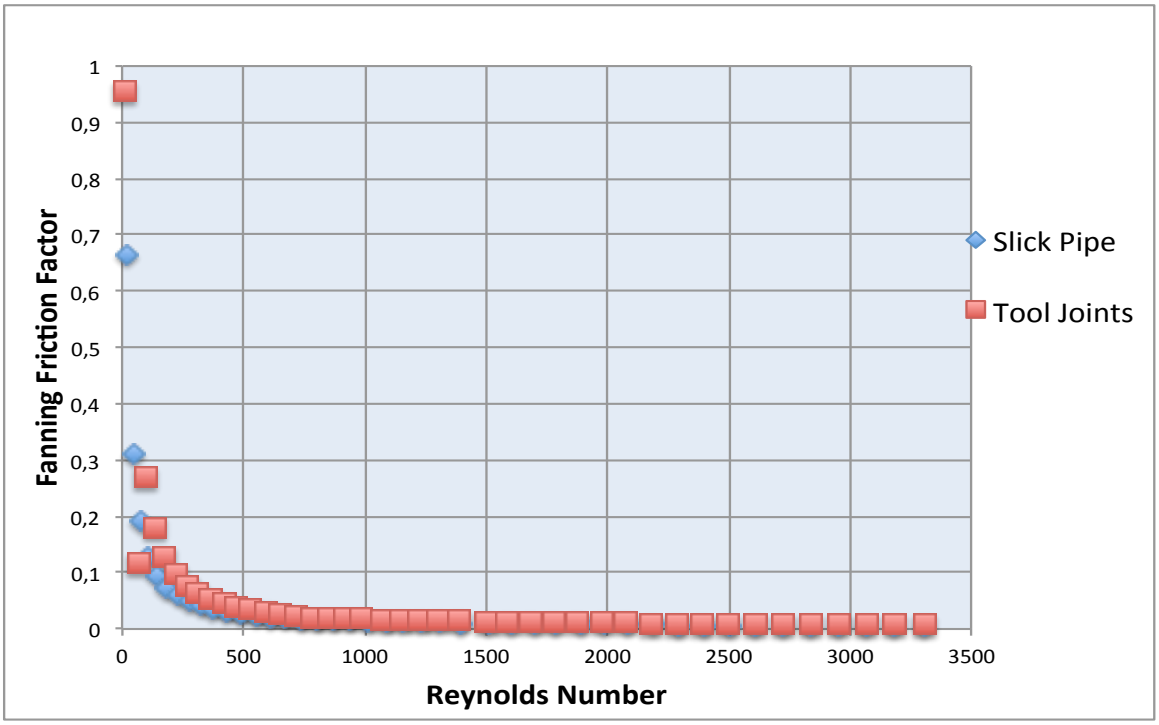

Figure 44: Measured Fanning friction factor plotted against Reynolds number for medium viscosity mud.

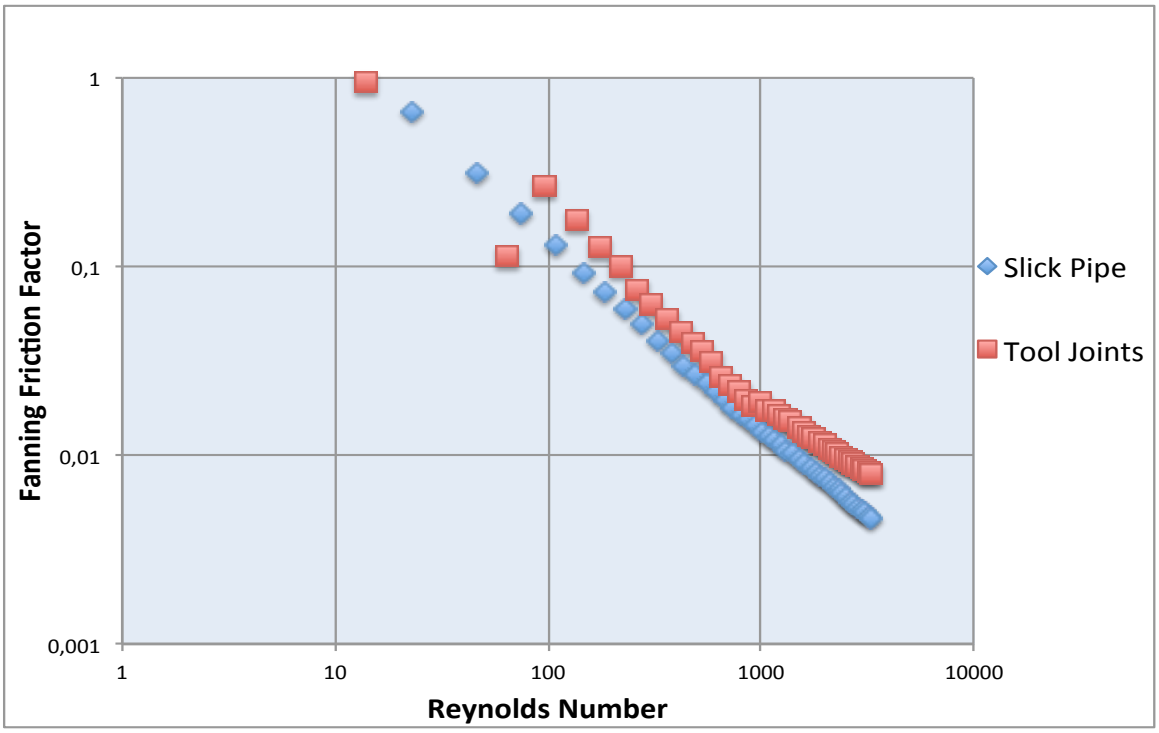

Figure 45: Measured Fanning friction factor plotted against Reynolds number for medium viscosity mud.

Figure 46 shows the effect of introducing an equivalent roughness in the string. The largest restriction, restriction 2, enhances the pressure drop from the tool joint section with 14.7 % while applying the smaller restriction, restriction 1, the pressure drop is decreased with 13 % compared to the tool joint section.

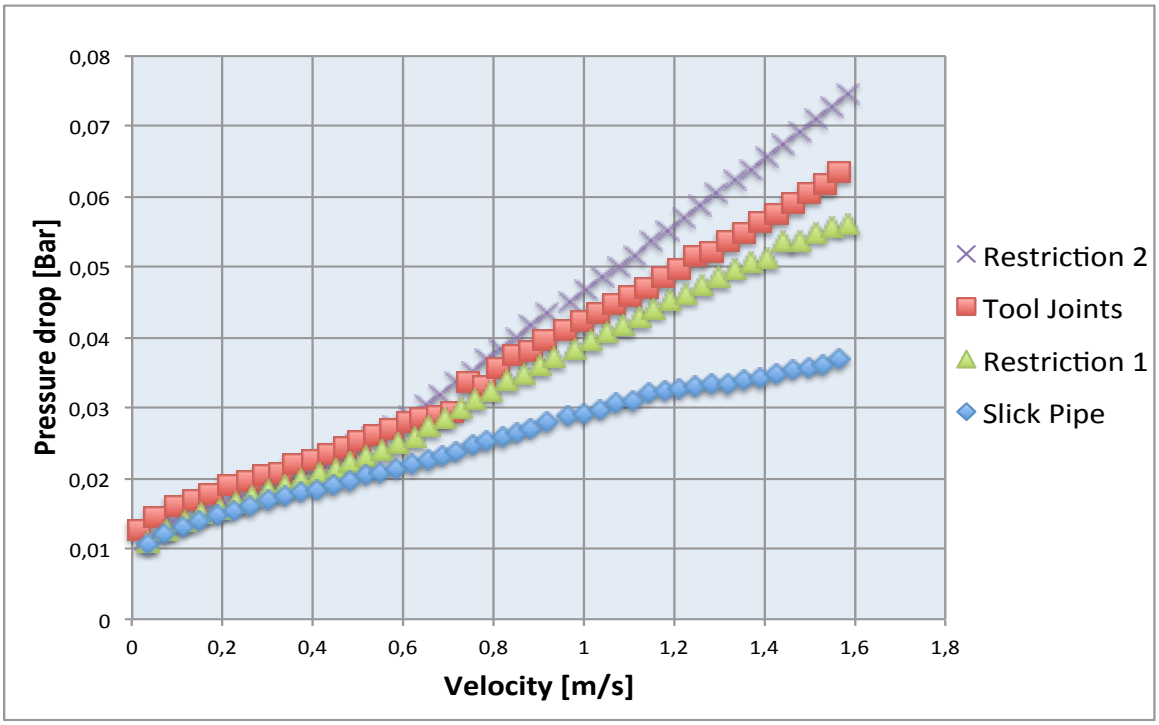

Figure 46: Measured hydraulic pressure loss plotted against velocity for Tool Joint, slick pipe and additional obstacle in for medium viscosity mud

5.5.4 High Viscosity Mud

When testing the high viscosity mud the test procedure was altered from the previous tests. Due to the high viscosity in the mud the flow meter started to generate noise at higher flow rates and it was decided to only test the fluid up to the pump limit of 25Hz. The high viscosity fluid introduced some unexpected result compared to published papers. There has not been reported additional pressure loss due to tool joints within the laminar region. As the previous results have shown the discrepancy in between the laminar region is small, but present. The trend in the high viscosity mud illustrates the effect additionally.

To neglect time dependent effects on the mud and errors connected to re-assemble and assemble the lab set up the sampling procedure was altered and the test carried out once more as described in the procedure. First the slick pipe configuration was tested, followed by the tool joint section once, then the same configurations were done again.

The discrepancy in the measured pressure loss, is shown in Figure 47. Utilizing a highly viscous base mud the measured pressure loss is approximately 9% higher at the highest flow rates in the tool joint section than in the slick pipe. Due to the higher slope in the tool joint section it is expected that the relative difference will increase with higher flow rates. For that reason the pressure loss would increase additionally with a higher flowrate, also within the laminar region.

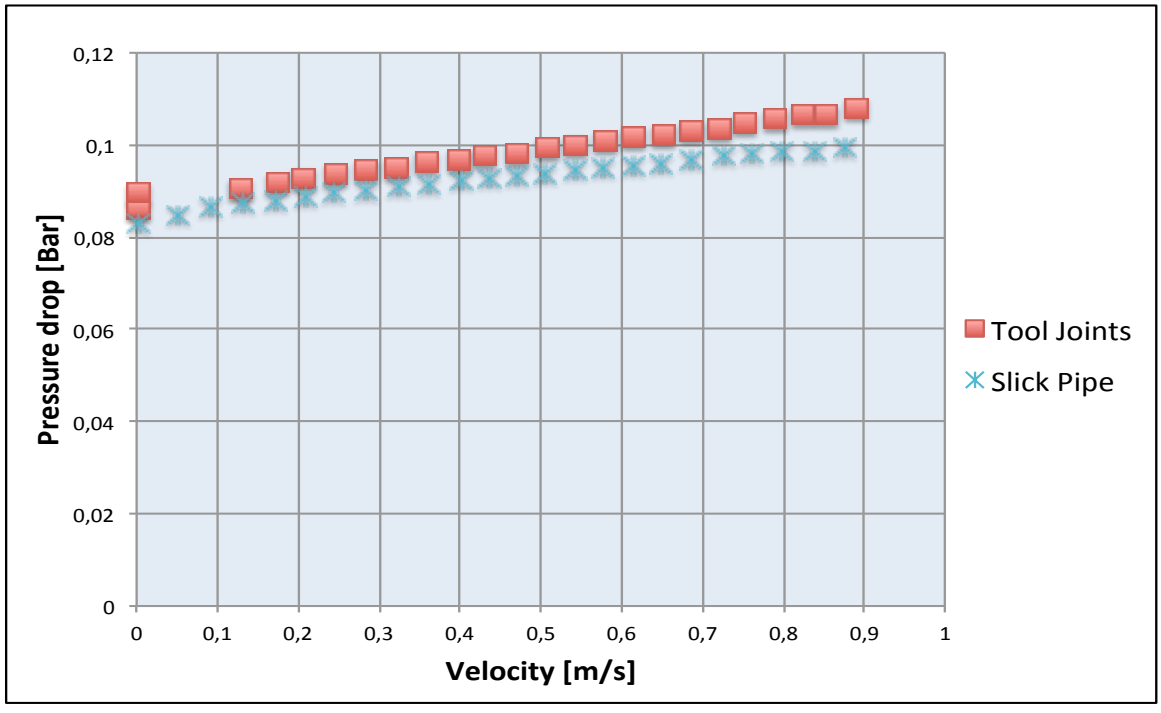

Figure 47: Measured hudraulic pressure loss plotted against velocity for high viscosity mud

Utilizing high viscosity mud it was not possible to reach turbulent flow due to limitations in the lab. Shown in Figure 48, the highest Reynolds number reached was only 600 with the resulting Fanning friction factor of 0.03. Due to the highly dominated viscous forces the friction factor is

extremely high, especially at lower flow rates. This is easier detectable in the logarithmic plot shown in Figure 49.

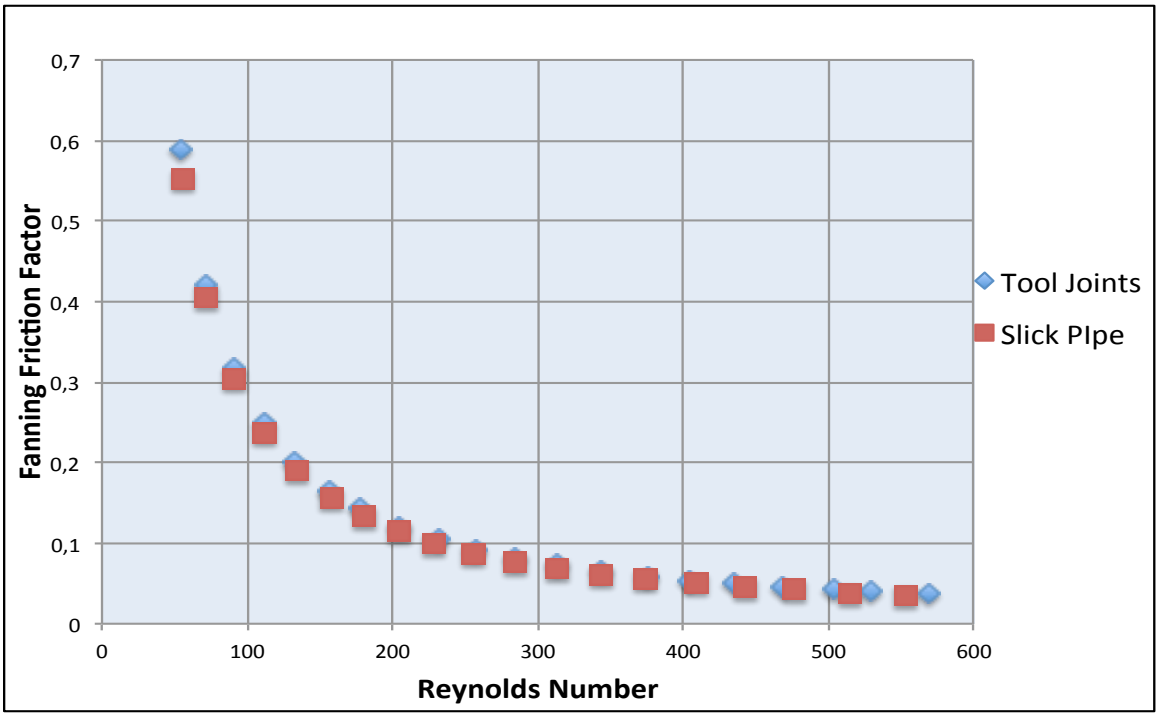

Figure 48: Measured Fanning friction factor plotted against Reynolds number for high viscosity mud

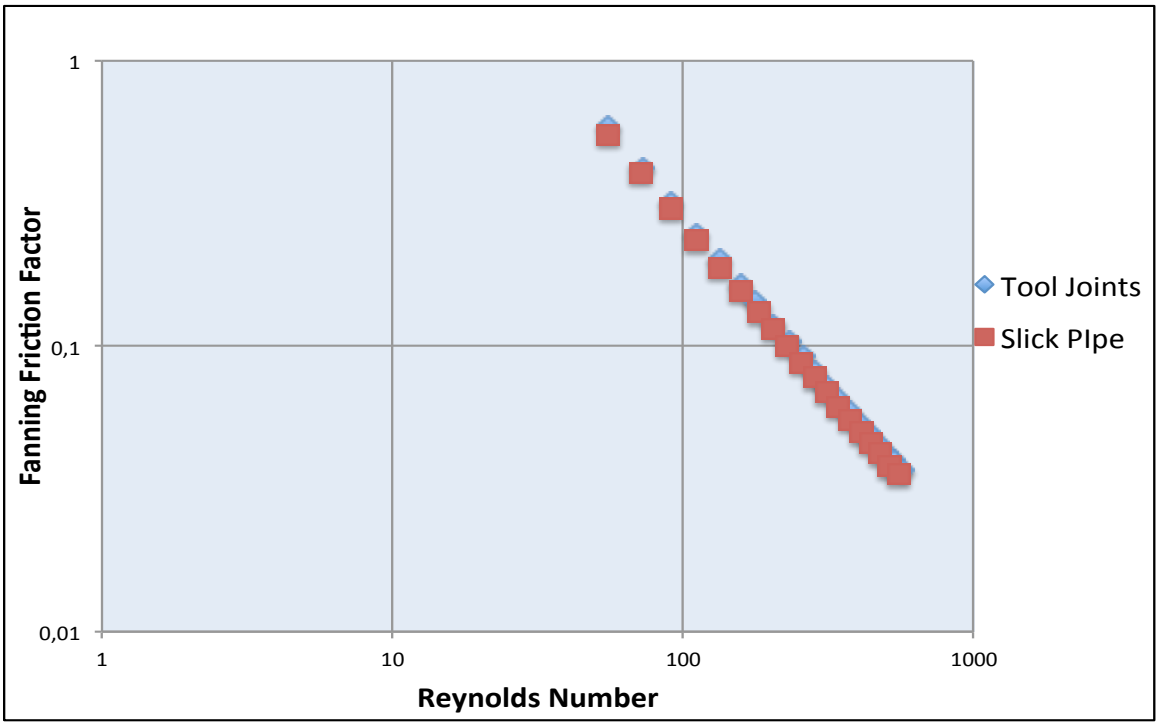

Figure 49: Logarithmic plot of measured Fanning friction factor against Reynolds number for high viscosity mud.

6 Discussion

The most important aspect, which has to be highlighted, is that the resulting pressure recordings are relative to each other. This means that even if the accuracy in the flow meter can be discussed, the consistency and amount of coinciding measurements support those relative differences between the slick pipe, tool joint section and the additional roughness.

In section 6.1 the experimental results are discussed, followed by an investigation of the accuracy in the existing models in section 6.2 In section 6.3 a modernization of the most corresponding model and a suggestive curve fitting method have been suggested and discussed before the accuracy in the experimental work and future recommendation are summarized in section 6.4

6.1 Discussion of Results

Comparing the tool joint section with the slick pipe section some distinct characterization showed in the results can be observed. Due to the presence of tool joint creating fluctuation in the velocity gradient the test carried out with tool joints in the string turns turbulent while the slick pipe does not. Due to the discrepancy in offset of turbulence it is possible to plot the relative differences between the tool joint section and the slick pipe section as in Equation 6.1, shown in Figure 50.

$$Relative\ difference = \frac{\Delta P_{Tj} - \Delta P_{Slick\ Pipe}}{\Delta P_{Slick\ Pipe}} \tag{6.1}$$

By plotting the relative difference for the low and medium viscosity and additionally for the tested flow rates for water in Figure 50, the difference between tool joint and slick pipe can be illustrated at all flow rates and a greater understanding of the tool joint effect can be obtained.

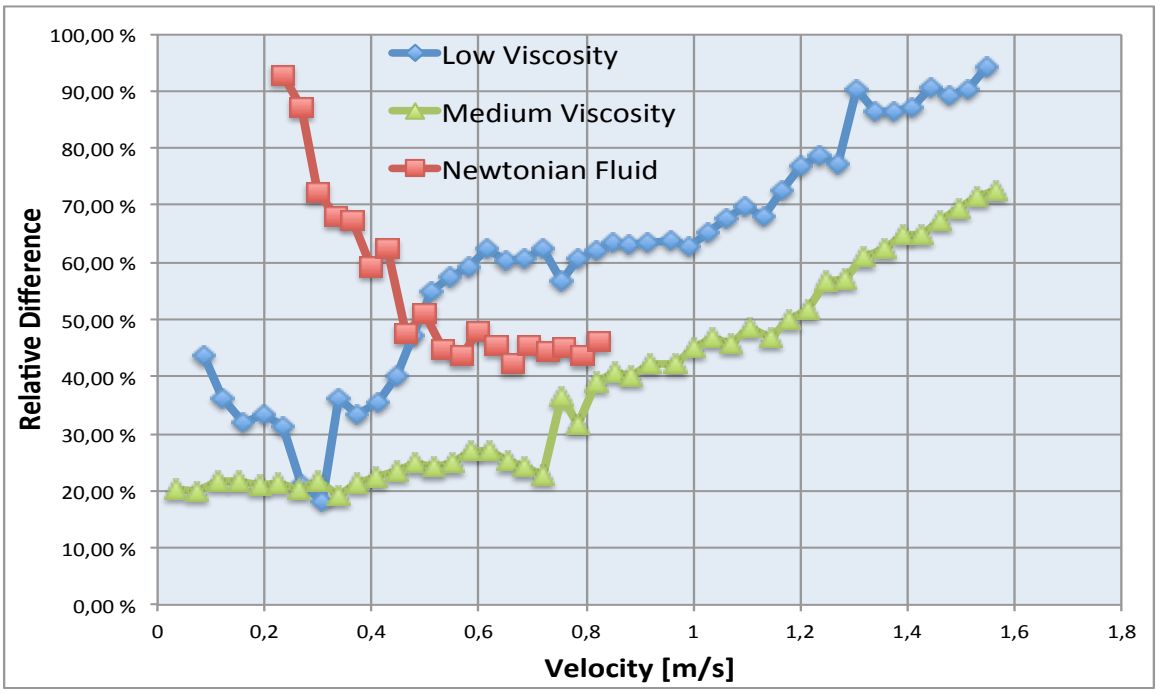

Figure 50: Measured relative difference between the tool joint and the slick pipe section

According to earlier studies there has been reported no tool joint effect in the laminar section. Based on the data obtained, showed in Figure 50, this have to be disregarded. There is no point, for none of the tested viscosities, where the pressure loss is enhanced less than 20% due to the tool joint effect.

One explanation for the enhanced pressure drop in the laminar region is the local occurrence of eddies due to the change in diameter. For the reason of the sequenced diameter changes, the ability to form a stable boundary layer is altered, which again causes larger eddies and thus a higher pressure drop according to Kolmogorov's theory, ref Chapter 3.3. As a result of the inability to form a stable viscous sublayer, one reasons for on-set of turbulence in the tool joint section can be explained.

The main difference between the Newtonian fluid and the measured muds is that there is no clear region of the flow turning turbulent in the slick pipe section for the muds, while water turns turbulent almost instantly. Due to turbulent flow regime the discrepancy between the tool joint section and the slick pipe section is most stable for water, at around 45%. Because of troubles measuring the low pressure differences in the Newtonian fluid test, the measured relative difference in the low velocity regions high and is not following the same trend line as the low viscosity and medium viscosity mud. Nevertheless, based on the trend in the Newtonian fluid, the discrepancy gradient between the tool joint section and the slick pipe section could decline and turn more stable once a enhanced turbulent region is reached in the muds.

Figure 51 visualize the effect of the viscous sublayer, were Fanning friction factor is plotted against Reynolds number with the low and medium viscosity mud. The high viscosity was neglected due to low Reynolds number measured and water due to the extremely high Reynolds number. In order to be able to visualize the effect of the sublayer Reynolds number lower than 1200 have not been included in the figure. Figure 51 show that the viscous forces due to boundary layer theory have some impact on both the tool joint section and the slick pipe section. In the slick pipe section the differences are decreasing as the mud moves towards more and more turbulent flow the effect of the viscous forces are decreasing. Due to no restrictions in the string the ability to form a sub layer with the rough pipe surface is present and the difference in friction factor evens out. In the tool joint section the less viscous fluid, causes an enhanced friction factor according to boundary layer theory.

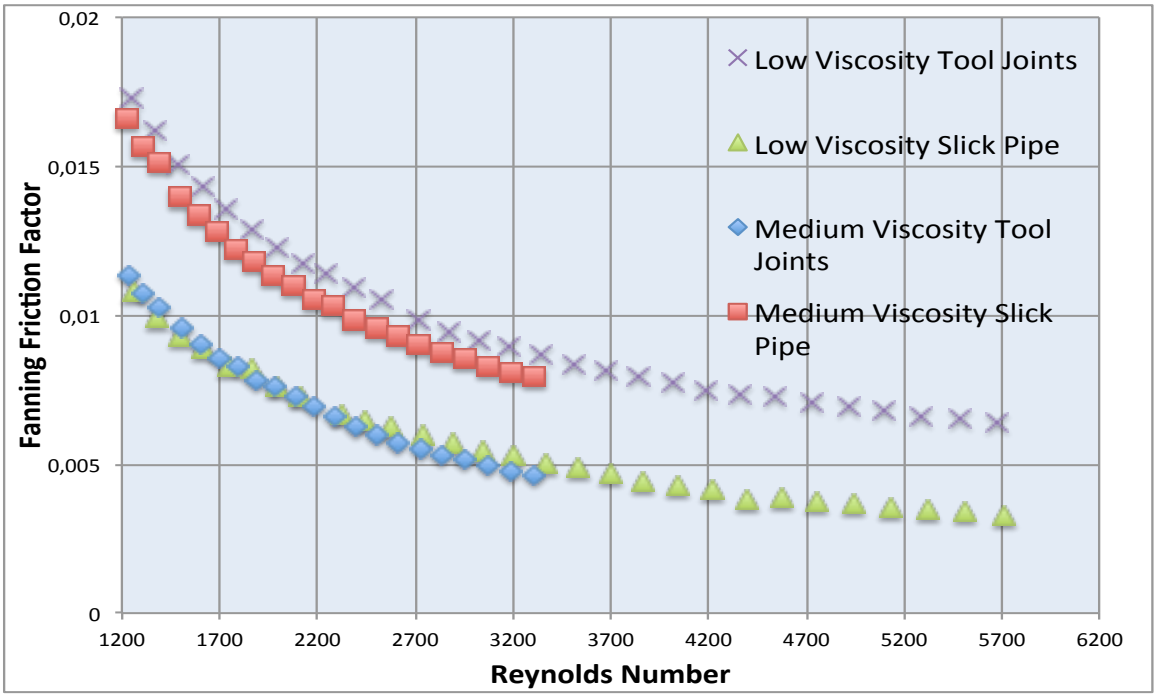

Figure 51: Fanning friction factor plotted against Reynolds number for the low and medium viscosity mud.

Comparing the tool joint section with the equivalent roughness section for the low viscosity mud and the medium viscosity mud the effect of sequenced tool joints can be highlighted, shown in Figure 52 and Figure 53. The Figures are the same as Figure 40 and Figure 43, but have been included again to ease understanding.

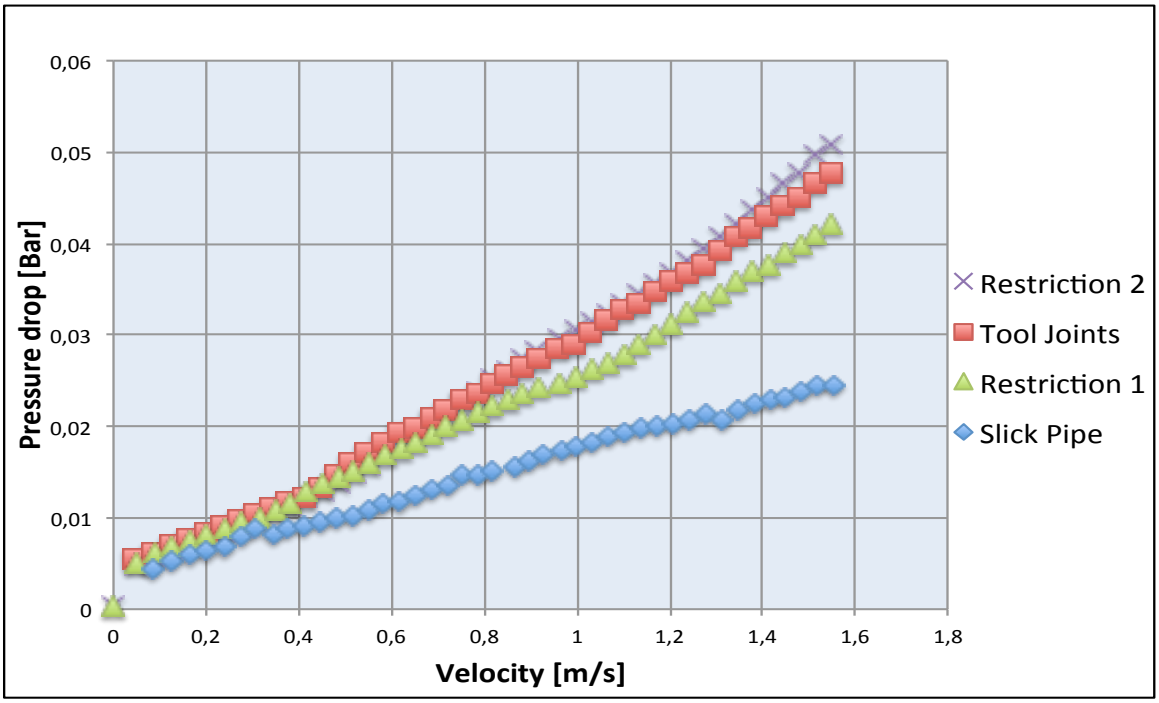

Figure 52: Additional roughness in the string compared with tool joints in the string for low viscosity fluid

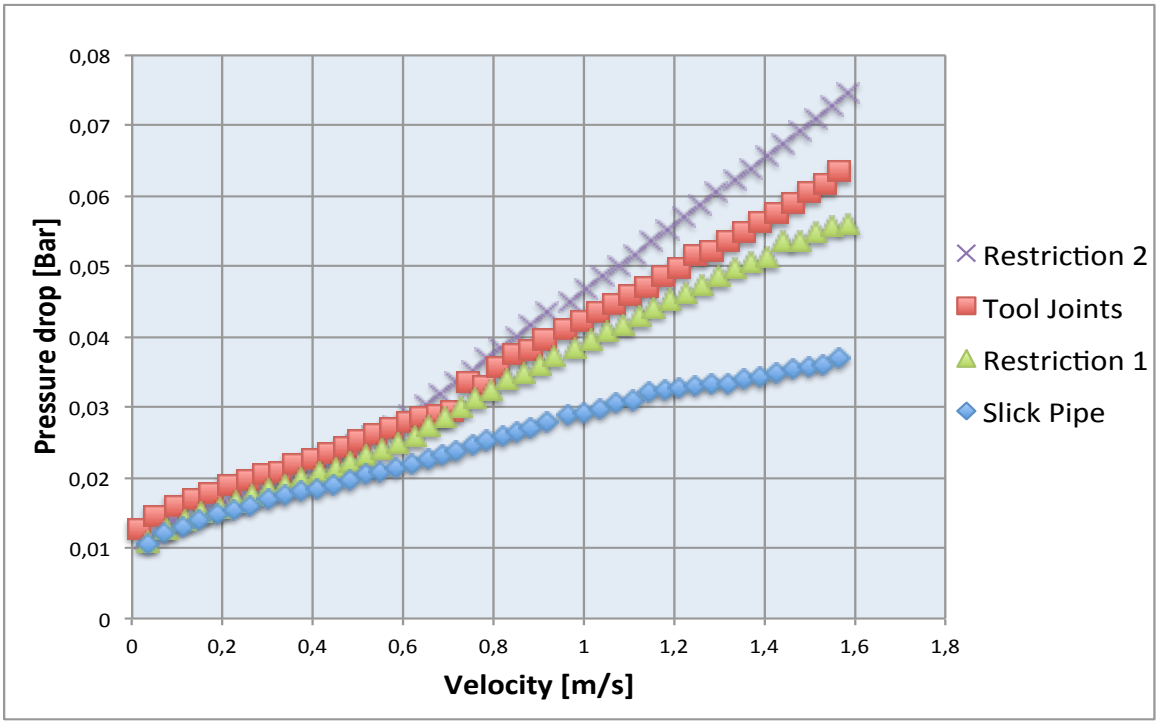

Figure 53: Additional roughness in the string compared with tool joints in the string medium viscosity mud.

Placing rough restriction with different diameter the main goal was to obtain a greater understanding and highlight the significance of tool joints in the string, thus find and equivalent obstruction causing the same pressure drop as tool joints.

Based on the data, continuous tool joints, introduces a higher pressure drop in the string than the smallest restriction. In the medium viscosity mud, the contribution from the rough interfaces higher than in the low viscosity mud due to an earlier on set of turbulence. Higher viscosity in the mud requires a rougher obstacle to turn the flow turbulent than low viscosity muds.

The additional rough restriction in the string is not larger than the tool joint section, but the rough interfaces create a rough abrupt obstacle in the well, with an angel of convergence and divergence of 90 degrees. Comparing the rough restrictions in the well it is possible to conclude that sequences tool joint in the string creates an equivalent pressure drop as placing a rough interface of significant diameter in the string and thus should be included in overall calculation of hydraulic frictional pressure loss.

6.2 Accuracy in Existing Model

To illustrate the accuracy in the existing models the medium viscosity and low viscosity mud have been applied for comparison. For the purpose to verify the existing models and thus the accuracy in the aperture the recorded readings for the low viscosity mud and the medium viscosity mud have been compared with the ordinary slick pipe calculations in Figure 54.

Assuming slick pipe, only the calculated low viscosity mud turns turbulent, while the measured pressure loss in the slick pipe does not show any indication of turbulent flow. Both the low viscosity mud and medium viscosity mud measured values is approximately between 0,01 or 0,015 bar lower than the calculated. There are three reasons for the discrepancy between the theorectical and measured pressure loss:

- The rheological model for applied is not applicable on the chosen rheology.
- The calculated model assumes too high friction factor. Previously published papers also highlights the effect of overestimated pressure loss in the laminar regions, ref. Chapter 2.
- The lab set up is not accurate enough, due to calibration errors or air in the system.

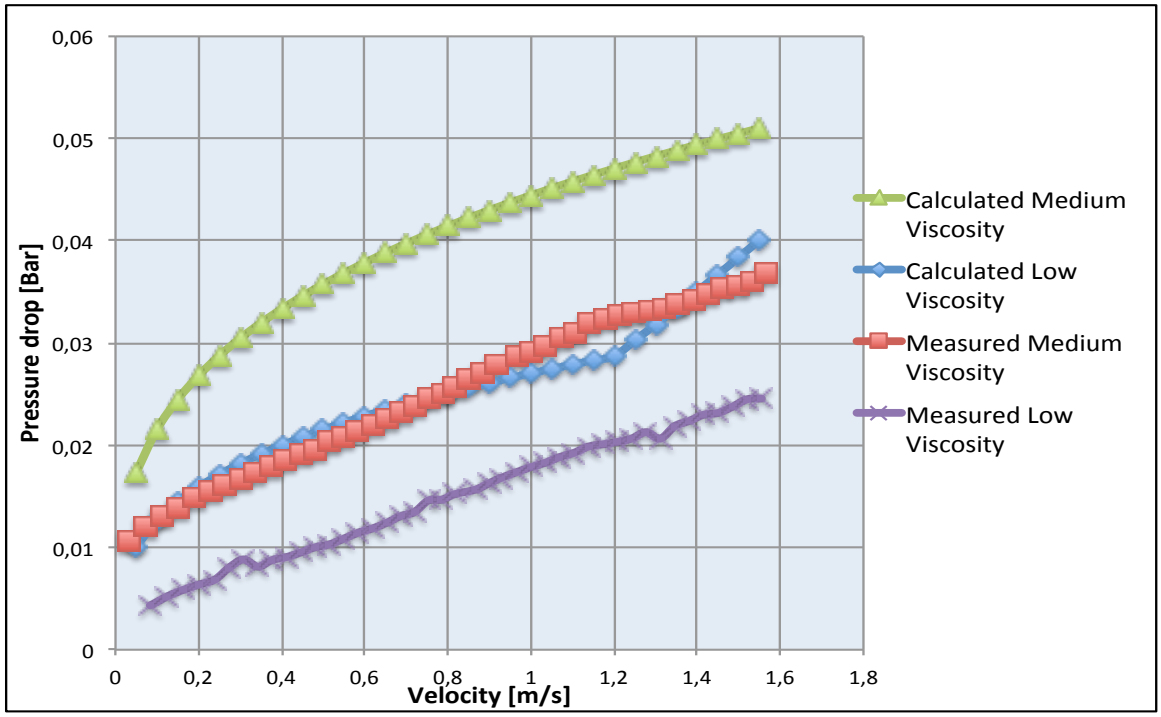

Figure 54: Calculated and measured pressure drop plotted against velocity for low and medium viscosity mud.

The trend in overestimated calculated pressure drop in the laminar region is consistent in the tool joint section for both viscosities. For the low viscosity mud the shift in the calculated flow regime clearer than for the medium viscosity mud, hence it is easier to visualize the effect of the different suggested models. By comparing the measured tool joint section with the calculated slick pipe section, it is possible to visualize the effect of incorporating tool joint in the calculation shown in Figure 55.

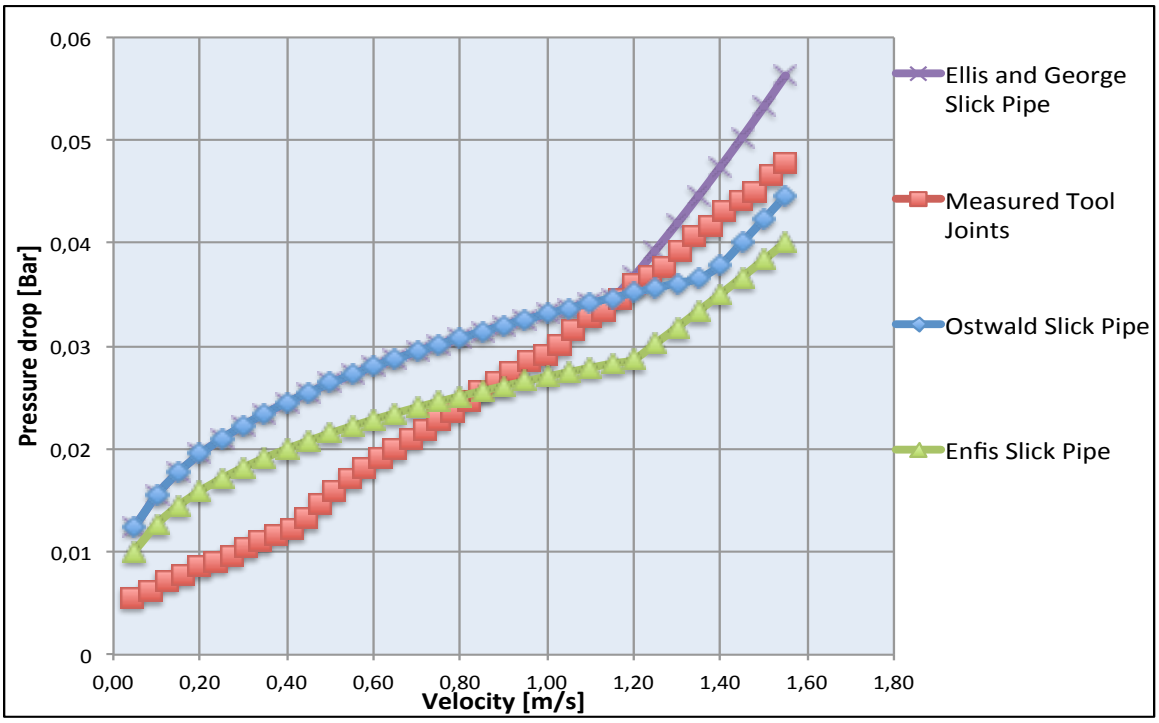

Figure 55: Pressure drop plotted against velocity for the low viscosity mud. Calculated values included are without tool joints while measured are with tool joints.

First, by looking at Calcadas suggested approach with Ellis and George correlation, the calculated estimation in the fluid is highly overestimated. The correlation suggested by Ellis and George do not include any flow index, n, in the calculation of friction factor, thus the pressure drop is highly overestimated. Applying Calcadas suggested model with Ostwald correlation, the discrepancy between the tool joint section decreased. By simply not including any correlation due to tool joints Ostwalds correlation would be within reason for the low viscosity fluid. One problem which might cause discrepancy within Ostwalds correlation is the steeper gradient compared to the measured value. If the fluid was subjected to a higher flow rate the discrepancy between the measured and calculated would be likely to increase.

Looking closer at Enfis suggested approach, the gradient of the slope in the measured and the calculated pressure drop similar, once Enfis model turn into turbulent flow. Applying Enfis approach without tool joint correlation the flow estimated pressure drop would be 17.5 % lower than the measured.

Including tool joint correlation the discrepancy in Figure 55 is significantly decreased, shown in Figure 56. Ellis and George correlation is significantly overestimated due to the elevated friction factor. Ostwald correlation causes a higher steep than the calculated, while the differences between Enfis suggested models varies from 6% at flow rate of 1.05m/s to 2.5% at 1.55m/s.

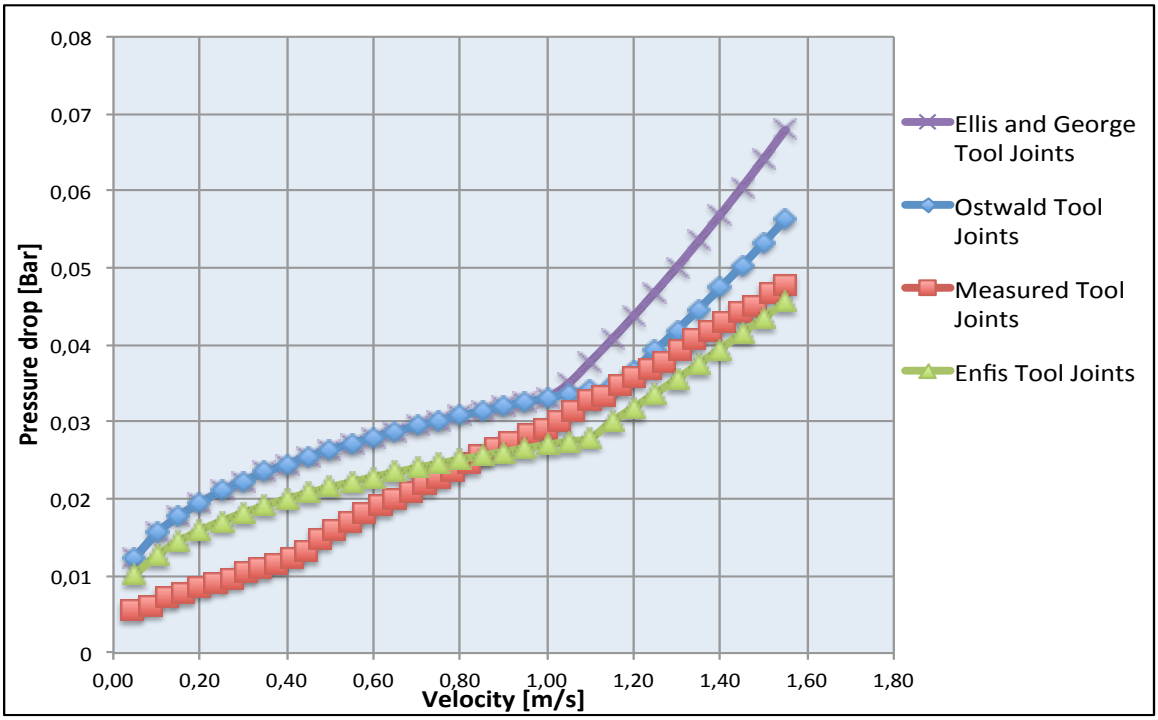

Figure 56: Pressure drop plotted against velocity for the low viscosity mud. Calculated values included are with tool joints and the measured values are with tool joints.

For low viscosity mud the neglecting of tool joints in the calculation causes the flow to turn turbulent at a later stage than incorporating tool joints in the estimation. Due to the dominating laminar regime in the slick pipe the discrepancy is higher than in the tool joint section.

For the medium viscosity mud it was harder to compare the calculated models with the measured values, for the reason that the calculated values does not turn turbulent.

In Figure 57 the difference between the measured pressure drop is plotted against the calculated values with tool joint correction. Neither Enfis suggested approach or Calcadas suggested approach with Ostwald correlation turns turbulent. While Enfis suggested model underestimates the pressure drop in the end both of Calcadas suggested friction correlation overestimates the values.

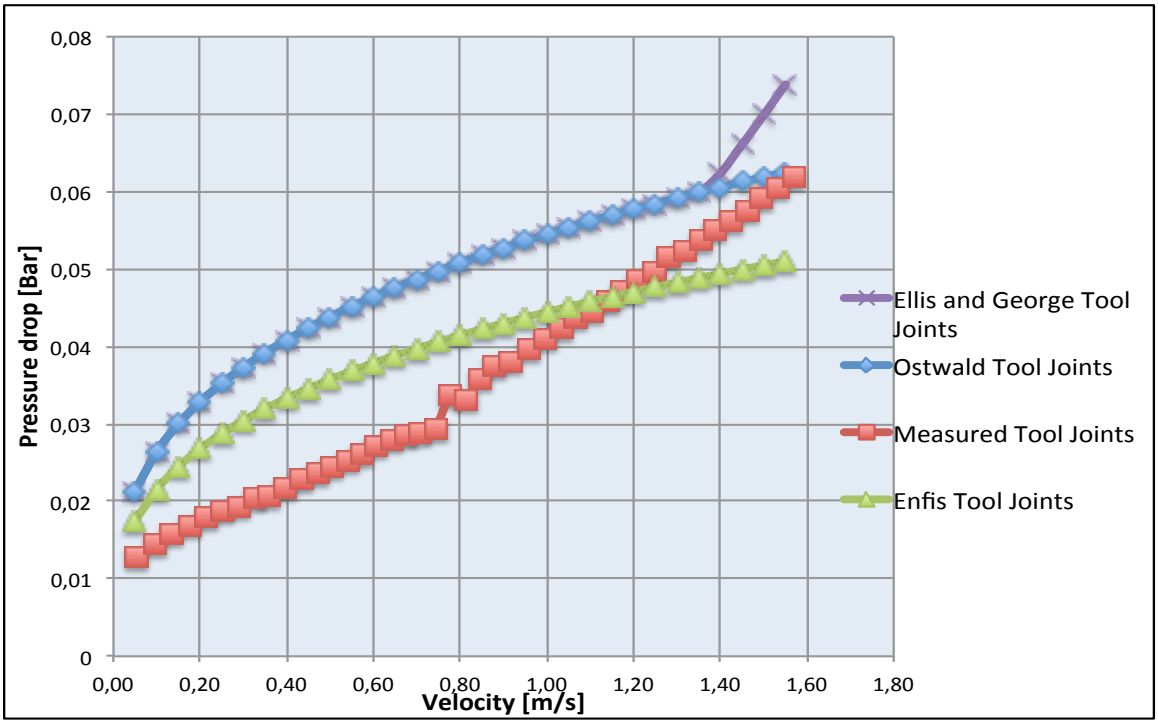

Figure 57: Pressure drop plotted against velocity for the medium viscosity mud. Comparison has been made between the suggested calculated models and the measured values.

On the basis the comparison of the models and the measured tool joint section it has to be emphasized that there are faults in the suggested models for offset of turbulence. Enfis suggested approach has to be concluded as within reason, for the low viscosity model, but not for the medium viscosity fluid. Calcadas suggested approach does not calculated results within reason for the tested viscosities for the reason that:

- Applying a slot approximation for the hydraulic radius highly overestimates the laminar pressure loss.
- The same shear stress is calculated in the narrow and in the wide zone and the contraction coefficient is slightly overestimated making the slope of the gradient higher, which will cause higher discrepancy with enhanced flow rate.

6.3 Suggested Modifications and Regression Constants

Due to the fact that the presence of tool joint introduce a equivalent pressure drop as a abrupt obstacle in the annular space and shift the transition from turbulent flow towards significantly lower flow rates, tool joint have to be included in the calculated hydraulic pressure loss. Three different approaches were investigated in order to provide more accurate results for on-set of turbulence and hydraulic pressure loss. All models suggested are in need for further investigation and experimental work. Since Enfis approach showed the most promising result, this has been used as a base.

6.3.1 Regression Factor

In Figure 61 it can be possible to curve fit the results between the slick pipe section and the tool joint section. Curve fitting of the results have been visualized on the both the low viscosity mud and the medium viscosity mud.

In hydraulic friction calculations the roughness is altered dependent on the material in use. Based on the old ideas for friction factor correlations due to roughness, a regression factor can be calculated on the basis of the increase friction by the presence tool joints in the string. In other words, by looking at the additional friction due to tool joints as a rough interface in the string, instead of a geometric obstacle in the well, a correlation can be suggested based on the measured pressure drop versus Reynolds number. This is the same approach as the old correlation suggested by e.g. Blasius and Dodge and Metzner. As Figure 58 display, the relationship between the tool joint section and the slick pipe section can be calculated as a function of Reynolds number applying regression and a regression constant can be obtained.

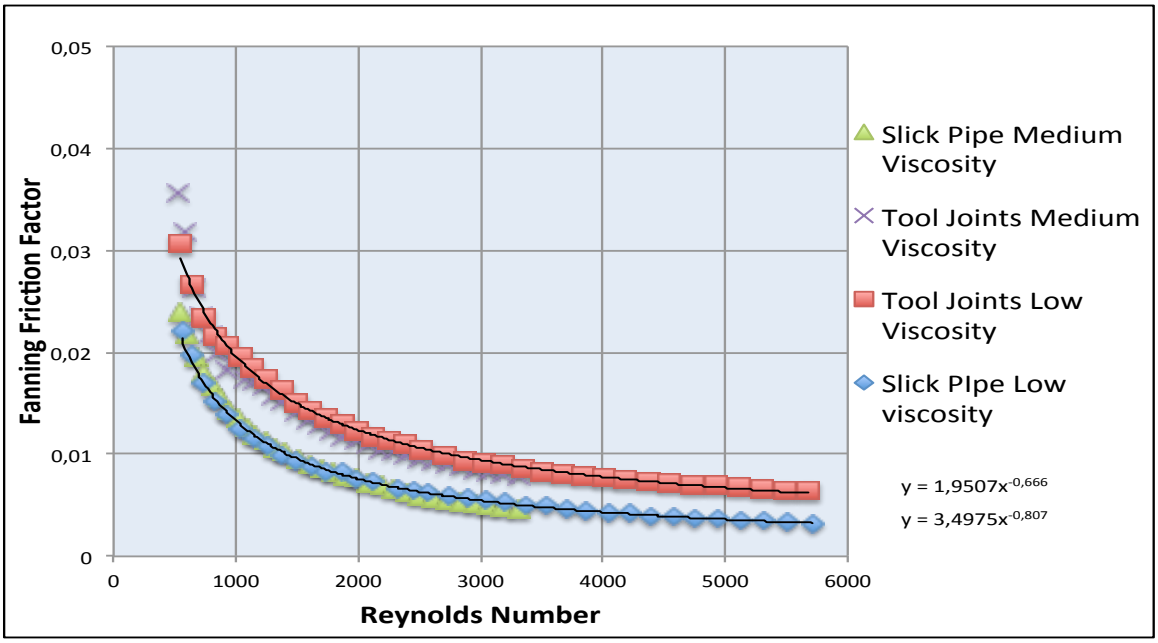

Figure 58: Fanning Friction Factor plotted against Reynolds number for the low viscosity and medium viscosity mud.

Dividing the regression from the tool joints section on the slick pipe section it is possible to create a relationship for the additional friction factor based on the Reynolds number, shown in Equation 6.2 Due to some instability in the Low Reynolds number only readings with higher Reynolds number than 500 have been included.

$$\%increase\ f = 1.7929 * \mathrm{Re}^{-0,141} \quad (6.2)$$

By calculation a factor for additional friction due to tool joints it can be possible to derive a database with altering parameters, such as: rheology, annular clearance and tool joint geometry.

The results of applying the regression factor for low viscosity mud is shown in Figure 59 and Figure 60 illustrates the results are overestimated at high flow rates. The positive feature by applying the regression factor on the low viscosity mud is that it more accurately estimates the on set of turbulence, compared with the previous analyzed models.

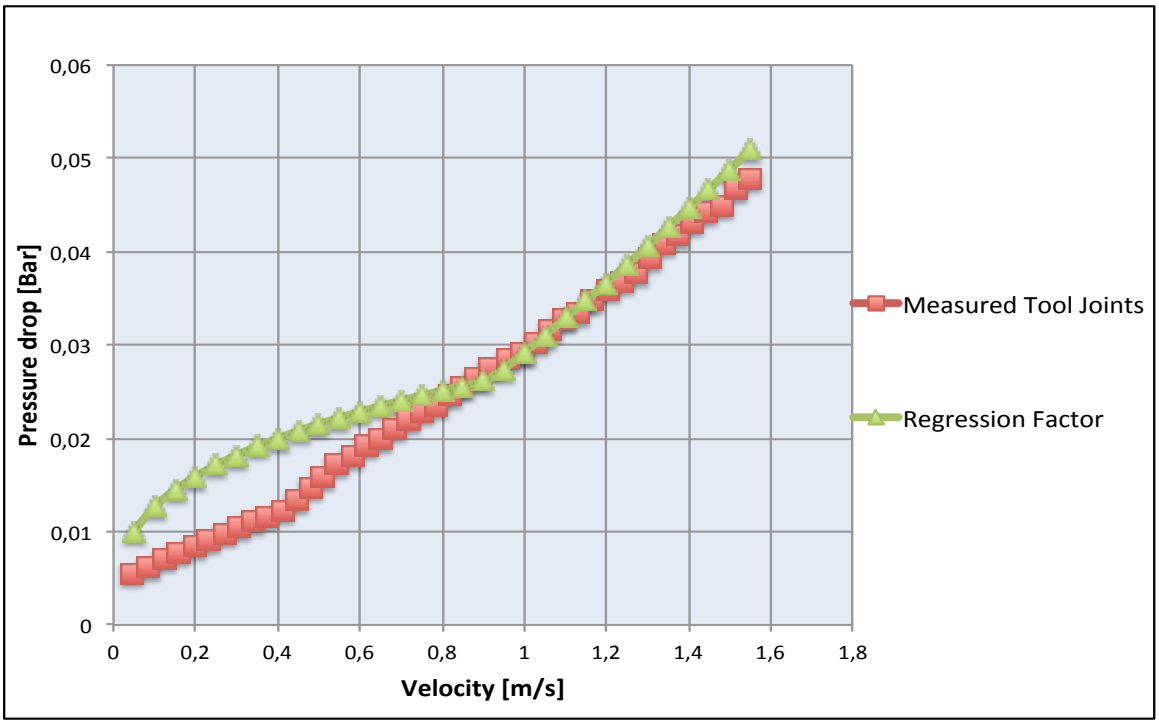

Figure 59: Measured tool joint section plotted against regression constant approach for low viscosity mud.

Approaching the medium viscosity mud with the cluster factor method the Equation becomes as shown in 6.3, With the responding results shown in Figure 60.

$$\%increase\ f = 1.9739 * \mathrm{Re}^{-0,146} \quad (6.3)$$

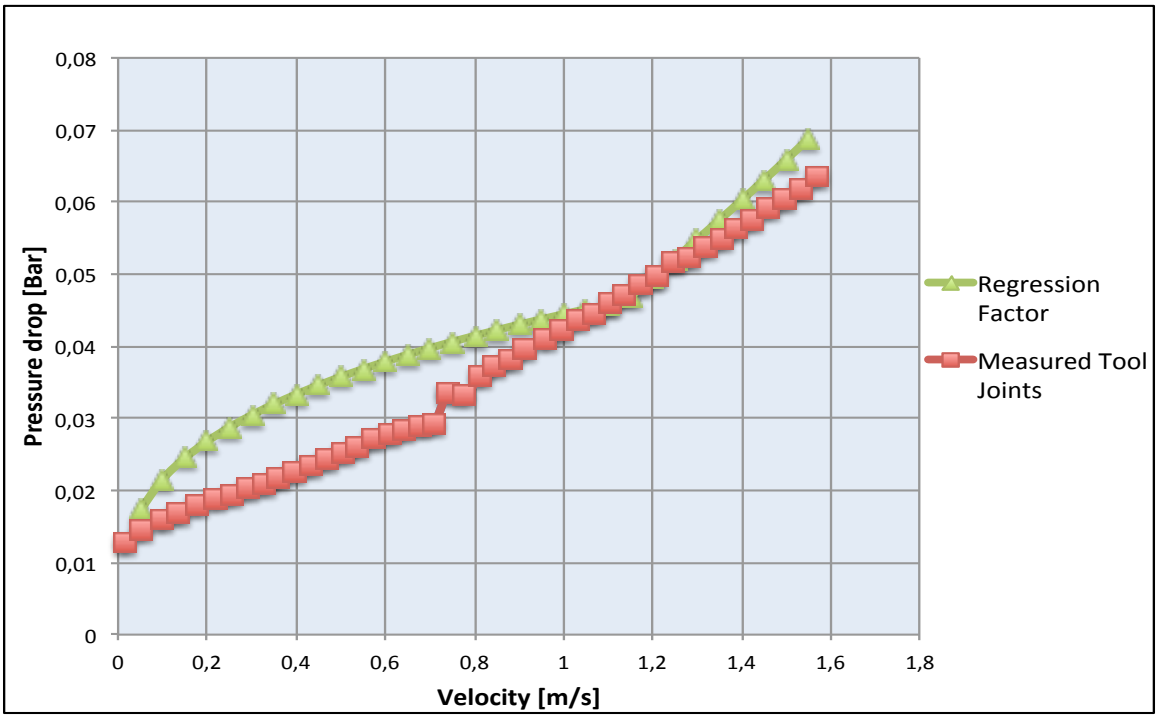

Figure 60: Measured tool joint section plotted against regression constant approach for medium viscosity mud.

Utilizing the regression factor method yields the best result on the medium viscosity mud of all models investigated. The equations for tool joint correction are highly sensitive on the Reynolds number at hand and due to the uncertainty in Reynolds number (almost 140 at the highest measured flow rate) the ability to accurately calculate correlation differs.

An important aspect of curve fitting the results is that the additional tool joint is a contribution or a additional friction factor, to the frictional factor already applied. In this investigation Dodge and Metzner have been applied. If another friction factor for slick pipe is utilize the results will be altered.

For that reason that the regression factor is a result of curve fitting the results it is not surprising that the calculated and estimated values comprehends the most. Nevertheless, it also visualize that by looking at tool joint as additional roughness, increasing the friction in the string, instead of a obstacle, the resulting estimated values could more accurately calculate of-set of turbulence and thus a correct pressure drop.

6.3.2 Relative Difference

The second mathematical approach was simply to calculate the relative difference between the measured tool joint section and the measured slick pipe, before averaging the value and thus apply it on the slick pipe equations. Utilizing the approach on the medium viscosity mud the discrepancy in Figure 57 is reduced due to and earlier on-set of turbulence, shown in Figure 61

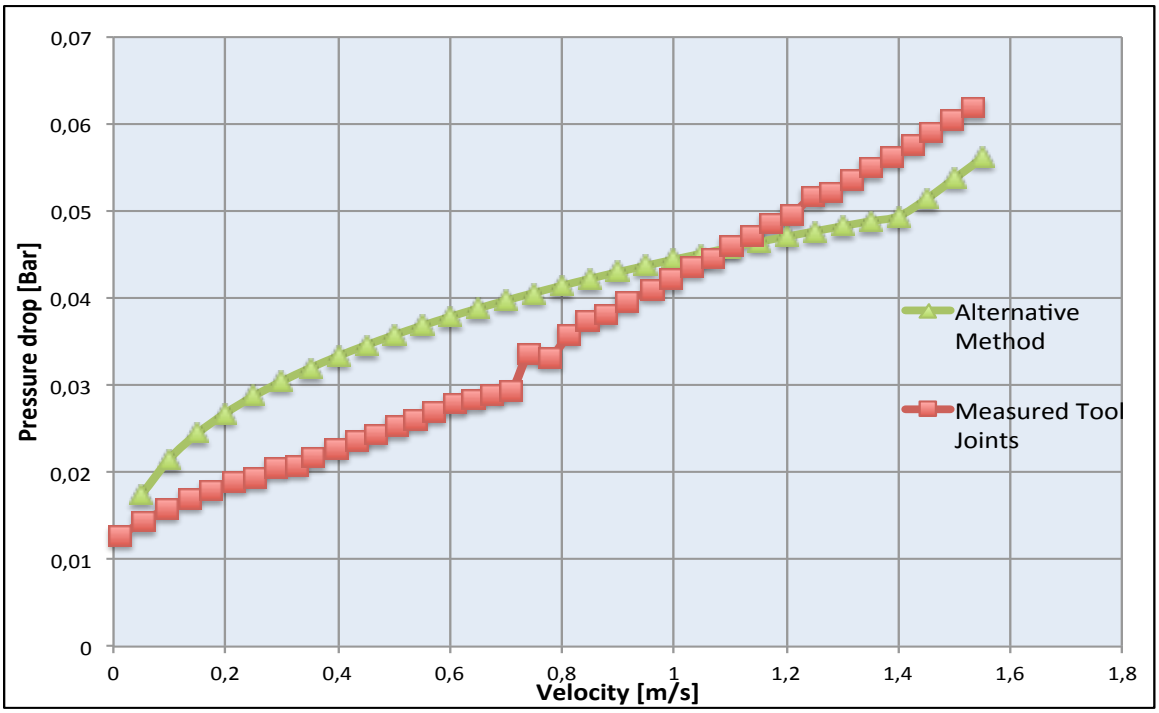

Figure 61: Relative difference approach on tool joint correction with medium viscosity mud.

Based on Figure 61 and applying the same method on the low viscosity mud the results are promising, but in need for further investigation. Due to viscosity changes, the relative difference varies and in reality this is just a simple way of curve fitting the results. On the other hand could a increased relative difference, calculated on the basis of the mud and geometry difference in the annular clearance be a simple way to roughly estimation in the field.

6.3.3 Modification of Enfis Suggested Model

Both Calcada and Enfis have contraction and enlargement angles of 18° and 36° respectively. Still both of them applies the coefficient suggested for angles larger than 45°, shown in equation 6.4 and 6.5 instead of equation 6.6 and 6.7.

Interval 45°<θ≤180.

$$K_e = (1 - R)^2 \tag{6.4}$$

$$K_c = 0{,}5\sqrt{(1 - R^2)\sin\frac{\theta}{2}} \tag{6.5}$$

Interval 0°<θ≤45.

$$K_e = 2.6\sin\frac{\theta}{2}(1 - R^2)^2 \tag{6.6}$$

$$K_c = 0.8\sin\frac{\theta}{2}(1 - R^2) \tag{6.7}$$

Utilizing the suggested expansion and contraction coefficients the discrepancy between the measured and the calculated frictional pressure drop decreases compared to Figure 56, shown in Figure 62. As there were no on set of turbulence, hence no change due to tool joints in the medium viscosity mud (ref. Chapter 6.1) the result of the modification have only been showed in the low viscosity mud.

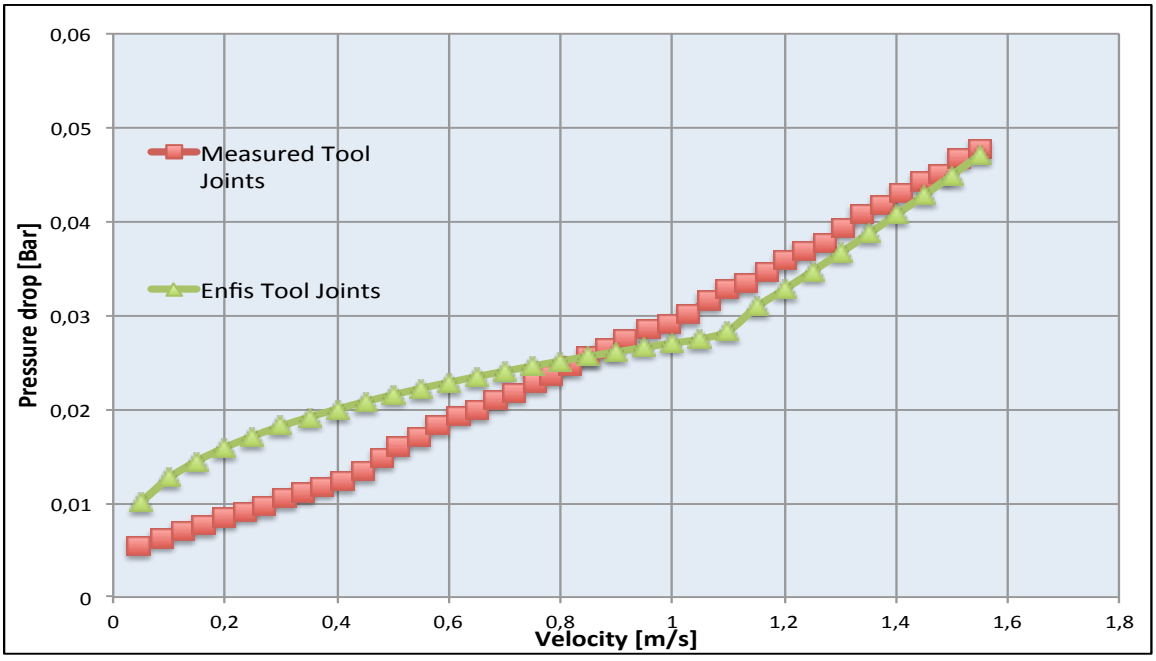

Figure 62: New friction coefficients applied on the low viscosity mud

Plotting the measured pressure drop against the calculated, for the measured flow rates, with the old and the new coefficients in Figure 63, the small difference is revealed. A fully accurate model would create a 45 degree slope. Based on Figure 66 the old coefficient has a steeper gradient than the new coefficient and will create larger differences at higher flow rates, than the old coefficient.

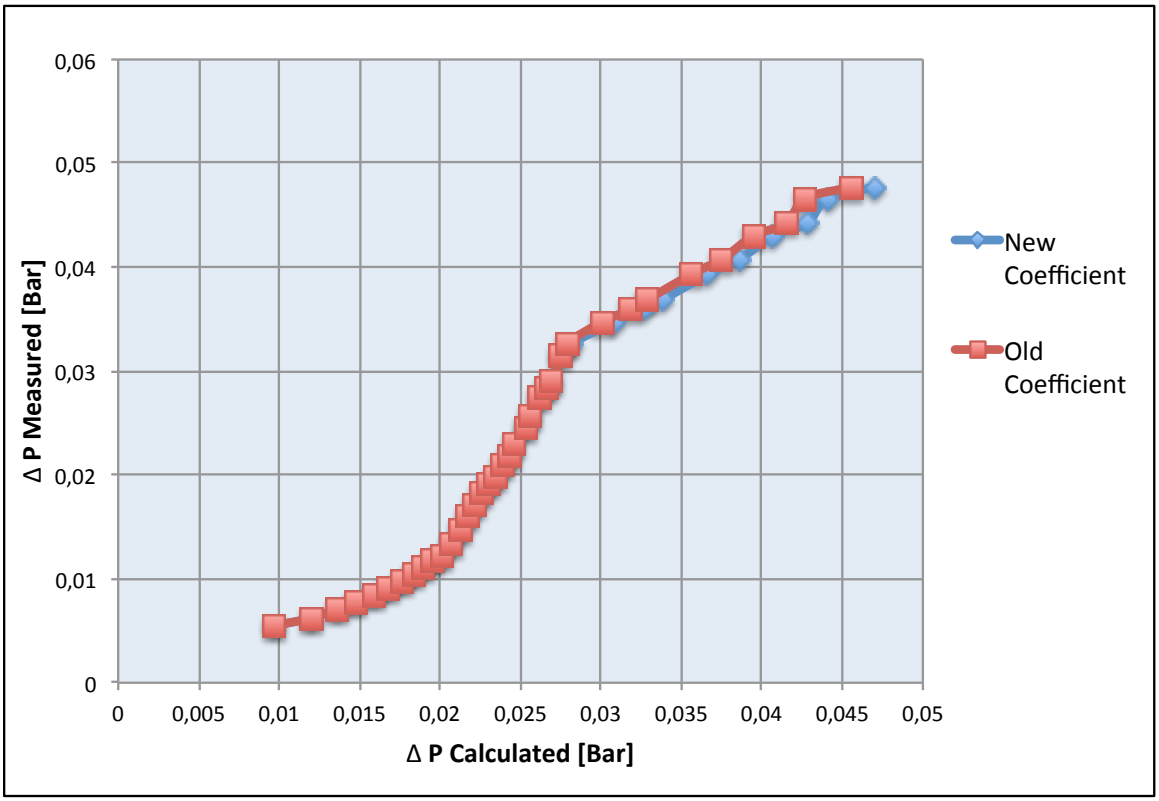

Figure 63: Measured pressure loss plotted against calculated for the new coefficient and the old.

6.4 Future Recommendations

Based on an overall comparison of the alternative method with the previously suggested models the regression factor method showed the most promising results. The results from the suggested model by Calcada did not yield accurate results, while the model suggested by Enfis matched the calculated results in the low viscosity mud but not in the medium viscosity mud. By highly underestimating the point of on-set of turbulence and thus overestimation in the pressure loss in the laminar region, the calculated results becomes wrong in the tool joint section. The laminar regions are equation based on slick pipe correlation and do not incorporate the effect of contraction and extraction in the string, which on-set the turbulence.

By looking at the tool joint as addiational roughness in the string, instead of a diameter contraction and expansion a more accurate picture could be obtained. Neglecting tool joint in the hydraulic pressure loss calculation would be the same as not altering the roughness if the material in use is changes from concrete to steel. Compared with Enfis suggested approach the regression factor is in need for a predetermined database. By creating a small scale experiments with the standard measurements with respect to tool joints size, annular clearance and standard mud.s it could be possible to easily calculate the effect of tool joint in similar wells, as the main goal of the investigation provided by Scheid et al (2009 and 2011) and Calcada et al (2012). Creating regression factors based on the diameter could be applied on the simple slick pipe calculation for the fluids and will be applicable on all friction factor correlations.

As mentioned, is the regression factor approach highly sensitive to Reynolds number in these experiments, hence the measurements in the flow meter. When working with extremely small measurable data the accuracy in the aperture is significant. As all laboratory experiments, this experiments has to highlight some important weak spots.

Based on the calculated errors in Chapter 5.4 and additional analysis utilizing the same approach, the end contribution on the Fanning friction factor and the Reynolds number is varied. Reaching the higher Reynolds number the errors decreases and more reliability can be given to the results. As the transformation from laminar to turbulent flow regimes accuracy at high flow rates and pressure losses, the calculated uncertainty is not high enough to alters the results.

A major set back in the readings was the inability to calibrate the pressure transducer with available methods in the lab. It was not possible to pressurize up the system in the lab to a known pressure before measuring the differential pressure. It was also not possible to measure the static differences by utilizing different water heights due to air bubbles in the system. In consultation with the provider of the aperture it was concluded that the pressure transducer did not need additional calibration.

Due to the limitation in the electrical wiring it was not possible to measure flow rates higher than 27Hz in the pump. Based on the 27 previous flow rates the 18 next was extrapolated. Based on the excessive amount of flow rates earlier the extrapolated vales does not create a lot of uncertainties. Even though thoroughly calibration by weighting the water, showed fairly accurate results in the flow meter a systematical error of 2% is to high for sensitive measurements. In order to improve future investigations the flow meter should be replaced with one or two more accurate aperture.

7 Conclusion

In this thesis tool joints have been investigated separately and not in the collaboration with string rotation, presence of cuttings and concentricity of the pipe, which all are major contributors on on-set of turbulence and enhanced pressure loss. Focusing on the tool joints separately it was possible to pinpoint the contribution and effect on the resulting hydraulic pressure drop. Based on the experimental data some main observation is highlighted:

- The presence of tool joints in the string highly increases the hydraulic pressure loss in the string, dependent on the flow rate and the viscosity of the mud.
- The highest measured enhanced pressure loss was registered in the low viscosity mud with more than 90% increased pressure loss. In the medium viscosity mud the highest measured pressure loss were more than 70%.
- Based on all test carried out there is a significant contribution from tool joints in the laminar flow region.
- Even though the high viscosity mud was not measured at the highest flow rates it supported the observation of increased pressure loss in the laminar region due to tool joints.
- Continuous tool joints in the string cause a pressure drop equivalent to a rough interface, blocking the fluid flow in the annulus.

Comparing the measure values with the existing models the findings were:

- Due to the choice of tool joints the flow turns turbulent at an earlier stage than the calculated, none of the existing models are able predict this fact.
- The pressure in the laminar region is highly overestimated compared to the measured values in all test conducted.
- Due to the choose in hydraulic diameter, the shear force in the narrow region and the friction factor correlation suggested by Calcada et al (2012) highly overestimate the hydraulic pressure loss.
- Enfis et al. (2011) coincide the most with the measured pressured loss of the previously suggested models
- Modification of Enfis et al. (2011) suggested model yielded better results than the old one.
- Instead of looking on tool joints as a restriction in the string it could be looked upon as additional roughness, and thus increase the ability to predict accurate pressure loss.
- At medium viscosity mud the regression factor is the only approach which predicts coinciding results as the measured pressure loss in the joint section

In order to further investigate the tool joint effect and be able to accurately calculate the hydraulic pressure loss, different studies can be taken on:

- By utilizing different geometrical variance in tool joint geometry, annular clearance, amount of tool joints in the string and varied rheological properties it can be possible to obtain a data base for the cluster factor.

- The test has to be carried out with improved laboratory and additional equipment with regards to flow rates

8 References

Ahmed, R., Enfis, M., Miftah-El-Kheir, H., Laget, M,. and Saasen,.A. 2011. The Effect of Drillstring Rotation on Equivalent Circulation Density: Modeling and Analysis of Field Measurements. SPE 135587. Presented at SPE Annual Technical Conference and Exhibition, 19-22 September 2010, Florence, Italy.

Bakker. A. 2002-2006. Lecture 8 – Turbulence. Applied Computational Fluid Dynamics. Link: http://www.bakker.org/dartmouth06/engs150/08-turb.pdf

Bakker. A. 2002-2006. Lecture 9 – Kolmogorov's theory. Applied Computational Fluid Dynamics. Link: www.bakker.org/dartmouth06/engs150/09-kolm.ppt

Bakker. A. 2002-2006. Lecture 4 – Classification of Flows. Applied Computational Fluid Dynamics Link: http://www.bakker.org/dartmouth06/engs150/04-clsfn.pdf

Bakker. A. 2002-2006. Lecture 11 – Boundary Layers and Separation. Applied Computational Fluid Dynamics Link: http://www.bakker.org/dartmouth06/engs150/04-clsfn.pdf

Burgoyne, A. T., Chenevert, M. E., Millheim. K. K., and Young. F. S. 1991. Applied Drilling Engineering, Vol 2. Texas: Monograph Series, SPE.

Calçada. L. A,. Eler, F. M., Paraiso., E. C. H., Scheid, C. M., and Rocha, D. C. 2012. Pressure drop in tool joints for the flow of water-based muds in oil well drilling. Brazilian Journal of petroleum and gas. Page 145-157. ISSN 1982-0593.

Cartalos, U and Piau. J.M., 1992. Pressure drop scaling laws and structural stress contributions for complex flows of flexible polymer solutions in thick solvents. Journal of Non-Newtonian Fluid Mechanics Volume 44, September 1992. Pages 55‑83.

Cartalos, U and Dupuis, D. 1993. An Analysis Accounting for the Combined Effect of Drillstring Rotation and Eccentricity on Pressure Losses in Slimhole Drilling. SPE/IADC 25769, The paper was prepared for presentation at the SPElIADC Drilling Conference held in Amsterdam 23-25 February 1993

Cengel Y, A. and Cimbala, J. M. 2010. Fluid Mechanics; Fundamentals and Applications, Second Edition in SI units.

Crane Company. 1981. Flow of Fluids through Valves, Fittings, And Pipe, Technical Paper 410, Crane Co., Chicago, IL,

Dodge, D.W. and Metzner, A.B. 1959. Turbulent Flow of non-NewtonianSystems, AIChE J. (1959) 5, No.2, 189-204.

Farshad. F.F., and Rieke. H. H. 2006. Surface-Roughness Design Values for Modern Pipes. SPE 89040. Journal SPE Drilling & Completion Volume 21, Number 3

Fester.V., Mbiya. B and Slatter. P. 2008. Energy losses of non-Newtonian fluids in sudden pipe contractions. Chemical Engineering Journal 145 (2008) 57–63

Finnemore, E, J., and Franzini, J, B. 2002. Fluid Mechanics with Engineering Applications Tenth Edition, Published by Mcgraw-Hill

Husveg, T. 2007.Operational Control of Deoiling Hydrocyclones and Cyclones for Petroleum Flow Control. Doctorial Thesis University of Stavanger. Stavanger. Norge.

Langlinais. J.P., Bourgoyne Jr., A.T. and Holden, W.R., 1983. Frictional Pressure Losses for the Flow of Drilling Mud and Mud/Gas Mixtures. SPE 11993. Presented at the 58th Annual Technical Conference and Exhibition held in San Francisco, CA, October 5-8, 1983

McCann, R.C., Quigley, M.S., Zamora, M., and Slater, K.S. 1995. Effects of High Speed Rotation on Pressure Losses in Narrow annuli. SPE 26343 J. SPE Drilling and Completion 10 (2): 96-103

McDonough. J. M. 2007. Introductory lectures on turbulence in physics, mathematic and modeling. Department of Mechanical Engineering and Mathematics University of Kentucky. Link: http://www.engr.uky.edu/~acfd/lctr-notes634.pdf

Metzner, A.B. and Reed, J.C. 1955. Flow of non-Newtonian Fluids- Correlation of the Laminar, Transition and Turbulent Flow Regions, AIChE J 1, No.4, 434-40

Moises, A.S., and Shah, S, N., 2000 Friction Pressure Correlations of Newtonian and Non-Newtonian Fluids through Concentric and Eccentric Annuli. SPE 60720. Presented at SPE/ICoTA Coiled Tubing Roundtable, 5-6 April 2000, Houston, Texas.

Ochoa, M, V. 2006. Analysis of Drilling Rheology and Tool Joint effect to reduce Hydraulic Calculations. Doctorial dissertation Texas A&M University

Ogugbue. C.C., Shah. S.N.2010. Laminar and Turbulent Friction Factors for Annular Flow of Drag-Reducing Polymer Solutions in Coiled-Tubing Operations. SPE 130579. Presented at the SPE/ICoTA Coiled Tubing and Well Intervention Conference and Exhibition held in The Woodlands, Texas, USA, 23–24 March 2011

Skalle, P. and Ventus Publishing. Drilling Fluid Engineering ©. Link: http://bookboon.com/no/laereboker/geoscience-eboker/drilling-fluid-engineering. Accessed 2011. ISBN 978-87-7681-929-3 2011.

Simoes, S,. Yu, M,. Miska, S and Takach, N, E,. 2007. The Effect of Tool Joints on ECD while drilling. SPE 106657. Presented at SPE Production and Operations Synposium, Oklahoma City, Oklahoma, USA., 31 March – 3 April 2007

Scheid C.M., Calcada L.A., Rocha, D.C., Aranha P.E., Aragao. A.F.L, and Leibsohn Martins. A., 2009. Prediction of Pressure Losses in Drilling Fluid Flows in Circular and Annular Pipes and Accessories. SPE 122072. Presented at Latin American and Caribbean Petroleum Engineering Conference, 31 May-3 June 2009, Cartagena de Indias, Colombia

Scheid C.M., Calcada L.A., Braga E.R., Paraiso,E.C..H and Martins, A.L. 2011. Hydraulic Study Of Drilling Fluid Flow in Circular and Annular Tubes. BRAZILIAN JOURNAL OF PETROLEUM AND GAS 239-253 1982-0593

Sletfjerding, E. 1999. Friction Factor in Smooth and Rough Gas Pipelines. PhD Dissertation Norwegian University of Science and Technology. Trondheim. Norge. 1999.

Shah. S: N., 1990. Effect of Pipe Roughness on Friction Pressures of Fracturing Fluids, SPE 18821. Production Engineering Volum 5, Number 2 May 1990. Pages 151-156.

Subramanian. R. and Azar. J. J., 2000. Experimental Study on Friction Pressure Drop for NonNewtonian Drilling Fluids in Pipe and Annular Flow. SPE 64647. Presented at International Oil and Gas Conference and Exhibition in China, 7-10 November 2000, Beijing, China

Mme, U. 2013. Using Lab View / Application of Field Data from Well C47. Internal Manual IPT NTNU

Van der Zande, M.J., Muntinga, J.H., and van den Broek, W.M.G.T. 1998. Emulsification of Production Fluids in the Choke Valve. SPE 49173. Presented at SPE Annual Technical Conference and Exhibition, New Orleans, Louisiana, 27-30 September 1998

White, F. M. 2008. Fluid mechanics (Sixth Edition ed.). McGraw-Hill, New York.

Internet pages:

Epifanov. V.M. Thermopedia. Boundary Layer. Accessed: 10.3.2013. Link: http://www.thermopedia.com/content/595/. DOI: 10.1615/AtoZ.b.boundary_layer

9 Nomenclature

Abbreviations

CFD	Computational Fluid Dynamics
ECD	Equivalent Circulation Density

Symbols

A_N	Narrow annulus
A_W	Wide annulus
A_0	Orifice Cross Sectional Diameter
D	Diameter
D_e	Effective Diameter
Ė	Energi Disipation
D_{TJ}	Tool Joint Diameter
K	Flow Consistency Index Poewer Law Fluids
Kc	Contraction Coeffient
Ke	Enlargement Coefficient
ΔP	Absolute Pressure Drop
L	Length
LP	Total Pipe Length
LEU	Tool Joint Length
Ldiss	Length Dissipation Zone
m_{diss}	Mass Dissipation Zone
n	Flow behaviour Power Law Fluids
R	Diameter Ratio (Dn/Dw)
r	Radius
Re	Reynolds Number
Q	Flow rate

Greek Letters:

$\bar{\bar{v}}$	Mean Fluid Velocity
μ	Fluid Viscosity
τ	Shear Stress
$\bar{\gamma}$	Shear Strenght
f	Friction Factor
δ	Boundary Layer Size
ε	Roughness
$\dot{\varepsilon}$	Energy Dissipation rater per unit mass
ρ	Fluid Density
ρ_c	Continous Phase Density

Appendix A: Theoretical Calculated Results

The theoretical difference of the Friction factor correlations and the effect of equivalent diameter have been given in order to illustrate the end effect on the resulting pressure the choice in the predetermine assumptions.

Effect of Friction Factor Correlation

In order to visualize the effect of chosen friction factor correlations for Newtonian fluids, described in Chapter 4, some assumptions has to be made:

- In most mathematical applications, roughness has not been measured by means of modernized equipment and thus roughness has to be assumed from standard tables. From the roughness chart shown in Figure 13, roughness of a steel pipe is $46*10^{-6}$ m. By assuming the same roughness in the inner pipe and outer pipe, roughness has been considered to be $96*10^{-6}$ m in both Colebrooks and Chens correlation.
- The equivalent diameter in the calculation of Reynolds number and pressure loss has been the slot. By utilizing $0.816(D_1-D_0)$ compared to simply D_1-D_2 the pressure drop is enhanced and the end result has some degree of conservatism in the estimation.

In Figure 64, the different friction factor correlation have been plotted against Reynolds number. Due to the surface roughness there is a relative large deviation between the Colebrooke-White and Chen correlations compared to Moore and Blasius suggested correlations.

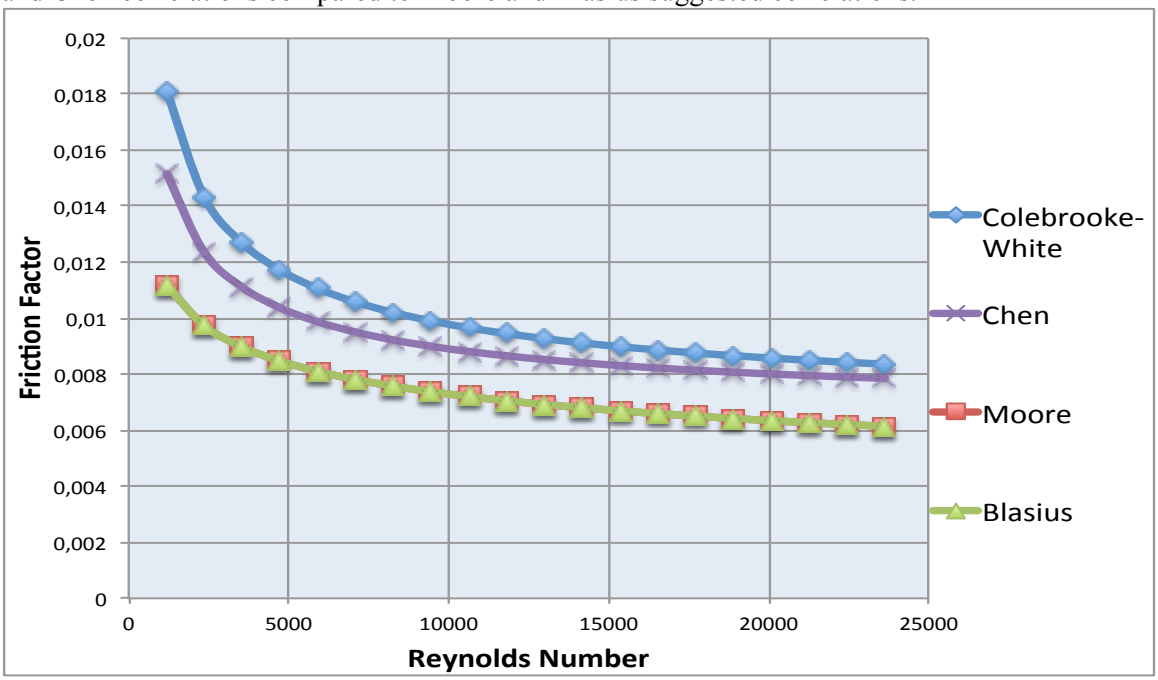

Figure 64: Theoretical calculated friction factor plotted against Reynolds number for the suggested correlations with Newtonian fluid.

Utilizing the universal pressure law it is possible to obtain a picture of the resulting theoretical calculated pressure loss with regard to velocity and distance in the pipe, shown in Figure 65. From Figure 65 it becomes clear that the selection of frictional correlation is essential. By applying the Blasius correlation compared to Colebrook equation a discrepancy of more than 25% can be detected due to the incorporation of roughness in the equation.

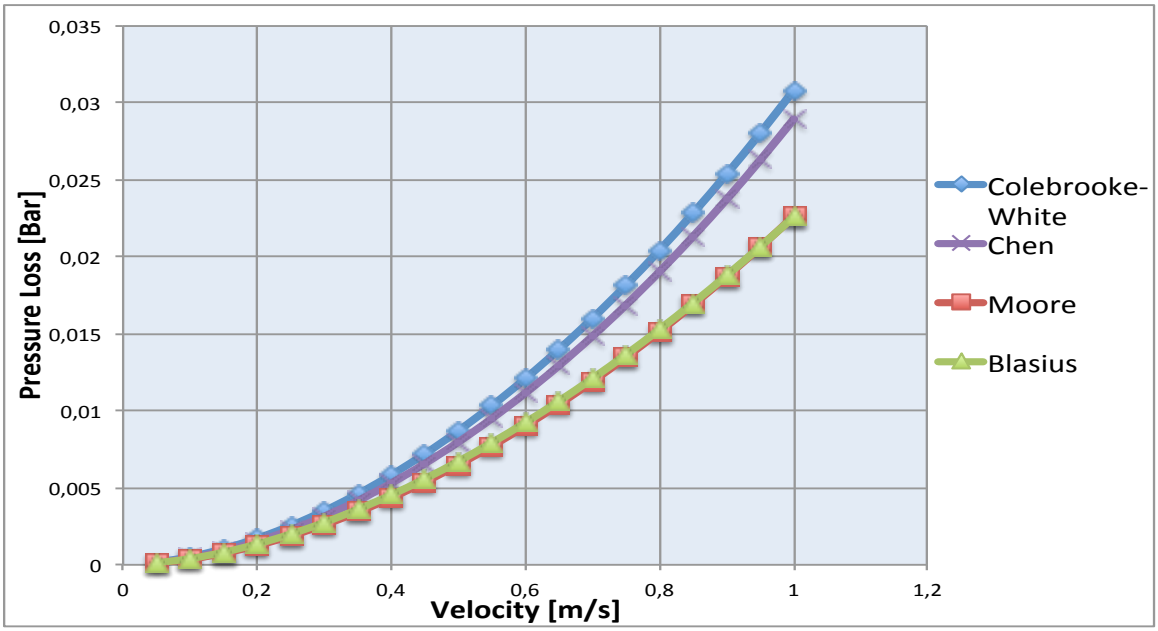

Figure 65: Theoretical calculated resulting pressure drop, plotted against velocity, due to the chosen friction factor correlation for Newtonian fluids

Effect of Equivalent Diameter

Dependent on the suggested hydraulic .the end estimate for velocity, Reynolds number and pressure drop in a pipe alters. To visualize the effect some assumptions were made:

- Newtonian Fluid
- Chen friction factor correlation has been applied in order to visualize the effect of the chose in equivalent diameter.
- Surface roughness is not altered by the equivalent diameter. In other words ε/D is considered constant

Based on Figure 66 there is no difference in applying Lamb correlation and the slot approximation, which both generates a higher pressure loss than applying the wetted perimeter.

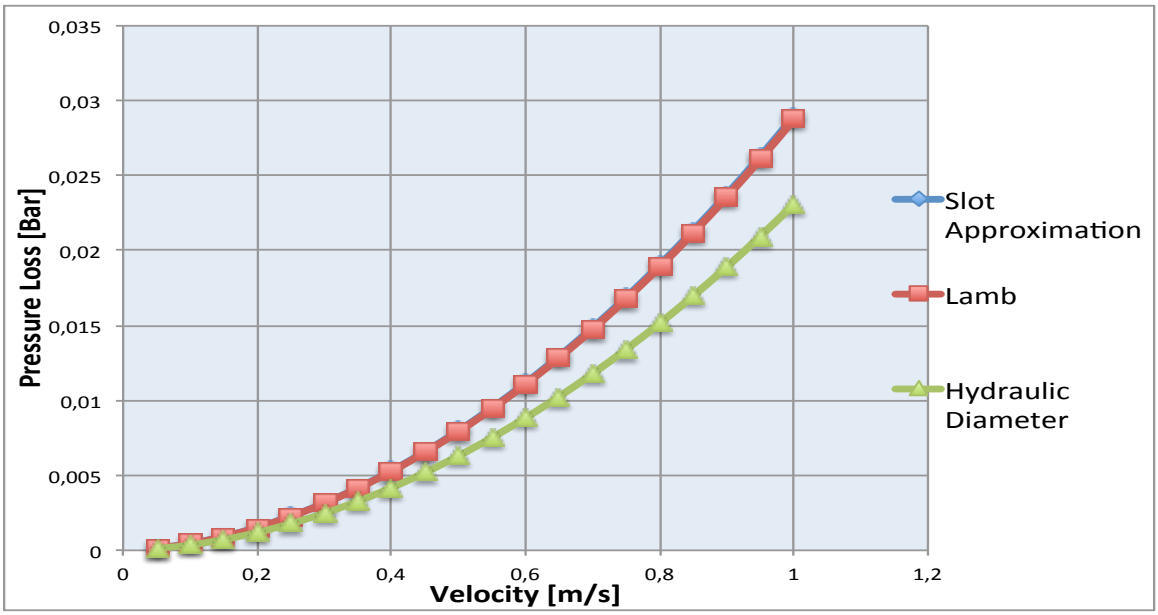

Figure 66: Theoretical effect of equivalent diameter on the velocity and resulting pressure drop for Newtonian fluids

Appendix B: Matlab Code for Noise Cancelling

```
%%This code was made in order to cancel out the pump noise in the
flowmeter
%and thus the responding pressure pulses and noise seen in the
%pressure transducers
%Author Sindre Eiane Aarsland
%5/4-2013

%%Load in input file
signal_input_1 = xlsread('40jmud7');
signal_input_1 = signal_input_1(:,3)
% signal_input_1=load('5hz_flowrate_water_test.txt');
% signal_input_1=load('5hz_p1_water_test.txt');
%signal_input_1=load('5hz_p2_wcater_test.txt');
%signal_input_1=load('5hz_deltap_water_test.txt');

%plot the signal without any filter applied
plot(signal_input_1);
%axis([0 6500 0 4])%(Pressure axis)
axis([0 6000 0 5])

legend('Unfiltered signal 5Hz');
grid on;
ylabel('samplings');
xlabel('input signal');
%% Fast Fourier Transformation in order to visualize the frequency
%in the signal and determine to utilize lowpass og bandpass filter

Fs = 100; %sampling time (REMEMBER TO CHANGE)
T = length(signal_input_1)/Fs; %Sample time
N = length(signal_input_1); %length of the signal

t = [0:N-1]'/N; %Defines the time
t = t*T; %define the time in secound

vector_fft = abs(fft(signal_input_1))/(N/2); %Defines the absolute value
of
%FFT
vector_fft = vector_fft(1:N/2).^2; %power of freqency
freq = [0:N/2-1]/T; % Corrosponding freqency in Hz
semilogy(freq,vector_fft);
legend('')
%% If the freqency spectrum is dominated by white noise a
% Lowpass filter is applied
Fpass = 1;    % Passband Frequency
Fstop = 20;   % Stopband Frequency
Apass = 1;    % Passband Ripple (dB)
Astop = 60;   % Stopband Attenuation (dB)
Fs    = 100;  % Sampling Frequency

h = fdesign.lowpass('fp,fst,ap,ast', Fpass, Fstop, Apass, Astop, Fs);

Hd = design(h, 'butter', ...
'MatchExactly', 'stopband', ...
```

```
'SOSScaleNorm', 'Linf');


lowpassed = filter(Hd,signal_input_1);
smoothing = smooth(lowpassed,250);

Subplot(311)
plot(signal_input_1,'g')
legend('Unfiltered Signal')
axis([0 6000 0 4])
%axis([0 6000 0 1])
xlabel('samplings')
ylabel('input signal')


hold on;
subplot(312)
plot(lowpassed,'b')
legend('Lowpassed Signal')
axis([0 6000 0 4])
%axis([0 6000 0 1])
xlabel('samplings')
ylabel('input signal')

%Smoothing the graph
subplot(313)
plot(smoothing,'r')
legend('Smoothed Signal')
axis([0 6000 0 4])
%axis([0 6000 0 1])
xlabel('samplings')
ylabel('input signal')

%%
plot(signal_input_1,'g')
legend('Unfiltered Signal 30Hz')
axis([0 6500 10.4 10.8])
%axis([0 6000 0 1])
xlabel('samplings')
ylabel('input signal')

%%
clear
%%
mean(lowpassed)
%mean(signal_input_1)
a=length(lowpassed);

b=std(lowpassed);

c=b/sqrt(a)
```

Appendix C: Experimental Uncertainty Analysis Example

To illustrate the impact of random and systematical errors one calculation example have been included below. The data is obtained from the slick pipe section in the low viscosity mud.

Q	0,0016700 m^3/s
$\bar{v}$	0,92812 m/s
P	0,0162 bar
Re	2372,609539
f	0,004927
δv_{Random}	0.00008591
δP_{random}	0,000056

$$\frac{\delta f_{sys}}{0.004927} = \sqrt{(\frac{0.001}{0,0162})^2 + (\frac{2 * 0.02}{0,9218})^2}$$

$$\delta f_{sys} = 0{,}000313$$

$$\sigma_{\Delta \bar{p}} = \frac{\sigma_{\Delta p}}{\sqrt{n}} = \delta \Delta P_{random} = 0.000056$$

$$\sigma_{\bar{v}} = \frac{\sigma_Q}{\sqrt{n}} = \delta v_{random} = 0.00008591$$

$$\frac{\delta f_{random}}{0.004896} = \sqrt{(\frac{0{,}000056}{0.0162})^2 + (\frac{2 * 0.00008591}{0{,}912})^2}$$

$$\delta f_{random} = 1{,}698 * 10^{-5}$$

$$\delta f = \sqrt{(1{,}698 * 10^{-5})^2 + (0{,}000313)^2}$$

$$\delta f = 0{,}00037$$

$$f = 0{,}00489 \pm 0{,}00037$$

And equivalent for Reynolds number

$$Re = 2372{,}60 \pm 102{,}25$$

Appendix D: Simoes et al. Suggested Correlations

Simoes et al. (2007) was placed in the Appendix due to no comparisons were carried out. As the regression constant suggested, Simoes et al .utilized the same principle only with CFD simulations. Since the correlations are based on predetermine assumptions, the prediction towards the chosen experimental geometry and mud would be wrong.

	Laminar	Turbulent	N
Region I	$f = 26.5638e^{-0.237\varepsilon} * Re^{-0.957}$	$f = 0.107262e^{-0.107\varepsilon} * Re^{-0.218}$	
Contraction Tapered shoulder	$f = 0.0782836\, e^{-0.060\varepsilon} Re^{0.654} * N^{-0.125}$	$f = 0.0000076e^{-0.060\varepsilon} Re^{2.8\ \ 8} * N^{1.409}$	$\frac{\rho l_1}{k(\frac{3n+1}{4n})^n * \frac{8v^n}{d_{eff}}} \frac{Q(2D_{H1}tan\beta - l_1 tan^2\beta}{\pi\left(D_{H1}^2 - D_{H1}l_1 tan\beta + \frac{{l_1}^2}{4}tan^2\beta\right)}^2$

Region III	Expansion Tapered shoulder	Region II	
$f = 0.372962e^{-0.264\varepsilon} * Re^{-0.987}$	$f = 0.141479e^{-0.065\varepsilon} * Re^{0.604} * N^{-0.117}$	$f = 16.97019e^{-0.0.050\varepsilon} * Re^{-0.873} * N^{-0.00675}$	$\frac{L_{Tj}}{D_{H2}}$
$f = 30.10606e^{-0.256\varepsilon} * Re^{-0.987}$	$f = 0.000028e^{-0.0007\varepsilon} * Re^{3.003} * N^{1.501}$	$f = 16.97019e^{-0.0.050\varepsilon} * Re^{-0.873} * N^{-0.00675}$	$\frac{\rho l_2}{k(\frac{3n+1}{4n})^n * \frac{8v}{d_{eff}}^n} \frac{Q(2D_{H1}tan\theta - l_1tan^2\theta}{\pi\left(D_{H1}^2 - D_{H1}l_1tan\theta + \frac{l_1^2}{4}tan^2\theta\right)^2}$

Figure 67: Simoes et al. suggested correlation for tool joint in the string.